

**SYNTHESIS AND POLYMERIZATION OF SPIRO-ORTHOESTERS CATALYZED BY
A CATIONIC INDIUM COMPLEX**

by

Chen Chang

B.Sc., The University of British Columbia, 2014

A THESIS SUBMITTED IN PARTIAL FULFILLMENT OF
THE REQUIREMENTS FOR THE DEGREE OF

MASTER OF SCIENCE

in

THE FACULTY OF GRADUATE AND POSTDOCTORAL STUDIES
(Chemistry)

THE UNIVERSITY OF BRITISH COLUMBIA

(Vancouver)

May 2017

© Chen Chang, 2017

Abstract

While numerous neutral indium complexes have been reported to be functional group tolerant Lewis acid catalysts for various transformations, there are only a handful of reported cationic indium complexes; these are mostly inactive in catalytic transformations. Herein, I describe the synthesis and characterization of a rare cationic indium alkyl complex bearing a chiral tridentate ligand, [(NNO)In(CH₂SiMe₃)(THF)][BAR^F] (**30**). Complex **30** is active towards reaction of 1,2-epoxy-7-octene and ε-caprolactone to form the corresponding spiro-orthoester (SOE1), where quantitative conversions of both substrates are achieved under 24 hours at 2.5% catalyst loading at 60 °C in benzene. Synthesis of spiro-orthoesters bearing various ether rings are also achieved with different lactone substrates. While preliminary polymerization studies of SOE1 by the cationic indium species **30** suggest the poor activity of this system towards polymerization of SOE1 at low temperature, polymerization of SOE1 complex **30** at 110 °C resulted in over 90% conversion of the monomer, and the resulting polymer was tentatively assigned as low molecular weight poly(ether ester). This thesis provides another example of the unusual reactivity of cationic indium complexes, where further investigation of various spiro-orthoesters synthesis and polymerization, as well as exploration of other cationic indium complexes, will be continued in the Mehrkhodavandi group.

Lay summary

Indium, a group 13 metal, has been an interested target in academia as its metal complexes have been reported to be active as Lewis acid catalysts for numerous chemical transformations. With several neutral indium based catalysts developed in the Mehrkhodavandi group, I investigate cationic variants of these indium complexes and their reactivity as catalysts. Herein, I describe the synthesis and characterization of a cationic indium complex $[(\text{NNO})\text{In}(\text{CH}_2\text{SiMe}_3)(\text{THF})][\text{BAR}^{\text{F}}]$ (**30**). Complex **30** catalyzes the formation of spiro-orthoesters (SOE), which is a potential building blocks for biodegradable polymers. Complete conversions of both substrates are achieved under 24 hours in appropriate conditions. As well, I have demonstrated that various spiro-orthoesters can be prepared from different starting materials. Preliminary polymerization studies of these SOEs by the cationic indium species **30** suggest the formation of poly(ether ester) which is potentially biodegradable. This thesis provides an example of the unusual reactivity of cationic indium complexes, where further investigation of various spiro-orthoesters synthesis and polymerization, as well as exploration of other cationic indium complexes, will be continued in the Mehrkhodavandi group.

Preface

This thesis summarizes the project that I worked on during my time in the Mehrkhodavandi group. The project was originally started by Dr. Insun Yu to investigate the reactivity of cationic indium complexes as polymerization catalysts. She synthesized the neutral indium alkyl complex **28** as well as the cationic ether adduct counterpart **29**. It was found that catalyst **29** was active towards the copolymerization of lactones and epoxides, where preliminary data suggested the product as alternating oligomers poly(CL-*co*-EOE). I repeated her experiments and identified the product as discrete spiro-orthoester (SOE1) and not oligomers.

Intensive structural analyses including NMR, FTIR, and GC-MS were conducted to confirm this result. I synthesized a THF adduct derivative catalyst **30**, which showed analogous reactivity to **29**. The efficiency of SOE1 synthesis was improved by varying reaction conditions; more than 75% isolated yield was obtained after 24 hours at 2.5% catalyst loading. Preliminary homopolymerization studies suggested the possibility to utilize **30** as a catalyst towards cyclic ester polymerization. Attempts to synthesize spiro-orthoesters bearing various sizes of lactones were also successful. Some polymerization studies suggested the difficulty of polymerizing spiro-orthoesters, where only low molecular weight poly(ether ester) was obtained through polymerization of SOE1 by **30** even at high temperature.

This work has enlightened various future directions to investigate cationic indium complexes and spiro-orthoesters. Further work to explore the substrate scope of this transformation and spiro-orthoesters polymerization will be continued by Hyuk Joon Jung in the group. As well, a manuscript for publication is in preparation.

Table of Contents

| | |
|---|------|
| Abstract | ii |
| Lay summary | iii |
| Preface | iv |
| Table of Contents | v |
| List of Tables | vii |
| List of Figures | viii |
| List of Abbreviations and Symbols | xi |
| Acknowledgements | xiii |
| Chapter 1: Introduction | 1 |
| 1.1 Sustainable synthesis | 1 |
| 1.2 Expanding monomers | 3 |
| 1.3 Spiro-orthoesters synthesis and polymerizations..... | 5 |
| 1.4 Neutral indium-based polymerization catalysts..... | 14 |
| 1.5 Cationic indium complexes..... | 19 |
| 1.6 Project overview | 23 |
| Chapter 2: Indium complexes synthesis and reactivity studies | 27 |
| 2.1 Synthesis and characterization of chiral proligand 27 | 27 |
| 2.2 Synthesis and characterization of neutral indium alkyl complex 28 | 29 |
| 2.3 Synthesis and characterization of cationic indium alkyl complex 30 | 30 |
| 2.4 Conclusion | 37 |

| | | |
|---|---|-----------|
| 2.5 | Experimental procedures | 38 |
| Chapter 3: Spiro-orthoester synthesis and polymerization | | 45 |
| 3.1 | Spiro-orthoester (SOE1) synthesis and characterization | 46 |
| 3.2 | Spiro-orthoester (SOE1) synthesis optimization | 55 |
| 3.3 | Homopolymerization studies of 30 with various monomers | 57 |
| 3.4 | Spiro-orthoesters synthesis with various lactones and EOE..... | 59 |
| 3.5 | Preliminary polymerization of SOE1..... | 65 |
| 3.6 | Conclusion | 71 |
| 3.7 | Experimental procedures | 71 |
| Conclusion and future work | | 79 |
| References | | 82 |
| Appendices..... | | 86 |
| Appendix A Characterization of compounds in solution..... | | 86 |
| Appendix B Characterization of compounds in the solid state..... | | 95 |
| Appendix C Spiro-orthoesters characterization..... | | 96 |
| Appendix D Spiro-orthoester (SOE1) polymerization | | 112 |

List of Tables

| | |
|---|----|
| Table 3.1. Synthesis of SOE1 by 30 | 56 |
| Table 3.2. Homopolymerization of various monomers by 30 | 59 |
| Table 3.3. Synthesis of spiro-orthoesters with different substrates by 30 | 60 |
| Table 3.4. Preliminary polymerization study of SOE1 by 30 | 66 |

List of Figures

| | |
|--|----|
| Figure 1.1 Change in bond distances in ethylene polymerization. | 3 |
| Figure 1.2 Three families of expanding monomers. | 4 |
| Figure 1.3. Proposed mechanism of acid catalyzed spiro-orthoesters synthesis. | 5 |
| Figure 1.4. Cationic polymerization of spiro-orthoesters. | 6 |
| Figure 1.5. Polymerization of spiro-orthoesters 1-3 with Al(acac) ₃ | 7 |
| Figure 1.6. Proposed mechanism for reversible poly(cyclic orthoester) formation..... | 9 |
| Figure 1.7. Stepwise spiro-orthoesters polymerization to afford poly(ether ester) | 10 |
| Figure 1.8. Proposed mechanism for poly(ether ester) formation. | 11 |
| Figure 1.9. Tunable poly(ether ester) for potential applications as new biodegradable materials..... | 12 |
| Figure 1.10. Radical copolymerization of olefins and spiro-orthoester with an exomethylene group (5) followed by cationic polymerization to form crosslinked polymers | 13 |
| Figure 1.11. Examples of recent reports of neutral indium based polymerization catalysts. .. | 15 |
| Figure 1.12. Ring opening polymerization of <i>rac</i> -lactide by 12 | 16 |
| Figure 1.13. Ligand tuning on tridentate dinuclear neutral indium complex (12)..... | 17 |
| Figure 1.14. Ring opening polymerization of <i>rac</i> -lactide by 13 | 18 |
| Figure 1.15. Examples of previously reported cationic indium complexes 14-22 | 20 |
| Figure 1.16. Synthesis of cationic indium complexes (23-26). | 21 |
| Figure 1.17. Polymerization of MMA by cationic indium complexes 23-26 | 22 |
| Figure 1.18. Synthesis of neutral (28) and cationic (29) indium complexes. | 23 |

| | |
|---|----|
| Figure 1.19. Attempts in homopolymerization of CL and epoxides by 29 | 24 |
| Figure 1.20. Attempts in copolymerization of CL and epoxides by 29 | 25 |
| Figure 2.1. Synthesis of proligand H(NNO) (27). | 28 |
| Figure 2.2. Synthesis of complex 28 | 29 |
| Figure 2.3. Molecular structure of 28 | 30 |
| Figure 2.4. Synthesis of complex 30 | 31 |
| Figure 2.5. 2D ^{13}C - ^1H HMBC NMR spectrum of 30 | 32 |
| Figure 2.6. 2D ^1H - ^1H COSY NMR spectrum of 30 | 33 |
| Figure 2.7. <i>SS</i> -Enantiomeric molecular structure of 30 • H_2O | 34 |
| Figure 2.8. <i>RR</i> -Enantiomeric molecular structure of 30 | 36 |
| Figure 3.1 SOE1 synthesis catalyzed by 30 | 45 |
| Figure 3.2. ^1H NMR spectrum of crude from reaction of EOE and CL in the presence of 30 over 16 h. | 46 |
| Figure 3.3. Possible structures of SOE1. | 47 |
| Figure 3.4. ^1H NMR spectrum of SOE1. | 48 |
| Figure 3.5. $^{13}\text{C}\{^1\text{H}\}$ NMR spectrum of SOE1. | 48 |
| Figure 3.6. ^{13}C - ^1H HSQC NMR spectrum of SOE1..... | 49 |
| Figure 3.7. ^{13}C - ^1H HMBC NMR spectrum of SOE1..... | 50 |
| Figure 3.8. Zoomed in ^{13}C - ^1H HSQC NMR spectrum of SOE1..... | 51 |
| Figure 3.9. GC-MS analysis of SOE1..... | 53 |
| Figure 3.10. Proposed mechanism for SOE1 formation catalyzed by 30 | 54 |
| Figure 3.11. FTIR Spectrum of SOE1. | 55 |

| | |
|---|----|
| Figure 3.12. Overlaid ^1H NMR spectra of reaction of CL and EOE in the presence of 30 at 80 °C and SOE1 polymerization by 30 at 80 °C. | 57 |
| Figure 3.13. Homopolymerizations of various monomers by 30 | 58 |
| Figure 3.14. Synthesis of SOE2. | 60 |
| Figure 3.15. ^1H NMR spectrum of SOE2. | 61 |
| Figure 3.16. $^{13}\text{C}\{^1\text{H}\}$ NMR spectrum of SOE2. | 61 |
| Figure 3.17. GC-MS analysis of SOE2. | 62 |
| Figure 3.18. Synthesis of SOE3 | 63 |
| Figure 3.19. ^1H NMR spectrum of SOE3. | 63 |
| Figure 3.20. $^{13}\text{C}\{^1\text{H}\}$ NMR spectrum of SOE3. | 64 |
| Figure 3.21. GC-MS analysis of SOE3. | 65 |
| Figure 3.22. Cationic polymerization of SOE1 by 30 | 66 |
| Figure 3.23. Overlaid ^1H NMR spectra of SOE1 polymerization at 110 °C overtime. | 67 |
| Figure 3.24. $^{13}\text{C}\{^1\text{H}\}$ NMR spectrum of SOE1 polymerization product. | 68 |
| Figure 3.25. FTIR Spectrum of SOE1 polymerization product. | 69 |
| Figure 3.26. MALDI-TOF mass spectrum of SOE1 polymerization product. | 70 |

List of Abbreviations and Symbols

| | |
|--------|---|
| EOA | 1,2-epoxyoctane |
| EOE | 1,2-epoxy-7-octene |
| SOE2 | 2-(hex-5-en-1-yl)-1,4,6-trioxaspiro[4.5]decane |
| SOE3 | 2-(hex-5-en-1-yl)-1,4,6-trioxaspiro[4.5]nonane |
| SOE1 | 2-(hex-5-en-1-yl)-1,4,6-trioxaspiro[4.6]undecane |
| H(NNO) | 2,4-di-cumyl-6-(((2-(dimethylamino)cyclohexyl)imino)methyl) phenol |
| AcOH | acetic acid |
| acac | acetoacetone |
| AGE | allyl glycidyl ether |
| BOE | bicyclic-orthoester |
| μ | bridging ligand |
| BL | γ -butyrolactone |
| MM2 | calculation for conformational analysis of hydrocarbons and other small organic molecules |
| CL | ϵ -caprolactone |
| COSY | correlation spectroscopy |
| CHO | cyclohexene oxide |
| D_M | dispersity |
| Et | ethyl |
| FTIR | fourier transform infrared spectroscopy |
| iPr | <i>iso</i> -propyl |
| GC-MS | gas chromatography mass spectrometry |
| τ | geometry index or structural parameter |
| HMBC | heteronuclear multiple-bond correlation spectroscopy |
| HSQC | heteronuclear single-quantum correlation spectroscopy |

| | |
|------------------|--|
| MALDI-TOF | matrix-assisted laser desorption/ionization time of flight mass spectrometry |
| Mes | mesityl |
| Me | methyl |
| MMA | methyl methacrylate |
| NMR | nuclear magnetic resonance spectroscopy |
| M_n | number average molecular weight |
| Ph | phenyl |
| PCL | poly(ϵ -caprolactone) |
| nPr | propyl |
| $^{13}C\{^1H\}$ | proton decoupled carbon |
| (\pm) | racemic |
| κ | relate to the coordination mode of ligand |
| r.t. | room temperature |
| SOC | spiro-orthocarbonate |
| SOE | spiro-orthoester |
| Boc | <i>tert</i> -butoxycarbonyl |
| tBu | <i>tert</i> -butyl |
| THF | tetrahydrofuran |
| VL | δ -valerolactone |
| M_w | weight average molecular weight |
| BAR ^F | tetrakis(3,5-bis(trifluoromethyl)phenyl)borate |

Acknowledgements

First, I would like to express my sincere gratitude to my supervisor Prof. Parisa Mehrkhodavandi. With limited experience in inorganic synthesis and polymer chemistry, I have struggled through the first half year of my graduate study. With her endless patience, support, and encouragement, I was able to push myself further and overcome challenges in front of me throughout my research. Parisa has been, not only an excellent advisor in chemistry, but also an exceptional mentor in a lot of other aspects in life. It has been a great time to have her as my supervisor and her enthusiasm in life and science will definitely impact my life and future after graduation.

I would also like to thank the MehrCats as well as former members from the group for their support and advice throughout my time in the lab. I would like to give special thanks to former coffee loving post-doctoral researcher, Dr. Paul Kelley for his continuous support and mentoring throughout my time here. I was also able to receive feedback and suggestion from former Ph.D. students, Dr. Insun Yu and Dr. Dinesh Aluthge regarding the ongoing project which, greatly assisted with the progress of my project. I would like to thank Love-Ese Chile, Emiliya Mamleeva, and Tannaz Ebrahimi, who helped me with experimental procedures and instrumentations. Lastly, I would like to give credits to Alexandre Bertrand Kremer, Xiaofang Zhai, Carlos Andres Dias Lopez, Hyuk Joon Jung, Chris Shyi and other former members of the group for their friendship and support. It was my pleasure to work with the MehrCats, where I grew and learnt a lot from. Big thanks to all of them.

Aside from the group, I would like to first thank the chemistry department for offering me this opportunity to continue my graduate study here at UBC. I would like to appreciate all the staff and faculty helped me with instrumentations and experiments throughout my studies. In particular, I would like to thank Maria Ezhova and NMR facility for NMR experiments; Dr. Yun Liang and the mass spectrometry facility for mass analysis and elemental analysis; Tannaz Ebrahimi, Dr. Brian Patrick, and the X-Ray crystallography lab for solid state structure analysis; Sheri Harbour for her help with documentation; and all staff in electronics, glass blowing, and mechanical shop for their help. In addition, I would like to thank Prof. Glenn Sammis, Prof. Suzana Straus, Prof. Laurel Schafer for their revision and suggestion on my project which helped me to redirect my project focus in a more clear and thoughtful manner. A special thank for Prof. Glenn Sammis for giving me the idea for spiro-orthoester as a potential product. Finally, I would like to thank all the friends, colleagues, professors that I have met in this department.

I am fortunate to join the NSERC CREATE sustainable synthesis program where I was able to widen my vision in an interdisciplinary fashion with aspects of green chemistry from chemistry, chemical engineering, and pharmaceutical sciences. I would like to thank Prof. Laurel Schafer and Adana Whitter for their support and mentoring in the program. As well, I would like to thank the program for providing an opportunity for an industrial internship experience.

Last but not least, I would like to thank my family and friends for their endless support and encouragement throughout my graduate studies. It has been a challenging period for me and I am glad that they are always there for me at difficult moments. I am proud of myself for the completion of the program and I hope that all of you are as well.

Chapter 1: **Introduction**

1.1 Sustainable synthesis

Over the last few decades, green chemistry, or sustainable chemistry, has become an emerging area of interest in both academia and industry.¹⁻⁶ Green chemistry focuses on development of green processes and products with minimization of hazardous material usage and generation. In the late 90's, the 12 principles of green chemistry were developed as guidelines for scientists and engineers to design methods to reduce waste generation, energy consumption, and pollution.⁷ While several aspects of green chemistry can be addressed in process and product designs, the Mehrkhodavandi group focuses on the development of catalysts for biodegradable polymers.

In the modern world, petroleum derived polymers and plastics have become some of the most significant materials since the invention of synthetic plastic in the early twenty century. Over last few decades, along with growing population, there has been an enormous growth in plastic demand. According to Statista, the production of plastics around the globe has more than tripled from 100 million metric tons to 311 million metric tons in the 25 years, between 1989 and 2014.⁸ Substantial plastic production has led to many issues associated with plastic disposal, which, has become a serious global concern, due to low-degradability of conventional plastics.⁹ Consequently, significant attention has been focused towards the development of biodegradable plastics; a more sustainable alternative to conventional petroleum derived polymers.

Biodegradable polymers can undergo rapid chemical decomposition under the influence of microorganisms in a suitable composting environment.¹⁰ For instance; most biodegradable polymers possess chemical motifs within the polymer backbone, where these linkages are constitutionally susceptible to hydrolysis and further degradation in a composting environment. One example of an important family of biodegradable polymers that receives considerable attention is aliphatic polyesters. With high biocompatibility, low toxicity, and biodegradability, aliphatic polyesters excel as superior candidates in bio-medical,¹¹ pharmaceutical,¹² food packaging,¹³ and agricultural applications.¹⁴ Interest in tunable biodegradable material has led to significant attention being focused on the development of functionalized polyesters to expand their uses in other applications.

Inspired by green chemistry and NSERC CREATE sustainable synthesis program at UBC, I joined the Mehrkhodavandi group and investigated indium based catalysts for biodegradable polymers. My project focused on exploration of reactivity of a cationic alkyl indium complex as a potential catalyst for the copolymerization of epoxides and lactones. While this project was originated by Dr. Yu, I extended the investigation and confirmed the identity of the resultant product as discrete spiro-orthoester and no copolymers. This catalytic transformation not only provides another example of the unusual reactivity of indium catalysts, but also showcases an alternative route to synthesize spiro-orthoesters efficiently. Moreover, previous reports show that cationic polymerization of spiro-orthoesters at high temperature undergoes double ring opening polymerization to yield to poly(ether ester)s, which can potentially be utilized as a new class of tunable biodegradable polymers.

1.2 Expanding monomers

In a typical polymerization process, volume shrinkage is an unavoidable defect for most polymers derived from monomers such as ethylene, vinyl chloride, methyl methacrylate, and styrene.¹⁵ One of the major causes for this phenomenon is the change in molecular distances between the monomer state and the polymer state. During the polymerization, monomers move from van der Waals distance to covalent distance to form polymers. The decrease in distances between each monomer leads to a decrease in the total volume of the material. In ethylene polymerizations, the distance between each monomers changes from a van der Waals distance of 3.40 Å to the covalent distance of a single C-C bond (1.54 Å), which results in a net decrease of 1.86 Å (Fig. 1.1.1). Despite the slight bond expansion of 0.20 Å, due to the change from the double C=C bond in ethylene (1.34 Å) to the single C-C bond in polyethylene (1.54 Å), polymerization of ethylene usually leads to an overall volume shrinkage of ~66%.¹⁵

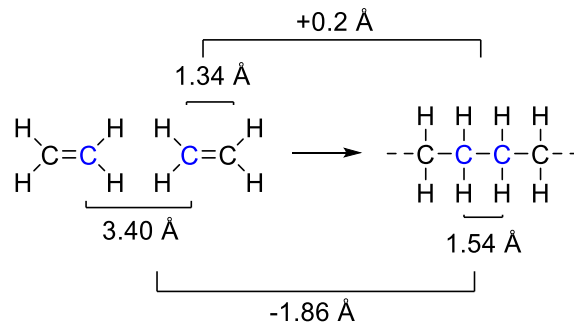


Figure 1.1 Change in bond distances in ethylene polymerization.

In material science, this unfavorable shrinkage can lead to a plethora of issues, such as accumulation of internal stress within polymers.¹⁶⁻¹⁷ As a consequence, efforts have been made towards the development of monomers that exhibit low volume shrinkage or expansion upon polymerization. Monomers of this type are critical for applications such as precision coating, dental fillings, and epoxy resin.¹⁸⁻²⁰

In 1973, Bailey reported the first example of monomers that showed low volume shrinkage upon polymerization.²¹ This discovery led to the development of three major families of expanding monomers over the following decades; spiro-orthoesters (SOE), bicyclic orthoesters (BOE), and spiro-orthocarbonate (SOC), (Fig. 1.1.2). The volume expanding nature is believed to be a result of a double ring opening process during polymerization. While many materials based on these structures have been developed in the past,²²⁻²⁴ several issues associated with monomer synthesis, polymerizability, and material properties have led to limited industrial applications.

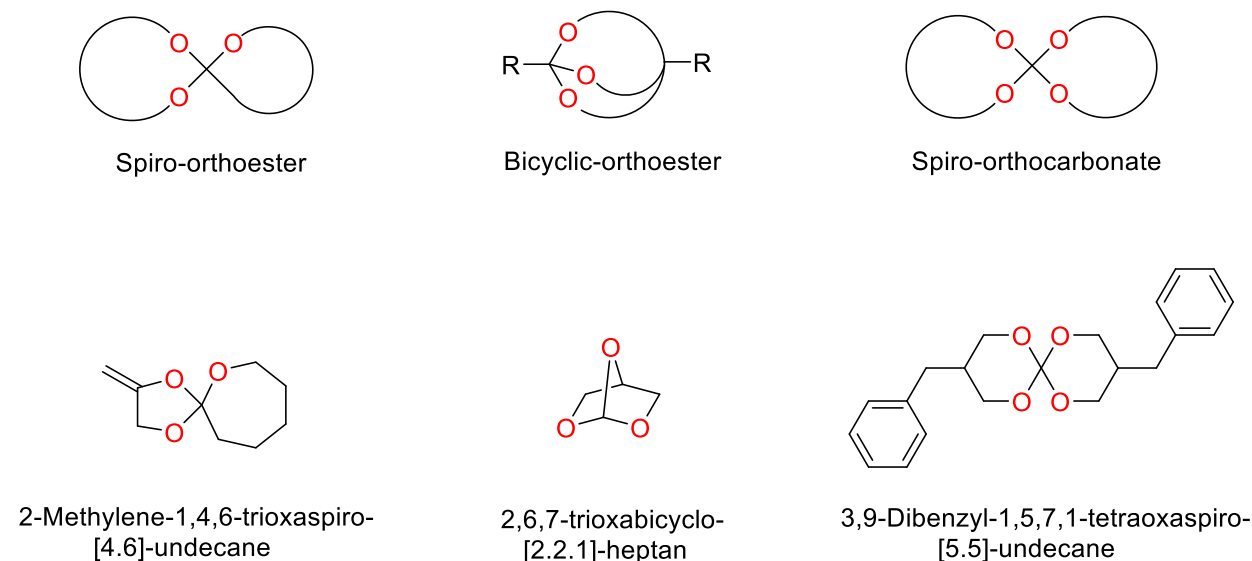


Figure 1.2 Three families of expanding monomers.²²⁻²⁴

1.3 Spiro-orthoesters synthesis and polymerizations

Among aforementioned expanding monomers, spiro-orthoesters are the most useful monomers, due to the ease of preparation compared to BOEs and SOCs. The first spiro-orthoester, 1,4,6-trioxaspiro-[4,4]-nonane was prepared by Bodenbenner in 1959 from the reaction of ethylene oxide and γ -butyrolactone in the presence of boron trifluoride (BF_3).²⁵ Several methodologies for the synthesis of spiro-orthoesters have been reported, most examples focusing on the acid-mediated reaction of epoxides and lactones.²⁶⁻³⁰ While both Lewis and Brønsted acids are reported to facilitate this transformation, the product yields are often low.

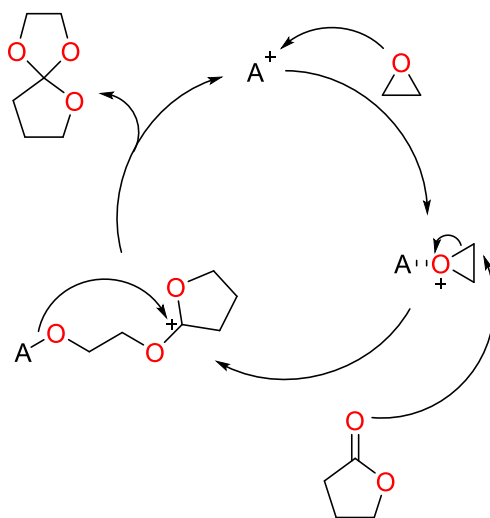


Figure 1.3. Proposed mechanism of acid catalyzed spiro-orthoesters synthesis.³¹

Figure 1.3 illustrates the proposed mechanism of acid catalyzed spiro-orthoesters formation.³¹ In the initiation step, the epoxide unit is activated by the acid catalyst A^+ . The electrophilic carbon of the activated epoxide undergoes nucleophilic attack via the carbonyl oxygen on the lactone. This attack leads to the ring opening of the epoxide to form a carbocation intermediate, where the carbocation is stabilized by two neighbouring oxygens. This reactive intermediate undergoes a back-biting cyclization to yield the desired spiro-orthoester.

Previous reports of spiro-orthoesters polymerization, mostly focused on catalysis via cationic initiators,³¹⁻³³ with a few examples of photoinitiators.³⁴⁻³⁶ The Bailey and the Endo group reported that spiro-orthoesters could be polymerized with cationic catalysts to form poly(ether ester)s through a double ring opening isomerization at elevated temperature.³⁶⁻³⁷ Based on NMR studies,³⁸ Matyjaszewski suggested that the cationic polymerization of 1,4,6-trioxaspiro-[4,4]-nonane employed a fast single ring opening polymerization of the lactone cyclic unit to form poly(cyclic orthoester), followed by a slow intramolecular rearrangement to afford the corresponding poly(ether-ester) (Fig. 1.4).

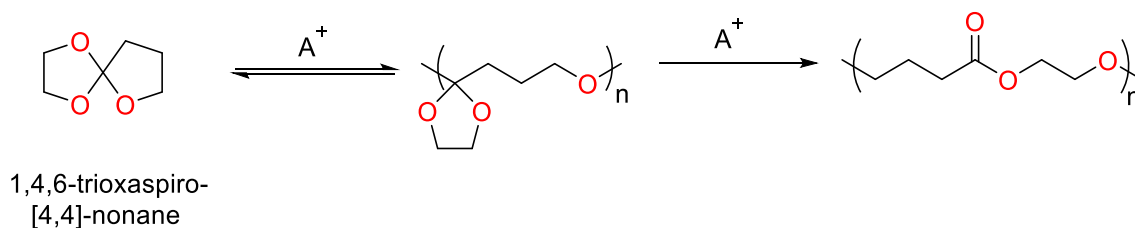


Figure 1.4. Cationic polymerization of spiro-orthoesters.³⁸

In 1990, Endo and coworkers reported the single ring opening polymerization of 2-methyl-1,4,6-trioxa-spiro[4,6]-undecane (**1**) from the cyclic ether ring, catalyzed by aluminium acetylacetonate ($\text{Al}(\text{acac})_3$) at room temperature to form the corresponding poly(cyclic orthoester) (Fig. 1.5).⁴⁰ The resultant polymer could be obtained in 75% after 10 days with a dispersity (D_M or M_w/M_n) of 1.85. However, polymerizations of spiro-orthoesters with five or six membered cyclic ether rings were unsuccessful. Based on force field calculations (model MM2), the polymerization was believed to be dependent on the strain energy of the monomer (**1**: 20 kcal/mol; **2**: 14 kcal/mol; **3**: 15 kcal/mol).⁴⁰

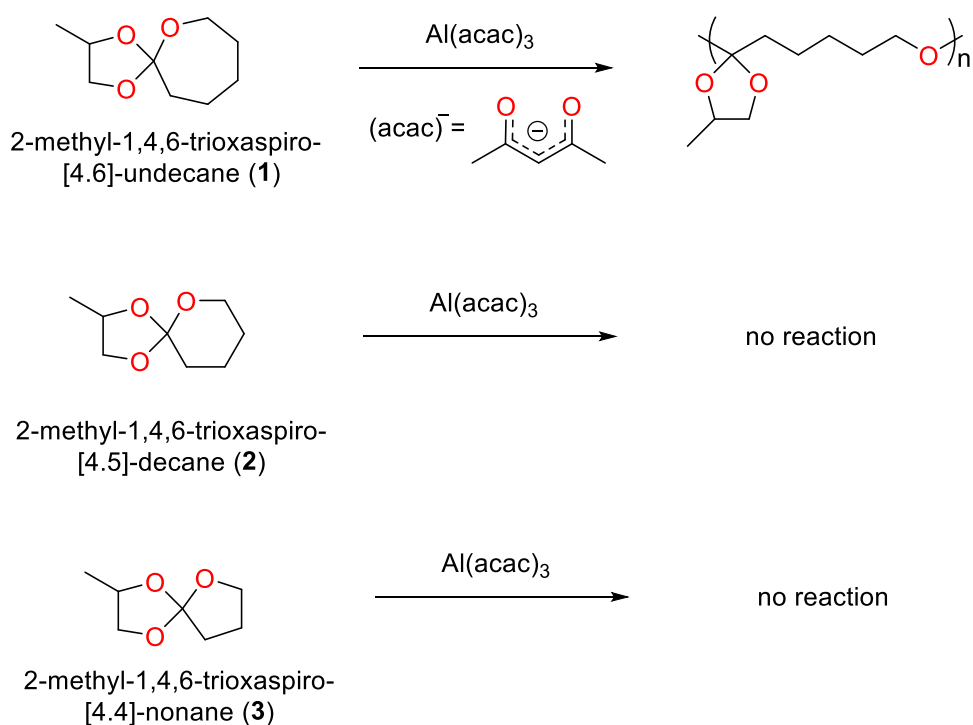


Figure 1.5. Polymerization of spiro-orthoesters **1-3** with $\text{Al}(\text{acac})_3$.⁴⁰

Poly(cyclic orthoester) rapidly decomposes to respective spiro-orthoester in the presence of an acid (Fig.1.6); this degradation can be monitored by changes in molecular weight over time.⁴¹ Further studies by Endo and coworkers also suggest a temperature dependence on spiro-orthoesters polymerization, which is consistent with the typical behaviors of equilibrium polymerization.⁴² In this case, polymerization of spiro-orthoesters selectively afford poly(cyclic orthoester) at low temperature ($< 10\text{ }^{\circ}\text{C}$).⁴³

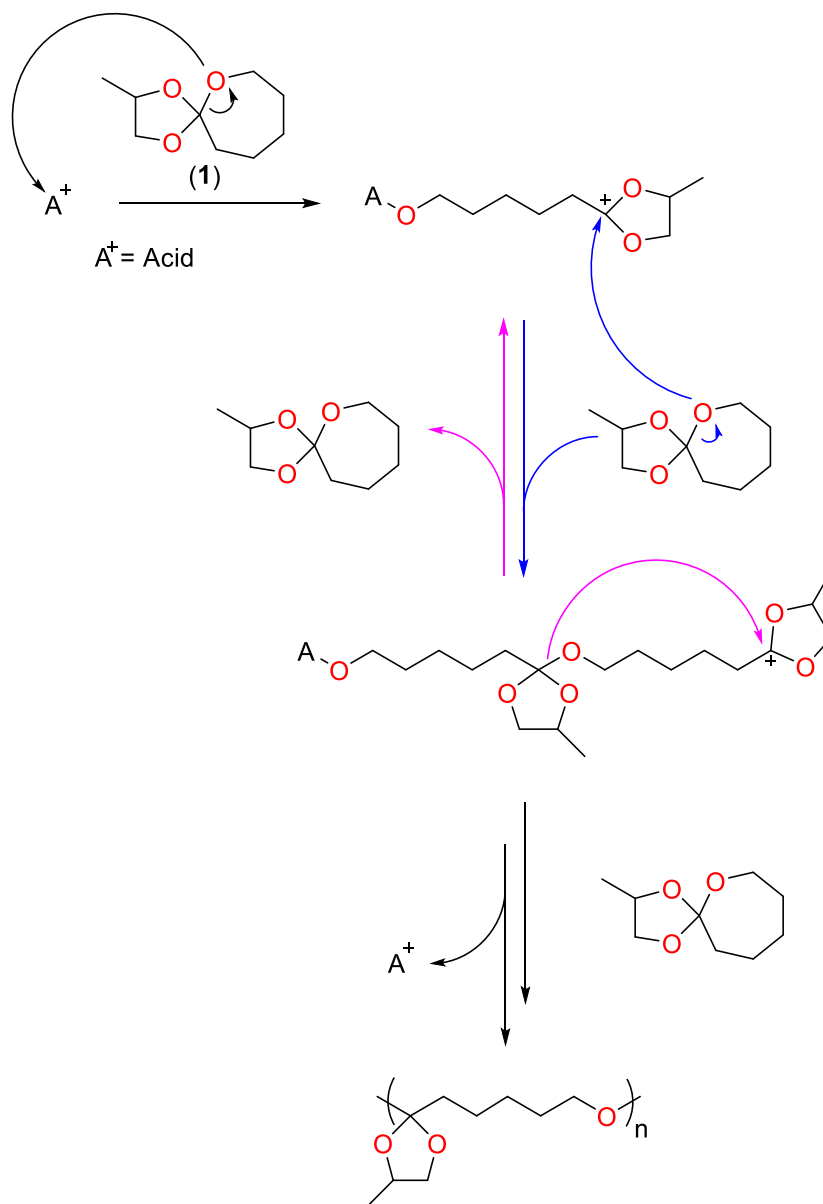


Figure 1.6. Proposed mechanism for reversible poly(cyclic orthoester) formation. Blue arrow indicates polymerization pathway while pink arrow illustrates the reverse depolymerization.⁴¹

In 1992, Endo and coworkers reported an intensive study on cationic ring-opening polymerization of spiro-orthoesters.⁴² Polymerizations of 1,4,6-trioxaspiro-[4.6]-undecane (**4**) were shown to be effective in the presence of SnCl₄ (2 mol%) at temperatures ranging from 0 °C to 120 °C. Polymers obtained at 0 °C were found to be poly(cyclic orthoester), exclusively. However, polymers obtained above 40 °C suggested the existence of poly(ether ester) type structure. This is indicative of a temperature-dependent isomerization that only occurs at higher temperature.

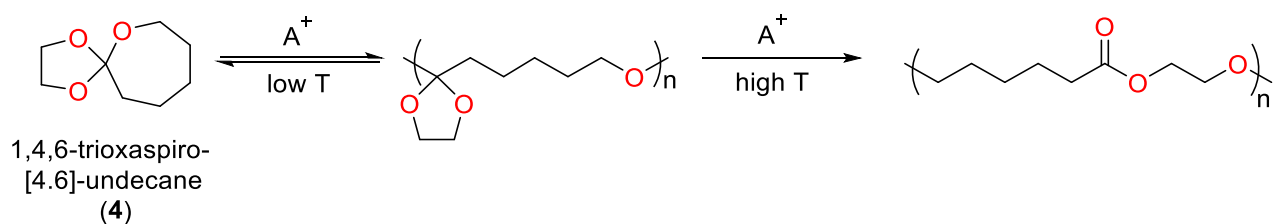


Figure 1.7. Stepwise spiro-orthoester polymerization to afford poly(ether ester).

Detailed ¹³C NMR measurements of the polymer mixture suggested the presence of a mixture of products between poly(cyclic orthoester) and poly(ether ester) even at 120 °C. This evidence suggested the difficulty to obtain complete isomerized poly(ether ester) as the molecular weight decreases dramatically with increasing reaction temperature.⁴² Moreover, the degree of isomerization was found to increase over time while the overall yield showed no dependence on the polymerization time. This suggests the single ring opening product, poly(cyclic orthoester) is formed prior to further isomerization to poly(ether ester) at elevated temperature (Fig. 1.7). Further investigation of this phenomenon by treatment of the pre-synthesized poly(cyclic orthoester) with

SnCl₄ at 120 °C yielded a partially isomerized product, which supports the aforementioned reaction pathway. A plausible mechanism for this isomerization was proposed by Endo and coworkers (Fig. 1.8).⁴²

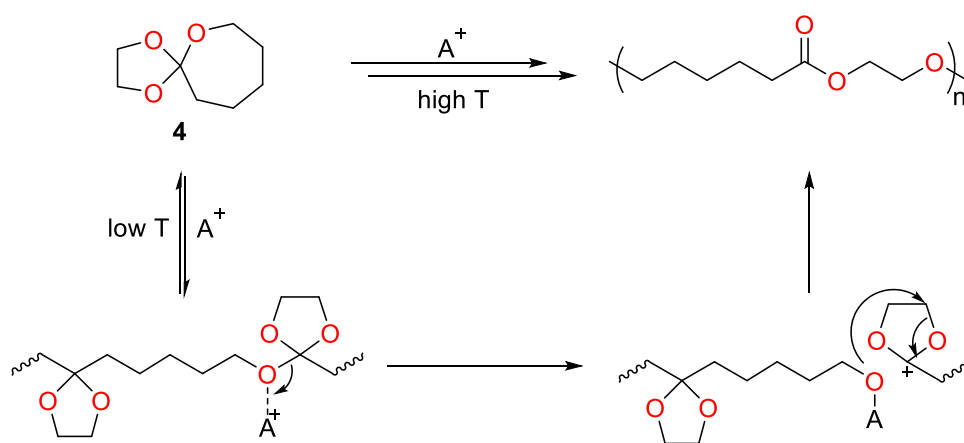


Figure 1.8. Proposed mechanism for poly(ether ester) formation.⁴²

The volume change during polymerization was investigated by Endo and coworkers, as the double ring opening event of spiro-orthoesters during polymerization should translate into a volume change, that is characteristic for an expanding monomer.⁴² A slight volume shrinkage was observed for 1,4,6-trioxaspiro-[4.6]-undecane based poly(cyclic orthoester); reduction of the shrinkage was found to be related with increasing the degree of isomerization. This result provided evidence that the double ring opening isomerization contributes to the reduction of volume shrinkage during polymerization.

In addition to the volume expansion, the resultant polymer from the double ring opening isomerization of spiro-orthoesters, poly(ether ester), possesses ester motifs along the polymer

chain. These linkages are susceptible to hydrolysis, which offers a potential use as a biodegradable alternative to conventional polymers. Moreover, a functional group on the epoxide starting material could allow the synthesis of various functional spiro-orthoesters, which could translate into a functionalized polymer backbone for post-synthetic modifications, such as intermolecular cross-linking, to enhance material property. Unfortunately, despite the promising nature of these polymers, homopolymerization of spiro-orthoesters often leads to low molecular weight oligomers.

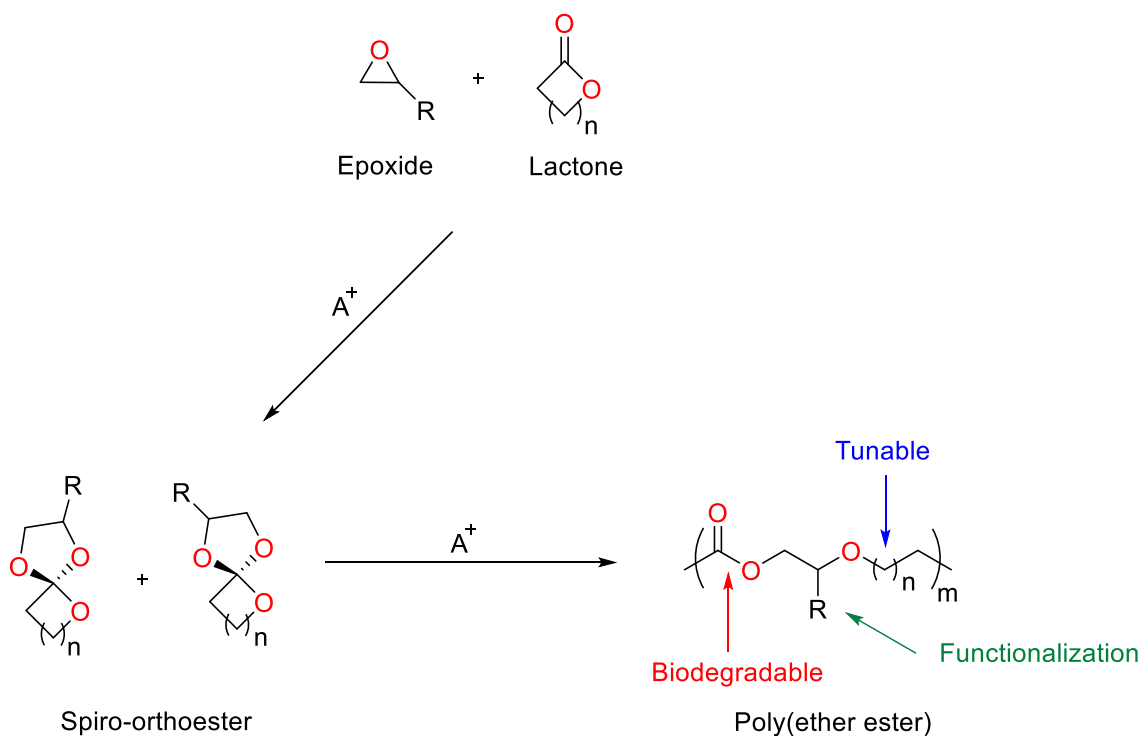


Figure 1.9. Tunable poly(ether ester) for potential applications as new biodegradable materials.

While numerous spiro-orthoester syntheses and their polymerizations have been reported in the late 90s, there are only a handful of reports associated with spiro-orthoesters in the recent literature.⁴⁴⁻⁴⁷ Due to the low molecular weight nature of the resultant polymer from homopolymerization of spiro-orthoesters, more attention has been focused on copolymerization of functionalized spiro-orthoesters with other monomers to improve the molecular weight. For instance, several reports have shown that a spiro-orthoester (**5**) with an exomethylene group can copolymerize radically with olefins such as styrene, acrylonitrile, and vinyl acetate (Fig. 1.10).⁴⁵⁻

47

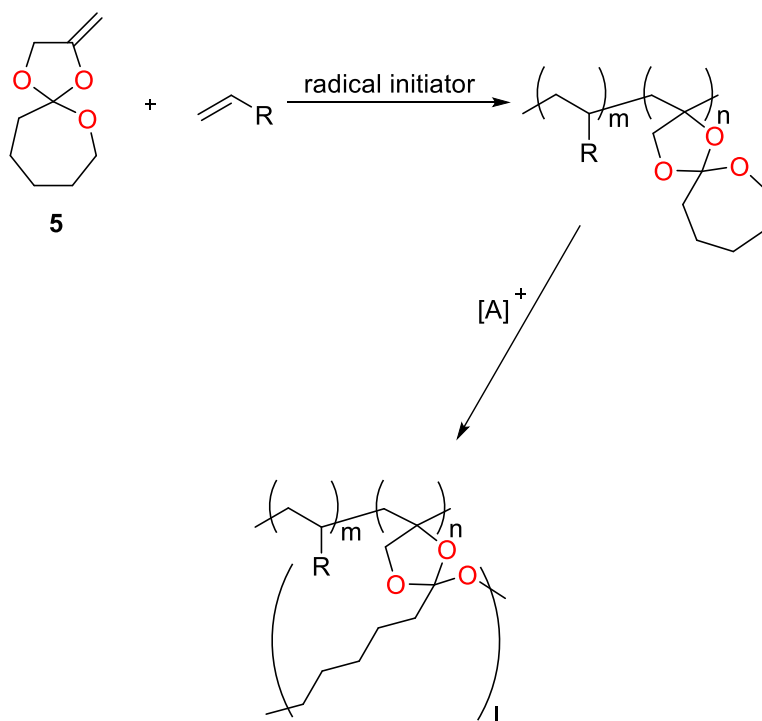


Figure 1.10. Radical copolymerization of olefins and spiro-orthoester with an exomethylene group (**5**) followed by cationic polymerization to form crosslinked polymers.⁴⁶⁻⁴⁷

Pendant spiro-orthoester groups can be further utilized as cross-linking agents through cationic polymerization. This alternative method allows the incorporation of spiro-orthoester moieties into polymer backbones that can be used to prevent volume shrinkage associated with cross-linking process.⁴⁵⁻⁴⁷ Although such methodology could provide plausible routes towards higher molecular weight species, the issue of low molecular weight homopolymers has not yet been addressed. This limitation remains one of the major challenges towards the usage of spiro-orthoester monomers as building blocks for tunable biodegradable materials without volume shrinkage.

1.4 Neutral indium based-polymerization catalysts

While intensive effort has been put towards the development of group 13 Lewis acid catalysts, most of these catalysts based on boron and aluminium suffer from limited substrate scope and instability in the presence of monomer impurities such as water or alcohol. As a consequence, more attention has been put towards the investigation of indium-based catalysts as they have been reported to be functional group tolerant Lewis acid catalysts in numerous organic transformations.⁴⁸⁻⁵⁰ In addition, indium salts are surprisingly stable towards moisture, which is an outstanding feature among group 13 elements. In the recent literature, neutral indium-based catalysts have also been reported as polymerization catalysts (Fig. 1.11).⁵¹⁻⁵⁶

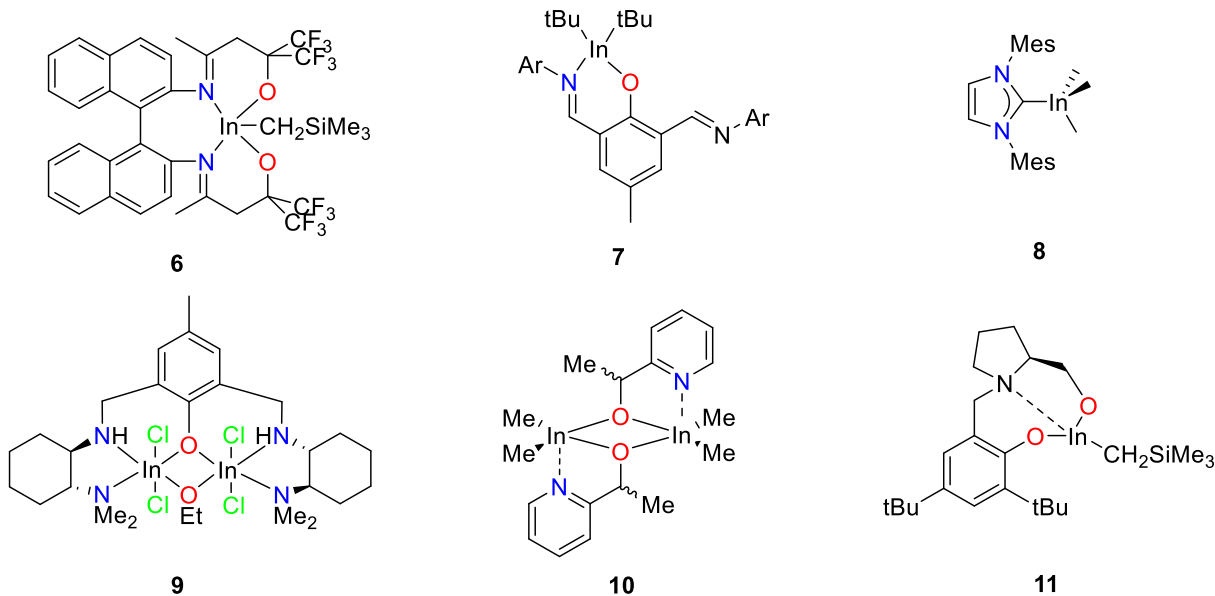


Figure 1.11. Examples of recent reports of neutral indium based polymerization catalysts.⁵¹⁻⁵⁶

In the Mehrkhodavandi group, previous efforts have been focused on the development of neutral indium(III) based catalysts for ring-opening polymerization of cyclic esters such as lactide, ϵ -caprolactone, and β -butyrolactone.⁵⁷⁻⁶³ In 2008, our group reported the first example of a highly active dinuclear asymmetrically bridged diaminophenolate indium catalyst (**12**) for the ring opening polymerization of lactide (Fig. 1.12).⁵⁷ Living polymerization of *rac*-lactide catalyzed by **12** yielded high molecular weight poly(lactide) with low dispersity and enriched isotactic microstructure. For example, 200 equivalents of *rac*-lactide are converted into poly(lactide) in 90% conversion in 30 minutes at room temperature, a result which is comparable to the most active systems for lactide polymerization.⁵⁷

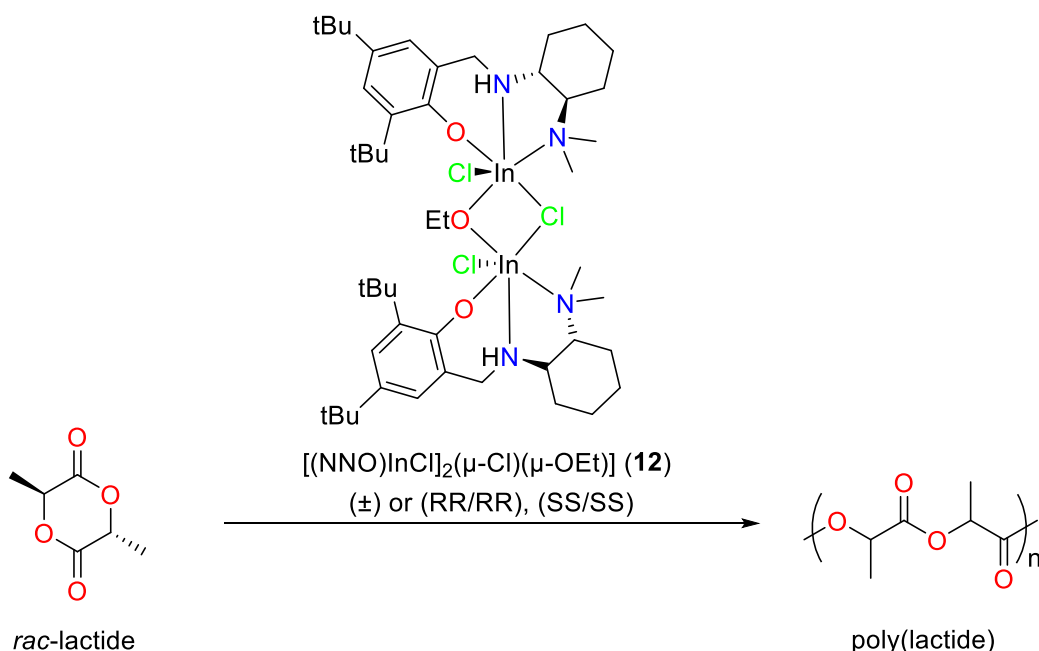


Figure 1.12. Ring opening polymerization of *rac*-lactide by **12**.⁵⁷

Several modifications of **12** were reported, to probe the role of the ligand towards the observed reactivity. For example, analogues with different halide ligands on the indium center were synthesized and characterized. The mechanistic study of living lactide polymerization by the complexes was described and the parent system **12** with chloride ligands was shown to be one of the most successful catalysts towards controlled ring opening polymerization of lactides.⁴⁵ Further investigation on tridentate ligand tuning on the catalyst was conducted by former Ph.D. researcher Dr. Kimberly Osten, which included modification of substituents on the 2,4 positions of the phenol ring and terminal amine, tuning electronics on the central amine to tertiary amine and imine, and changing the linker between two amines (Fig. 1.12).⁵⁹⁻⁶² These results allowed us to gain important insights into the tridentate ligand system, that is utilized in various research projects in our group.

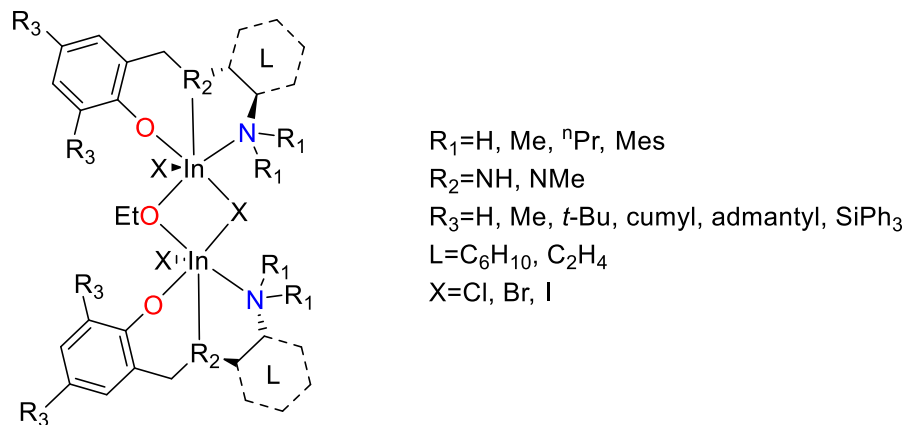


Figure 1.13. Ligand tuning on tridentate dinuclear neutral indium complex (**12**).⁵⁹⁻⁶²

With the success of first generation catalysts, the Mehrkhodavandi group expanded the investigation towards tetradentate ligand scaffolds and reported a site-selective dinuclear indium complex bearing a chiral salen ligand (**13**) as an excellent catalyst for controlled ring opening polymerization of lactide (Fig. 1.13). In comparison to the tridentate system, the activity of **13** towards ring opening polymerization of lactide is an order of magnitude lower. However, due to the site-selective nature of **13**, polymerization of *rac*-lactide yields highly isotactic poly(lactide)s.⁶³ Both of these reported systems have demonstrated the potential for indium complexes to be used as efficient Lewis acid catalysts towards polymerization of cyclic esters.

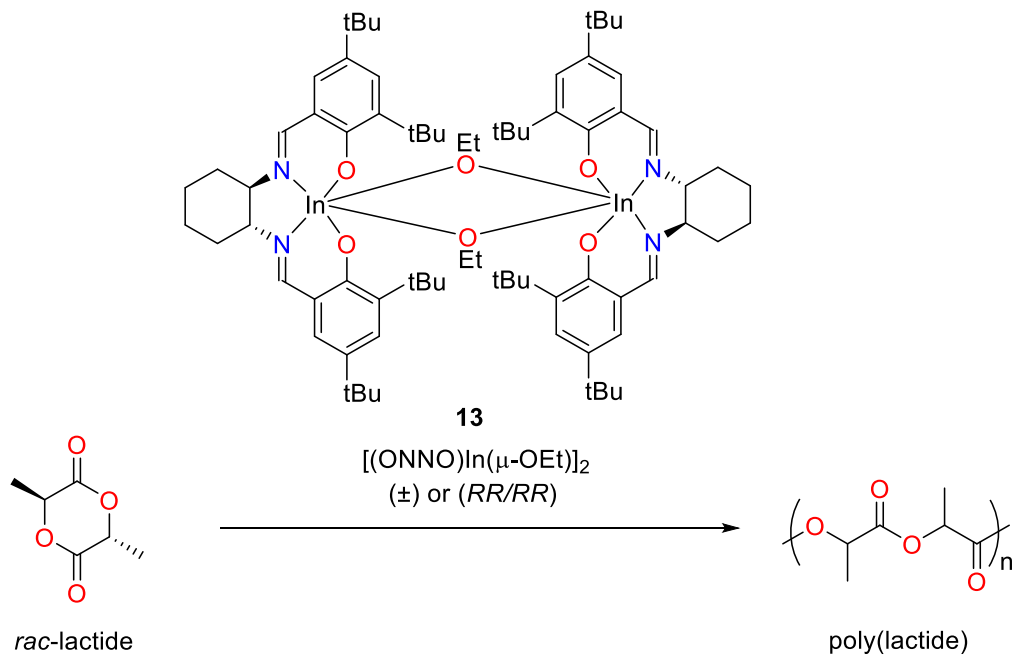


Figure 1.14. Ring opening polymerization of *rac*-lactide by **13**.⁶³

While previous efforts in Mehrkhodavandi group focused on indium complexes and their reactivity towards ring opening polymerization of various monomers to form biodegradable polymers, a majority of the research has been conducted with neutral indium complexes. With limited reports of active cationic indium complexes, expanding our knowledge of indium reactivity, through the development of cationic indium species and the exploration of their reactivity has been a new direction in the group.

1.5 Cationic indium complexes

Cationic group 13 metal complexes are attractive targets in academia due to their Lewis acidic nature which makes them potent candidates for a wide range of Lewis acid mediated reactions. In particular, attention has been drawn to cationic aluminum species as they possess great stability and reactivity in catalytic polymerization of epoxides⁶⁴⁻⁷⁴ and cyclic esters.⁷⁵⁻⁷⁸ Although extensive effort has been expended on the investigation of cationic aluminum complexes⁶⁴⁻⁷⁸, there are few examples of cationic indium complexes,⁷⁹⁻⁸⁷ and most are reported to be catalytically inactive (Fig. 1.15).

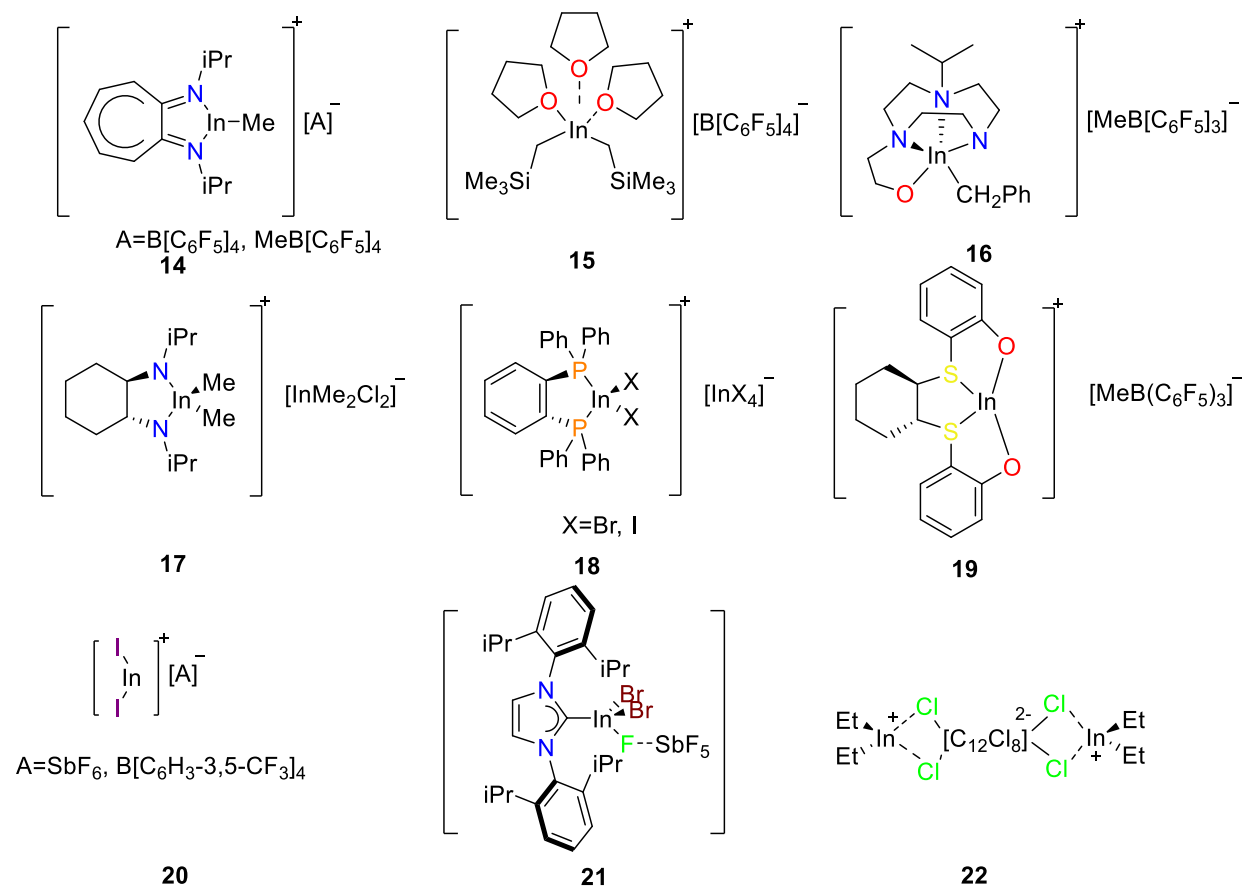


Figure 1.15. Examples of previously reported cationic indium complexes **14-22**.⁷⁹⁻⁸⁷

Previous reports suggested that cationic indium complexes could be synthesized from their neutral counterparts via protonolysis,⁸¹ halide abstraction,⁸⁵⁻⁸⁶ and alkyl abstraction.^{79,82,84,87} With the numerous neutral indium catalysts developed by the Mehrkhodavandi group,⁵⁷⁻⁶² former Ph.D. graduate, Dr. Insun Yu investigated the chiral tridentate diaminophenolate system and synthesized a group of cationic indium alkyl complexes through protonolysis with strong Brønsted acids (Fig. 1.16).⁸⁸ These cationic indium complexes bearing different counterions (**23-26**) were fully characterized and summarized in her thesis.⁸⁸

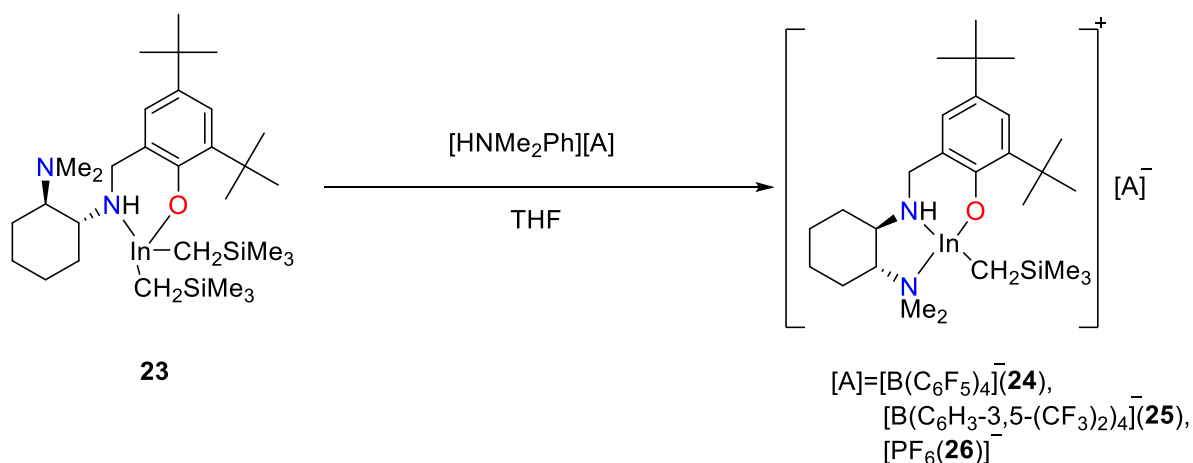


Figure 1.16. Synthesis of cationic indium complexes (**23-26**).⁸⁸

Interestingly, preliminary results by Dr. Yu show that these cationic indium complexes (**23-26**) show catalytic activity towards the polymerization of a polar conjugated monomer, methyl methacrylate (MMA) (Fig. 1.17),⁸⁸ however, the reactivity was low in comparison to the well-known Sm and Zr systems for MMA polymerization,⁸⁹⁻⁹⁰ While these preliminary results suggest only modest reactivity for these indium cations, they show the potential of cationic indium complexes as catalysts towards polymerization of polar conjugated monomers.

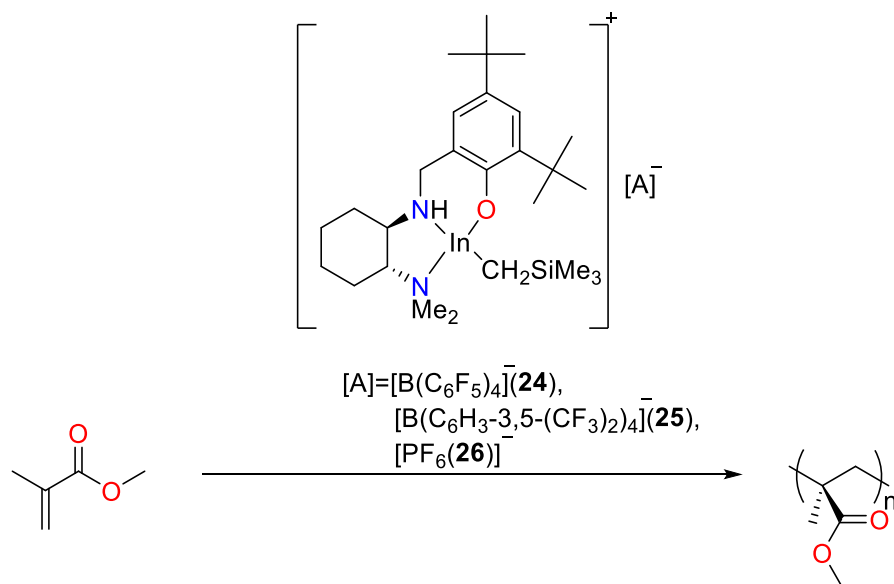


Figure 1.17. Polymerization of methyl methacrylate (MMA) by cationic indium complexes **23-26**.⁸⁸

Recent reports^{85-87,91,92} have shown the reactive nature of several cationic indium complexes towards alkene and alkyne cyclization,^{85,86} but there are rare examples of indium cations being utilized as polymerization catalysts. In the Mehrkhodavandi group, we are interested in developing cationic indium complexes and exploring their reactivity as potential polymerization catalysts for biodegradable polymers.

1.6 Project overview

With several active indium catalysts being reported by the Mehrkhodavandi group,⁵⁷⁻⁶³ development and investigation of cationic indium complexes constitutes one of the new foci in the group. With extensive knowledge of the diaminophenolate system, former post-doctoral researcher, Dr. Insun Yu, investigated cationic indium counterparts of pre-existing systems. She was able to synthesize an alkyl indium species through the reaction of a diaminophenolate ligand, 2,4-di-cumyl-6-(((2-(dimethylamino)cyclohexyl)imino)methyl) phenol (\pm)-H(NNO) (**27**) and $\text{In}(\text{CH}_2\text{SiMe}_3)_3$. Moreover, the corresponding cationic complex was generated through a protonolysis reaction with a strong Brønsted acid (Fig. 1.18). Complexes **28** and **29** were fully characterized by various NMR spectroscopic techniques and the solid state structures were determined by X-ray crystallography.⁹³

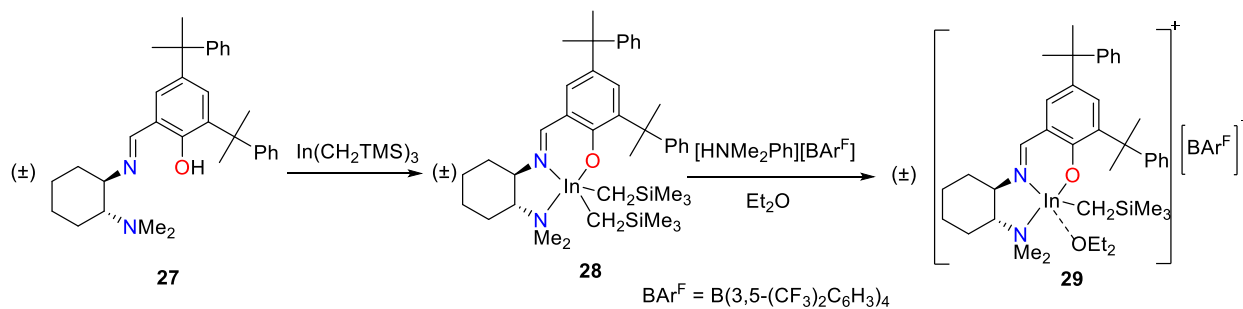


Figure 1.18. Synthesis of neutral (**28**) and cationic (**29**) indium complexes.

The aforementioned cationic complex **29** was subjected to several polymerization studies with different monomers such as ϵ -caprolactone (CL) and functional epoxides including 1,2-epoxyoctane (EOA), 1,2-epoxyoctene (EOE) and allyl glycidyl ether (AGE). Homopolymerization of ϵ -caprolactone with **29** in benzene at 70 °C showed 97% monomer conversion in 87 hours while attempts to homopolymerize epoxides with **29** under identical reaction condition yielded >99% unreactive monomers (Fig. 1.19).

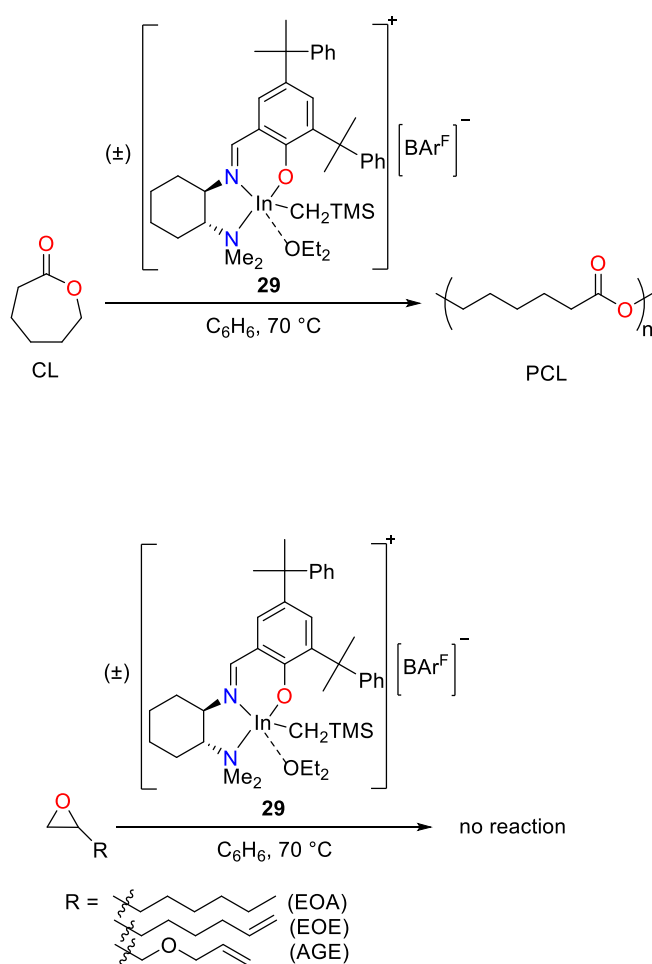


Figure 1.19. Attempts in homopolymerization of CL and epoxides by **29**.

Interestingly, attempts to copolymerize ϵ -caprolactone and epoxides showed an increase in epoxide conversion in the presence of catalyst **29**. Reaction of 500 equivalents of 1:1 mixture of CL and epoxide, in refluxing benzene for 87 hours resulted in 85-97% conversion of CL and 75-88% conversion of epoxides (Fig. 1.20). The resulting mixture contained ~20% poly(caprolactone) (PCL) and the product could be obtained in 60% isolated yield after separation of the PCL. With initial characterization by different NMR techniques and MALDI-TOF mass spectrometry, these isolated products were tentatively assigned as alternating oligomers.

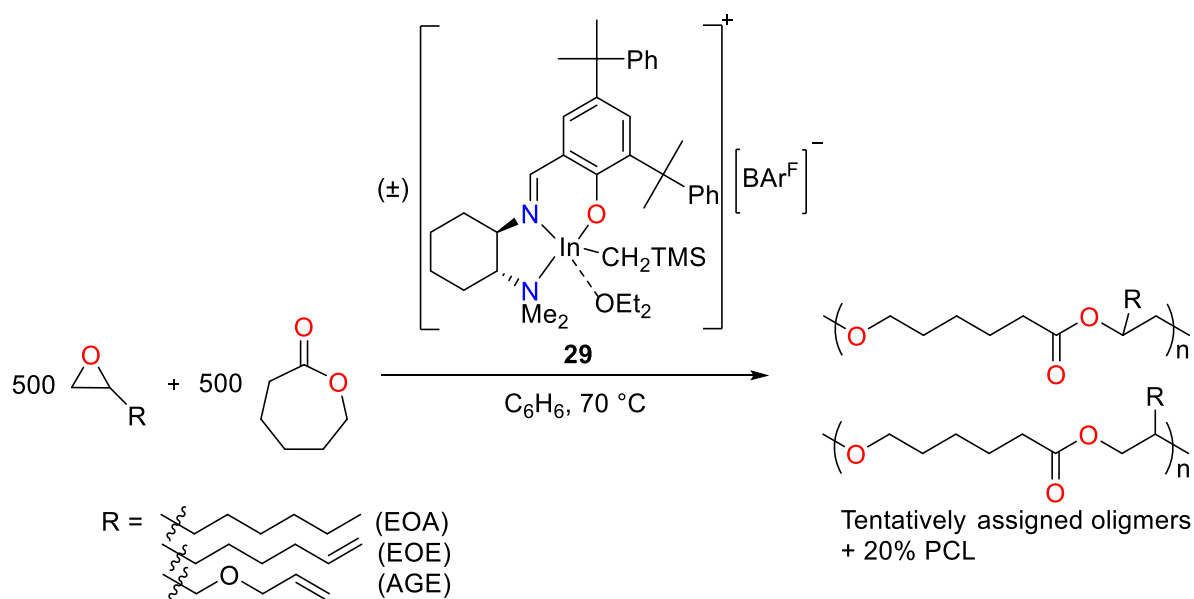


Figure 1.20. Attempts in copolymerization of CL and epoxide by **29**.

While these preliminary results demonstrated interesting catalytic reactivity of the cationic indium system, further investigation of the nature of these products was essential to understand this transformation as well as to identify the product. After I took over the project, I reproduced

experiments from synthesis of ligands and catalysts to reaction investigations. I developed a more facile synthesis of a new THF coordinated cationic indium complex (**30**). Homopolymerization studies of different lactones and epoxides were conducted to further explore the reactivity of the cationic indium complexes. I was able to characterize the isolated product from these reactions and confirm their identities as discrete spiro-orthoester (SOE1) and not oligomers.¹⁰⁶ Modifications and optimizations of procedures reported by Dr. Yu led to improved reaction efficiencies where quantitative conversions of both substrates could be achieved in less than 24 hours. I was able to synthesize and isolate spiro-orthoesters with different lactone units under analogous reaction conditions. Preliminary investigations of spiro-orthoesters polymerization were also conducted.

Chapter 2: Indium complexes synthesis and reactivity studies

As discussed in Chapter 1, the Mehrkhodavandi group is interested in developing cationic indium complexes and investigating their reactivities as polymerization catalysts. While synthesis and characterizations of the neutral alkyl indium complex **27** and its cationic counterpart bearing a coordinated ether (**29**) were reported by former post-doctoral researcher, Dr. Yu (Fig. 1.18), their reactivity have not been investigated intensively. Herein, I repeated the synthesis of complex **27** and described the synthesis and characterization of a new THF coordinated cationic indium complex **30** through the modification of the previous synthetic procedure for complex **29**.

2.1 Synthesis and characterization of chiral proligand **27**

The chiral proligand was synthesized according to procedures modified and optimized by the Mehrkhodavandi group (Fig. 2.1).⁵⁷⁻⁶² Commercially available (\pm)-*trans*-1,2-diaminocyclohexane was protected with one equivalent of hydrochloric acid prior to asymmetric protection of one amine by a *tert*-butoxycarbonyl (Boc) protecting group.⁹⁴ Upon basic work-up, the primary amine was methylated twice via reductive aminations with HCHO and sodium cyanoborohydride. Deprotection with HCl afforded the desired *trans*-*N,N*-dimethylcyclohexyl-1,2-diamine intermediate. Condensation reactions between amine intermediate and 2,4-cumyl di-substituted salicylaldehyde in MeOH formed imine proligand H(NNO) (**27**), respectively. Upon recrystallization in petroleum ether, the desired yellow solid product was isolated in more than 74% purified yield.

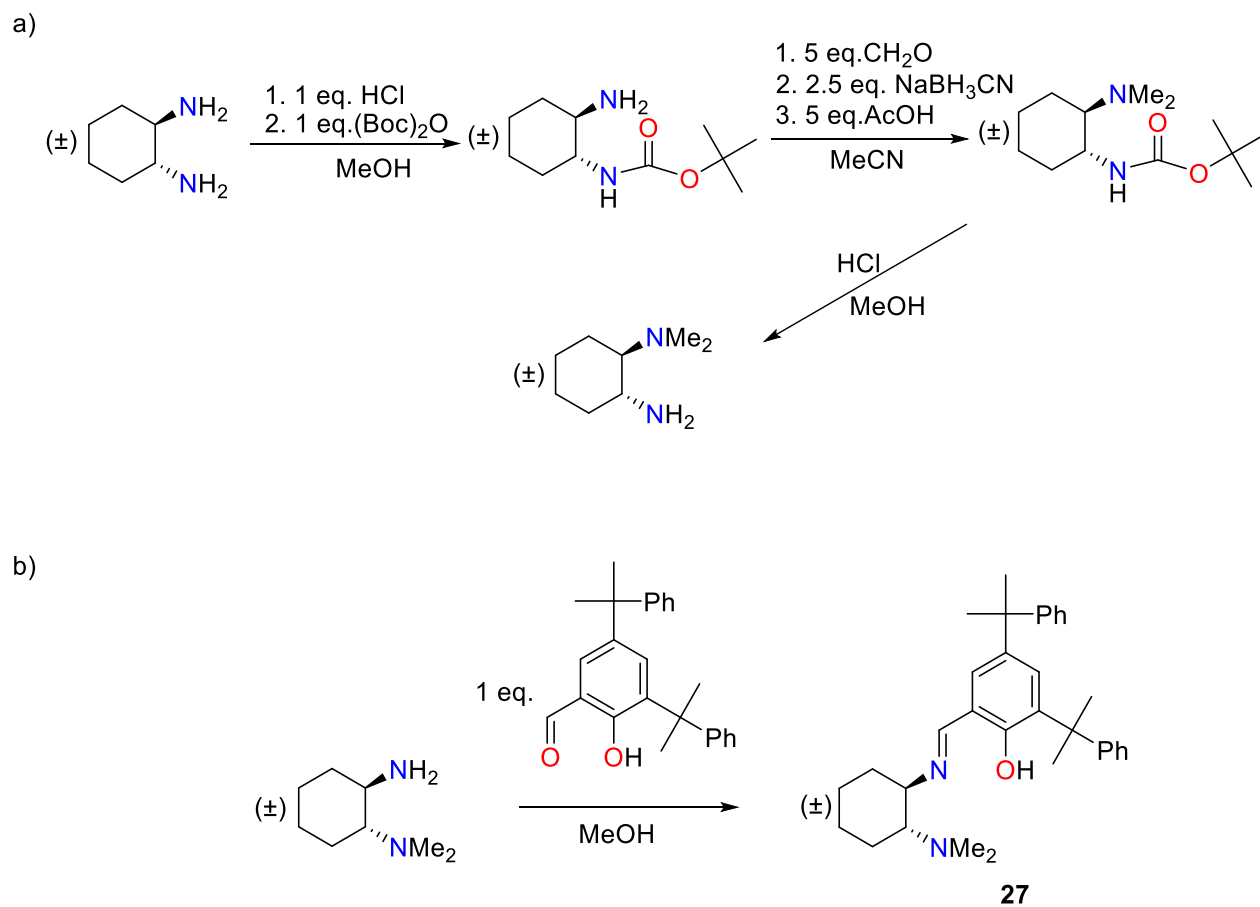


Figure 2.1. Synthesis of proligand H(NNO) (**27**).⁶⁵ a) Synthesis of *trans*-*N,N*-dimethylcyclohexane-1,2-diamine. b) Condensation reaction to form H(NNO).

2.2 Synthesis and characterization of neutral indium alkyl complex **28**

The neutral indium alkyl complex **28** was synthesized according to procedures determined by Dr. Yu (Fig. 1.18).⁸⁸ $\text{In}(\text{CH}_2\text{SiMe}_3)_3$ was prepared according to a known literature procedure.⁹⁵ The reaction of (\pm)-**27** with one equivalent of $\text{In}(\text{CH}_2\text{SiMe}_3)_3$ in Et_2O at 25 °C formed the corresponding dialkyl complex $(\text{NNO})\text{In}(\text{CH}_2\text{SiMe}_3)_2$ (**28**). Upon removal of Et_2O *in vacuo*, the product was obtained as bright yellow solid in 78% purified yield through recrystallization in acetonitrile (Fig. 2.2).

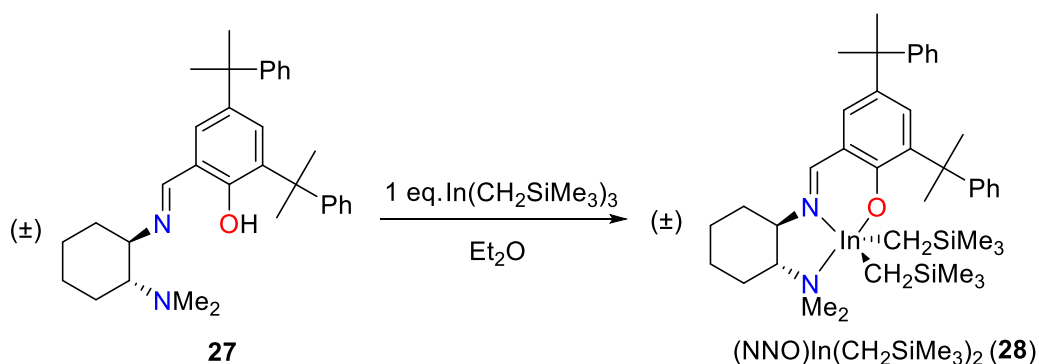


Figure 2.2. Synthesis of complex **28**.

The solid state structure of **28**, determined by Dr. Yu via single crystal X-ray crystallography, features a distorted square pyramidal indium center ($\tau = 0.36$) with a κ^3 -bound ancillary ligand. The ^1H and $^{13}\text{C}\{^1\text{H}\}$ NMR spectra of **28** are in agreement with the solid state structure (Fig. 2.3).

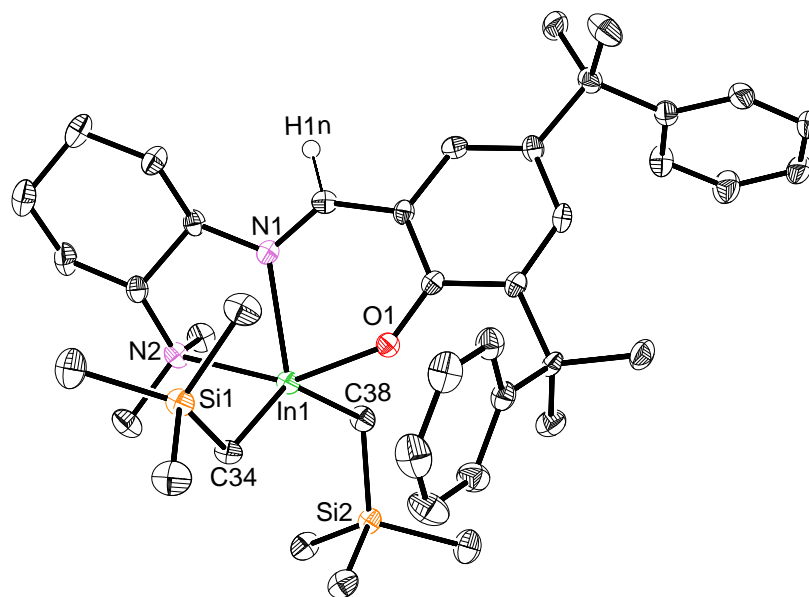


Figure 2.3. Molecular structure of **28** (depicted with ellipsoids at 50% probability and most hydrogen atoms omitted for clarity). Selected bond lengths (Å): In1-C34 2.176(4), In1-C38 2.195(4), In1-O1 2.187(3), In1-N1 2.260(3), In1-N2 2.510(4). Selected bond angles (°): O1-In1-C34 94.80(13), O1-In1-C38 93.72(13), O1-In1-N1 81.02(11), O1-In1-N2 152.14(10), N1-In1-N2 71.20(11), N1-In1-C34 117.56(13), N2-In1-C34 99.69(13), N1-In1-C38 111.67(13), N2-In1-C38 94.61(14), C34-In1-C38 130.76(14).

2.3 Synthesis and characterization of cationic indium alkyl complex **30**

The cationic alkyl indium complex [(NNO)In(CH₂SiMe₃)(THF)][BAr^F] (**30**) was synthesized through modification of procedures determined by Dr. Yu (Fig. 1.18). Instead of using diethyl ether as solvent, the reaction of complex **28** and one equivalent of [HNMe₂Ph][BAr^F] (BAr^F = B(3,5-(CF₃)₂C₆H₃)₄) was carried out in THF at room temperature to form the corresponding complex **30** along with byproducts NMe₂Ph and SiMe₄ (Fig. 2.4). Upon removal of THF *in vacuo*,

the yellow residue was washed repetitively with hexane to remove byproduct NMe₂Ph. The desired product was precipitated in hexane to form yellow powder and the supernatant was decanted. The solid was dried under vacuum to remove hexane residue prior to analysis.

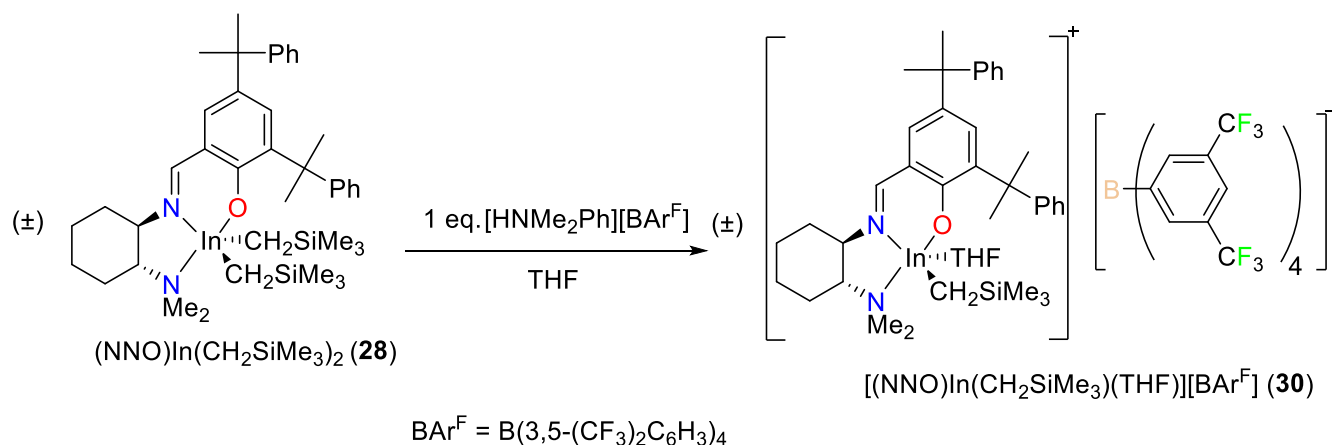


Figure 2.4. Synthesis of complex **30**.

Complex **30** was shown to have one coordinated THF molecule by ¹H-NMR spectroscopy, ¹³C{¹H}-NMR spectroscopy, ¹H-¹H-COSY NMR spectroscopy, ¹³C-¹H HSQC NMR spectroscopy, and ¹³C-¹H HMBC NMR spectroscopy. For example, ¹H NMR signal at 8.37 ppm was assigned to the imine –CH=N– proton from on the chiral ligand backbone based on previous assignment of the ligand. Correlations between –CH=N– proton to ¹³C signal at 167.5 ppm, 131.6 ppm, 117.2 ppm, and 61.2 ppm, were observed on HMBC, where the first three carbon were assigned to carbons on the phenol ring and the last one was assigned to diaminocyclohexane –CH– (Fig. 2.5).

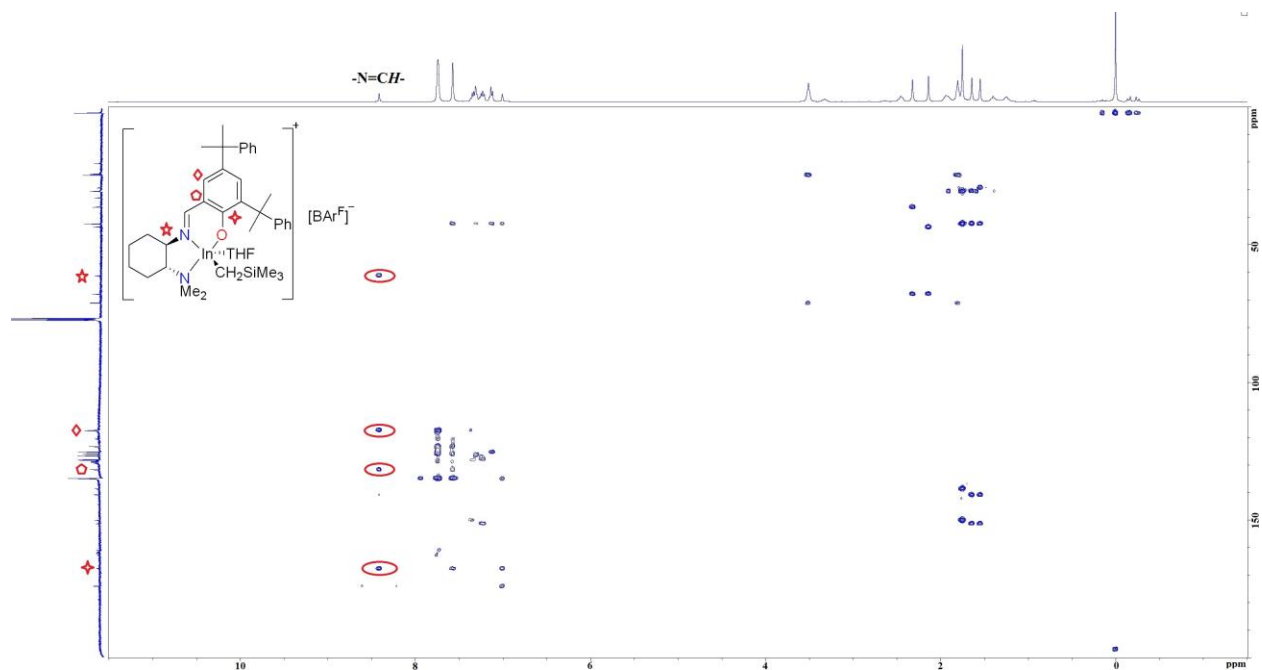


Figure 2.5. 2D ^{13}C - ^1H Heteronuclear Multiple Bond Correlation (HMBC) NMR spectrum (CDCl_3 , 25 $^\circ\text{C}$) of $(\pm)[(\text{NNO})\text{In}(\text{CH}_2\text{SiMe}_3)(\text{THF})][\text{BAR}^{\text{F}}]$ (**30**).

^1H -NMR signals at 3.49 ppm and 1.78 ppm were assigned to a molecule of tetrahydrofuran in the absence of correlations between these protons with the rest of the signals on ^1H - ^1H COSY NMR spectroscopy (Fig. 2.6). As these protons at 3.49 ppm and 1.78 ppm are shifted compared to free THF molecules (3.76 ppm and 2.36 ppm, respectively) and attempts to remove the THF molecule under vacuum were unsuccessful, the THF molecule is likely coordinated to the cationic indium metal center.

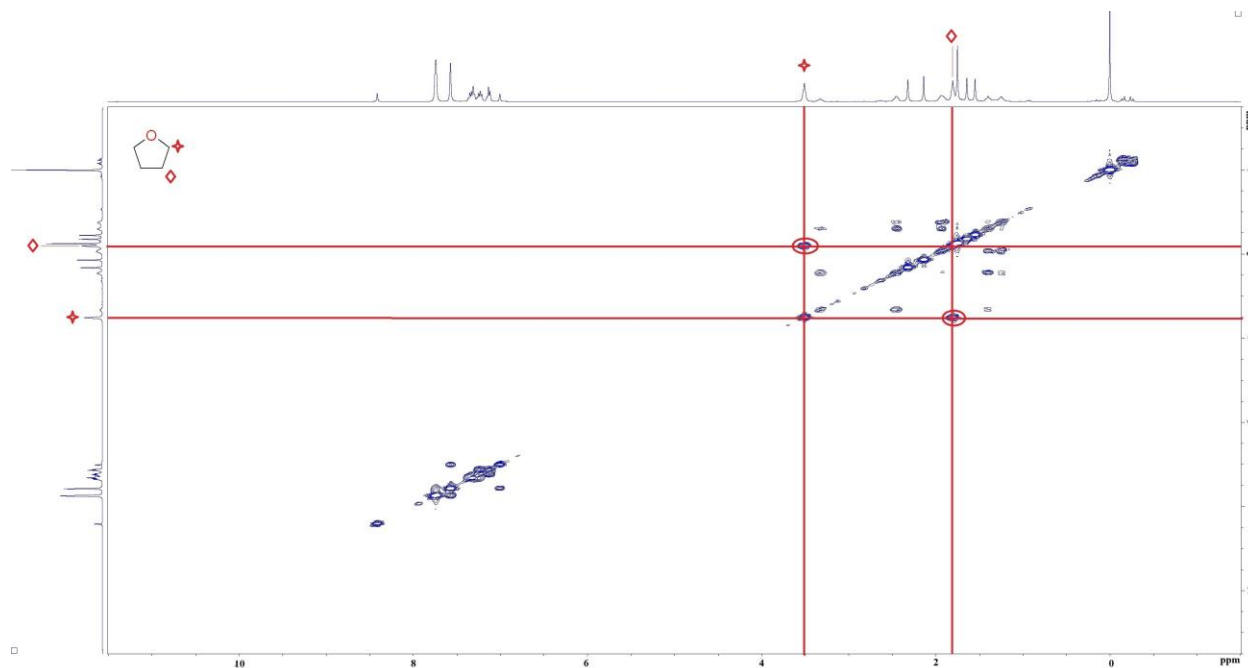


Figure 2.6. 2D ^1H - ^1H COSY NMR spectrum (CDCl_3 , 25 $^\circ\text{C}$) of (\pm) - $[(\text{NNO})\text{In}(\text{CH}_2\text{SiMe}_3)(\text{THF})][\text{BAR}^{\text{F}}]$ (**30**).

The ^1H NMR spectrum of **30** shows an AB doublet centered at -0.25 ppm corresponding to one $\text{In}-\text{CH}_2\text{SiMe}_3$ ligand which is shifted downfield compared to the corresponding protons of complex **28**. The rest of the ^1H -NMR signals and ^{13}C -NMR signals were assigned through ^1H - ^1H COSY NMR data to identify proton-proton interactions, ^{13}C - ^1H HSQC NMR data to identify one bond CH coupling, and ^{13}C - ^1H HMBC NMR data to identify long range CH couplings.

First attempts to obtain single crystals from a mixture of THF and hexane yielded contaminated single crystals due to adventitious water (Fig. 2.2.4). The solid state structure of **30**• H_2O illustrates a distorted square pyramidal indium center ($\tau = 0.20$), which is similar to its neutral counterparts **28**. However, the In-C bond distance is shorter (2.144 \AA) in comparison to the neutral system (2.176 \AA and 2.195 \AA).

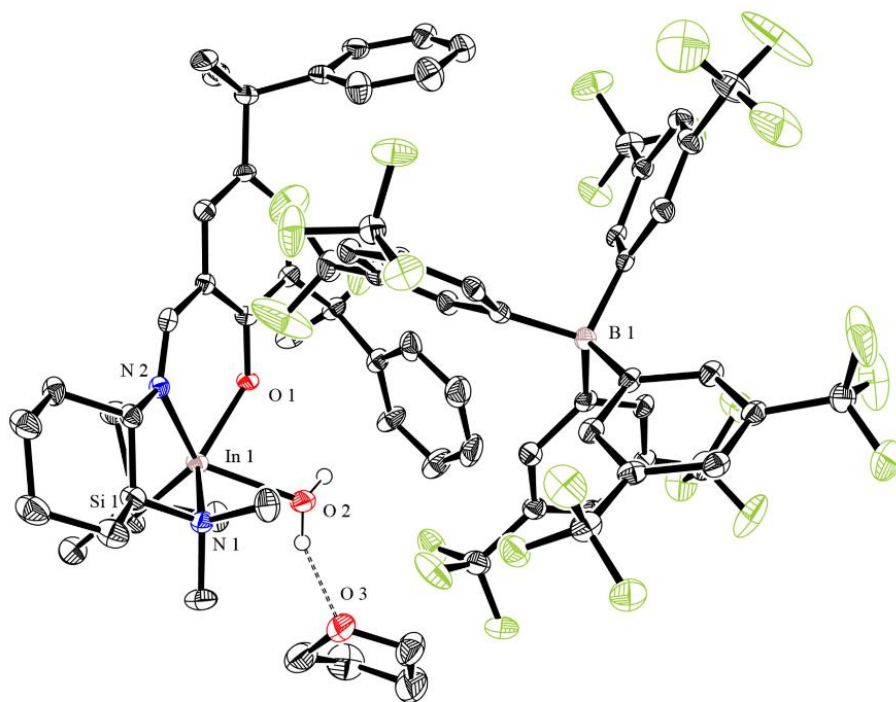


Figure 2.7. *SS*-Enantiomeric molecular structure of **30**·H₂O (depicted with ellipsoids at 50% probability, *RR*-**30**·H₂O, and most hydrogen atoms omitted for clarity). Selected bond lengths (Å): In1-O1 2.094(2), In1-O2 2.229(3), In1-N2 2.201(3), In1-N1 2.334(3), In1-C4 2.144(4). Selected bond angles (°): O1-In1-O2 77.36(10), O1-In1-N2 84.81(10), O1-In1-N1 134.87(10), O1-In1-C4 118.72(13), O2-In1-N1 83.72(11), N2-In1-O2 127.08(11), N2-In1-N1 74.67(11), C4-In1-O2 109.25(14), C4-In1-N2 122.93(14), C4-In1-N1 106.12(13).

The serendipitous water molecule also gives some insight into the reactivity of the cationic complex. The water molecule is coordinated to the cationic indium center while the THF molecule was shown to hydrogen bond to the proton on the water molecule. Interestingly, the distance between the oxygen of the water molecule and the metal center is longer (2.229 Å) than previously reported neutral indium aquo complexes (2.121 Å~ 2.162 Å)⁹⁶⁻¹⁰¹ as well as indium hydroxide complexes (2.016 Å ~2.214 Å).^{54,57,60,102} This result was unexpected as water molecules should in

theory, coordinate stronger to the cationic metal center than their neutral counterparts due to the positive charge. Moreover, the metal alkyl group was found to remain unreactive in the presence of trace water, which demonstrated the robustness of the cationic indium system.

In order to avoid water contamination, crystallization solvents were rigorously dried in the presence of sodium benzophenone over a week prior to usage. A single crystal of X-ray quality of **30** was obtained in the mixture of dried THF and hexane. The solid state structure of **30** also features a distorted square pyramidal indium center ($\tau = 0.12$). The indium alkyl distance in **30** was found to be shorter (2.119 Å) than those in **28** (2.176 Å and 2.195 Å), **29** (2.116 Å and 2.135 Å) and **30**•H₂O (2.144 Å). This value is also shorter than values observed in the solid structures of reported alkyl indium cations (2.128-2.136 Å).⁷⁹⁻⁸² The solid state structure of **30** was found to be in agreement with the solution structure based on NMR spectroscopy (Fig. 2.8).

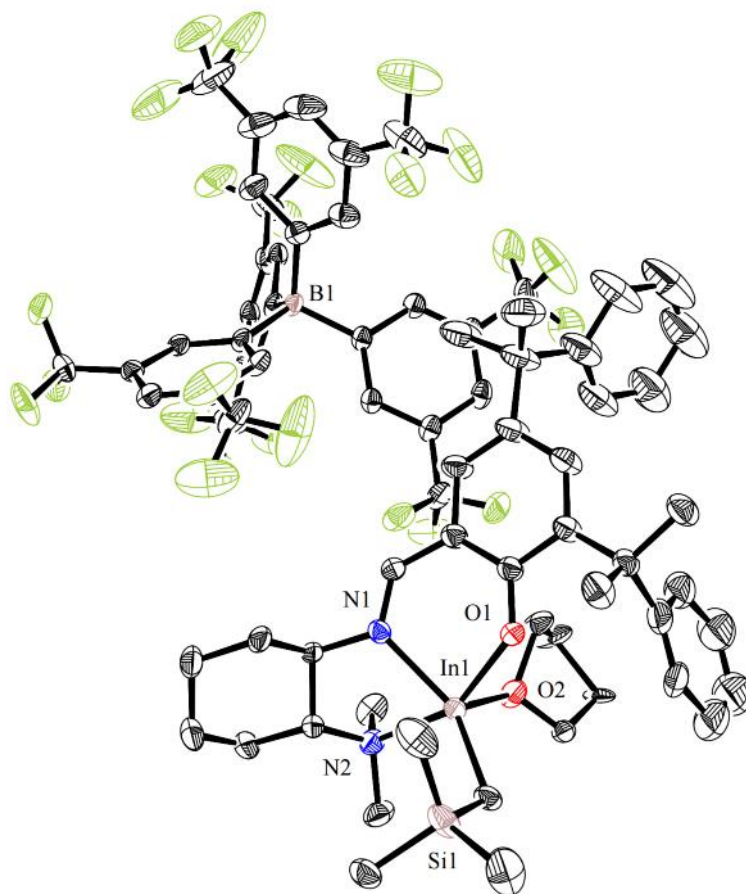


Figure 2.8. *RR*-Enantiomeric molecular structure of **30** (depicted with ellipsoids at 50% probability, *SS*-**30**, and most hydrogen atoms omitted for clarity). Selected bond lengths (Å): In1-O1 2.108(3), In1-O2 2.218(3), In1-N1 2.168(4), In1-N2 2.413(4), In1-C28 2.119(4). Selected bond angles (°): O1-In1-O2 89.25(14), O1-In1-N1 83.22(13), O1-In1-N2 151.61(13), O1-In1-C28 101.64(15), O2-In1-N2 83.15(14), N1-In1-O2 105.93(13), 1-In1-N2 72.78(13), C28-In1-O2 109.60(16), C28-In1-N1 144.15(16), C28-In1-N2 106.68(16).

The In-O bond between the metal center and the coordinated THF molecule is shorter (2.218 Å) compared to that of the ether adduct **29** (2.263 Å) and the water adduct **30** (2.229 Å), which suggests a stronger coordination of the THF molecule to the cationic indium. In comparison to the previous reported cationic alkyl indium complex with coordinated THF molecules,⁸⁰ the In-O distance is also much shorter (2.425 Å for **15**). This result showcases the effect of ligand designs that tunes the electronics of the cationic indium center; where ligand substitution of trimethylsilylmethylene groups to a tridentate NNO ligand alters the metal substrate interactions dramatically. This also suggests possible ligand design to further enhance the reactivity of the cationic indium complex.

2.4 Conclusion

In this chapter, the synthesis of an unusual cationic indium complex supporting a chiral tridentate ligand **30** was discussed. Protonolysis of the neutral alkyl indium complex **28** with a strong Brønsted acid leads to the corresponding complex **30** in over 75% yield. The structure of **30** was confirmed by various NMR spectroscopy techniques as well as X-ray diffraction experiments, where a single crystal of **30** was obtained through recrystallization in hexane. The indium alkyl bond length of **30** was found to be shorter than the neutral counterpart as well as other cationic indium species in the literature, which could be rationalized by the more electrophilic nature of the cationic indium center. Single crystal of **30**•H₂O was also obtained with adventitious water in the solvent. The unreactive nature of the indium alkyl bond in presence of water contaminant demonstrates the robustness of our system; which exhibits a plausible direction

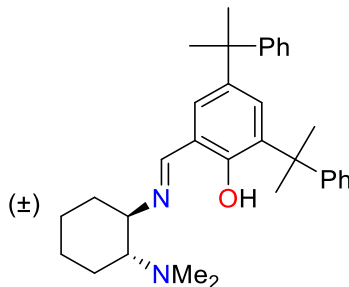
towards development of air-tolerant indium catalysts. Further investigation of other cationic indium species based on ligand design and various ligand platforms will be continued in the group.

2.5 Experimental procedures

General Considerations. Unless otherwise indicated, all air- and/or water-sensitive reactions were carried out under dry nitrogen using either an MBraun glove box or standard Schlenk line techniques. NMR spectra were recorded on a Bruker Avance 300 MHz, 400 MHz and 600 MHz spectrometer. ^1H NMR chemical shifts are reported in ppm versus residual protons in deuterated solvents as follows: δ 7.27 CDCl_3 and δ 7.16 C_6D_6 , $^{13}\text{C}\{^1\text{H}\}$ NMR chemical shifts are reported in ppm versus residual ^{13}C in the solvent: δ 77.2 CDCl_3 and δ 128.39 C_6D_6 . $^{19}\text{F}\{^1\text{H}\}$ NMR chemical shifts are reported in ppm and externally referenced to neat CFCl_3 at 0 ppm. Diffraction measurements for X-ray crystallography were made on a Bruker X8 APEX II diffraction and a Bruker APEX DUO diffraction with graphite monochromated Mo- $K\alpha$ radiation. The structures were solved by direct methods and refined by full-matrix least-squares using the SHELXTL crystallographic software of Bruker-AXS. Unless specified, all non-hydrogens were refined with anisotropic displacement parameters, and all hydrogen atoms were constrained to geometrically calculated positions but were not refined. EA CHN analysis was performed using a Carlo Erba EA1108 elemental analyzer. The elemental composition of unknown samples was determined by using a calibration factor. The calibration factor was determined by analyzing a suitable certified organic standard (OAS) of a known elemental composition.

Materials. Hexane was collected from a Solvent Purification System from Innovative Technology, Inc. whose columns are packed with activated alumina. Et₂O, THF were distilled from Na/benzophenone ketyl and degassed through a series of freeze-pump-thaw cycles. CDCl₃ and C₆D₆ were dried over CaH₂ and Na/benzophenone ketyl, respectively, collected by vacuum distillation and degassed through a series of freeze-pump-thaw cycles. Dimethylanilinium tetrakis[3,5-bis(trifluoromethyl)phenyl]borate ([HNMe₂Ph][BAr^F]) was generated by reacting dimethylanilinium chloride with NaBAr^F in Et₂O at room temperature for 4 h. The salt was filtered through a fine frit by vacuum filtration. The collected solvent was removed under high vacuum, and addition of hexane to the residue precipitates a white solid. The white solid was washed with hexane several times before drying under high vacuum for 4 h. (Trimethylsilyl)methylmagnesium chloride (1.0 M in Et₂O), dimethylanilinium chloride ([HNMe₂Ph]Cl) and sodium tetrakis[3,5-bis(trifluoromethyl)phenyl]borate (Na[BAr^F]), were purchased from Aldrich and/or Alfa Aesar and used as received. *trans*-*N,N*-dimethylcyclohexyl-1,2-diamine and In(CH₂SiMe₃)₃ were synthesized according to previously reported procedures

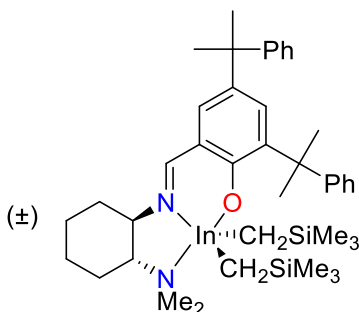
Synthesis of H(NNO) (27).



A Schlenk flask was charged with 3,5-dicumylsalicylaldehyde (1.7 g, 4.8 mmol) and methanol (10 mL) was added to the flask via cannula under a nitrogen atmosphere. A catalytic amount of 85% formic acid, followed by (±)-*trans*-*N,N*-dimethyl-1,2-cyclohexanediamine (1.2 g, 8.2 mmol), were added to the reaction mixture. The reaction mixture was stirred at r.t. The methanol was removed under vacuum, the residue was re-dissolved in petroleum ether (15 mL) and the resulting product recrystallized through slow evaporation overnight at room temperature. The product was collected as a yellow solid by filtration, washed with cold petroleum ether (3 × 5 mL), and dried under vacuum for 4 hours. (1.7 g, 74%). ¹H NMR (300 MHz, CDCl₃) δ 13.56 (1H, br. s., Ar-OH), δ 8.21 (1H, s, -N=CH-Ar), δ 7.34 - δ 7.10 (11H, m, ArH), δ 7.01 (1H, s, ArH), δ 3.12 (1H, dt, 3J_{H-H} = 4.3, 10.2 Hz, -CH- of DACH), δ 2.64 - δ 2.36 (1H, m, -CH- of DACH), δ 2.20 (6H, s, -N(CH₃)₂), δ 1.89 - δ 1.63 (17H, m, -CH₂- of DACH and -CH₃ of cumyl), δ 1.63 - δ 1.39 (2H, m, -CH₂- of DACH), δ 1.37 - δ 1.03 (3H, m, -CH₂- of DACH). ¹³C{¹H} NMR (101 MHz, CDCl₃) δ 163.6 (N=CH-Ar), δ 158.1 (Ar C), δ 150.9 (Ar C), δ 150.7 (Ar C), δ 139.0 (Ar C), δ 135.8 (Ar C), δ 128.7 (Ar C-H), δ 128.0 (Ar C-H), δ 127.7 (Ar C-H), δ 127.6 (Ar C-H), δ 126.8 (Ar C-H), δ 125.6 (Ar C-H), δ 125.5 (Ar C-H), δ 124.9 (Ar C-H), δ 118.2 (Ar C), δ 69.8 (C-H of DACH), δ 66.5 (C-H of DACH), δ 42.4 (Ar-C- of cumyl), δ 42.2 (Ar-C- of

cumyl), δ 40.7 (-N(CH₃)₂), δ 34.9 (-CH₂- of DACH), δ 31.0 (-CH₃ of cumyl), δ 30.9 (-CH₃ of cumyl), δ 29.8 (-CH₃ of cumyl), δ 29.1 (-CH₃ of cumyl), δ 25.2 (-CH₂- of DACH), δ 24.6 (-CH₂- of DACH), δ 24.0 (-CH₂- of DACH). Anal. Calcd. For C₃₃H₄₂N₂O: C 83.11; H 8.77; N 5.80. Found: C 83.91; H 8.96; N 5.64.

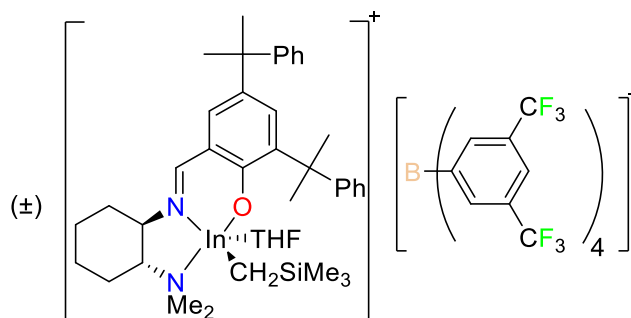
Synthesis of (NNO)In(CH₂SiMe₃)₂ (28).



A 20 mL scintillation vial was charged with proligand H(NNO) (**27**) (185 mg, 0.384 mmol) in Et₂O (10 mL). ((Trimethylsilyl)methyl)indium In(CH₂SiMe₃)₃ (155 mg, 0.385 mmol) was added to the stirring mixture dropwise. The reaction mixture was stirred for 4 h at room temperature. The solvent was removed to dryness *in vacuo*. Acetonitrile (ca. 5 mL) was added to the residue to precipitate a yellow solid, and the solution was filtered through a fine frit to collect the yellow solid. The collected solid was washed with acetonitrile (3 × 3 mL) and dried under high vacuum for 4 hours. (232 mg, 78%). ¹H NMR (300 MHz, CDCl₃) δ 8.07 (1H, s, -N=CH-Ar), δ 7.29 - δ 7.22 (4H, m, ArH of cumyl), δ 7.21 - δ 7.11 (5H, m, ArH of cumyl), δ 7.07 - δ 7.00 (m, 2H, m, ArH of cumyl and ArH), δ 6.73 (1H, d, 4J_{H-H} = 2.6 Hz, ArH), δ 3.02 (1H, dt, 3J_{H-H} = 4.0, 10.8 Hz, -CH- of DACH), δ 2.70 (1H, dt, 3J_{H-H} = 2.7, 11.0 Hz, -CH- of DACH), δ 2.15 (6H, s, -N(CH₃)₂), δ 2.04 - δ 1.94 (1H, m, -CH₂- of DACH), δ 1.94 - δ 1.76 (3H, m, -CH₂- of DACH), δ

1.72 (3H, s, -CH₃ of cumyl), δ 1.61 (6H, s, -CH₃ of cumyl), δ 1.54 (3H, s, -CH₃ of cumyl), δ 1.51 - δ 1.39 (1H, m, -CH₂- of DACH), δ 1.39 - δ 1.09 (3H, m, -CH₂- of DACH), δ -0.09 (9H, s, -Si(CH₃)₃), δ -0.12 (9H, s, -Si(CH₃)₃), δ -0.63 (2H, d, $2J_{H-H}$ = 9.9 Hz, 2H, In-CH₂-Si(CH₃)₃), δ -0.82 (2H, d, $2J_{H-H}$ = 6.3 Hz, In-CH₂-Si(CH₃)₃). ¹³C{¹H} NMR (101 MHz, CDCl₃) δ 172.8 (N=CH-Ar), δ 169.7 (Ar C), δ 151.7 (Ar C), δ 151.5 (Ar C), δ 141.3 (Ar C), δ 133.2 (Ar C), δ 133.1 (Ar C), δ 131.3 (Ar C-H), δ 128.0 (Ar C-H), δ 127.7 (Ar C-H), δ 127.1 (Ar C-H), δ 126.3 (Ar C-H), δ 125.5 (Ar C-H), δ 124.8 (Ar C-H), δ 118.1 (Ar C), δ 66.4 (C-H of DACH), δ 65.6 (C-H of DACH), δ 42.8 (Ar-C- of cumyl), δ 42.2 (Ar-C- of cumyl), δ 39.9 (-N(CH₃)₂), δ 36.5 (-N(CH₃)₂), δ 31.2 (-CH₂- of DACH), δ 31.0 (-CH₃ of cumyl), δ 30.9 (-CH₂- of DACH), δ 28.2 (-CH₂- of DACH), δ 25.6 (-CH₂- of DACH), δ 25.1 (-CH₃ of cumyl), δ 21.1 (-CH₃ of cumyl), δ 3.1 (-Si(CH₃)₃), δ 2.9 (-Si(CH₃)₃), δ -0.56 (In-CH₂-), δ -2.2 (In-CH₂-). Anal. Calcd. For C₄₁H₆₃InN₂OSi₂: C 63.88; H 8.24; N 3.63. Found: C 64.17; H 8.07; N 3.61.

Synthesis of [(NNO)In(CH₂SiMe₃)(THF)][BAR^F] (30).



A 20 mL scintillation vial was charged with (NNO)In(CH₂SiMe₃)₂ (**28**) (100 mg, 0.130 mmol) in THF (3 mL). [HNMe₂Ph][BAR^F] (128 mg, 0.130 mmol) in THF (2 mL) was added to the stirring solution of complex 1 dropwise. The reaction mixture was stirred for 4 h at room temperature. The

solvent was removed *in vacuo* to obtain a yellow residue and hexane (3 mL) was added to the residue. After stirred for 30 min, the supernatant was decanted off to remove the byproduct HNMe₂Ph. This step was repeated at least 3 times. The yellow solid was precipitated out from a mixture solution of hexane and THF. The product was washed with hexane (2 × 3 mL) and dried under high vacuum for a few hours. (156 mg, 75%). ¹H NMR (300 MHz, CDCl₃) δ 8.37 (1H, s, -N=CH-Ar), δ 7.70 (8H, br. s., ortho *H* of BAr^F), δ 7.53 (5H, m, para *H* of BAr^F and Ar*H*), δ 7.34 - 7.31 (2H, m, Ar*H* of cumyl), δ 7.29 (2H, d, Ar*H* of cumyl), δ 7.21 - δ 7.17 (3H, m, Ar*H* of cumyl), δ 7.12 - δ 7.07 (3H, m, Ar*H* of cumyl), δ 6.97 (1H, m, Ar*H*), δ 3.49 (4H, q, -CH₂- of THF), δ 3.27 (1H, m, -CH- of DACH), δ 2.41 (2H, br. m, -CH- and -CH₂- of DACH), δ 2.26 (s, 3H, s, -N(CH₃)₂), δ 2.08 (3H, s, -N(CH₃)₂), δ 1.93- δ 1.87 (3H, m, -CH₂- of DACH), δ 1.78 (4H, q, -CH₂- of THF), δ 1.71 (6H, s, -CH₃ of cumyl), δ 1.60 (3H, s, -CH₃ of cumyl), δ 1.51 (3H, s, -CH₃ of cumyl), δ 1.35 - δ 1.29 (m, 2 H, -CH₂- of DACH), δ 1.25 - δ 1.18 (m, 2 H, -CH₂- of DACH), δ -0.10 (s, 9H, s, -Si(CH₃)₃), δ -0.17 - δ -0.32 (2H, m, In-CH₂-Si(CH₃)₃); ¹³C{¹H} NMR (151 MHz, CDCl₃) δ 173.9 (N=CH-Ar), δ 167.5 (Ar C), δ 162.4 - 160.9 (B-C of BAr^F), δ 151.2 (Ar C), δ 150.0 (Ar C), δ 140.7 (Ar C), δ 138.6 (Ar C), δ 135.0 (Ar C-H), δ 134.8 (*ortho* C-H of BAr^F), δ 131.6 (Ar C-H), δ 129.1 (-CF₃ of BAr^F), δ 128.6 (Ar C-H of cumyl), δ 128.2 (Ar C-H of cumyl), δ 128.0 (Ar C), δ 126.6 (Ar C-H of cumyl), δ 126.0 (Ar C-H of cumyl), δ 125.9 (Ar C), δ 125.2 (Ar C-H of cumyl), δ 125.2 (Ar C-H of cumyl), δ 123.2 (Ar C), δ 120.5 (Ar C), δ 117.5 (*para* C-H of BAr^F), δ 117.2 (Ar C), δ 71.1 (THF O-CH₂-), δ 67.8 (-CH-N(CH₃)₂ of DACH), δ 61.2 (-CH-N= of DACH), δ 43.5 (-N(CH₃)₂), δ 42.3 (Ar-C- of cumyl), δ 42.3 (Ar-C- of cumyl), δ 36.3 (-N(CH₃)₂), δ 32.9 (-CH₂- of DACH), δ 30.6 (-CH₃ of cumyl), δ 30.5 (-CH₃ of cumyl), δ 29.3 (-CH₃ of cumyl), δ 29.3 (-CH₃ of cumyl), δ 24.7 (THF -CH₂-), δ 24.2 (-CH₂- of DACH), δ 24.2 (-CH₂- of DACH), δ 20.4 (-CH₂- of

DACH), δ 2.11 (-Si(CH₃)₃); ¹⁹F{¹H} NMR (282 MHz, CDCl₃): δ -62.3. Anal. Calc. For C₇₃H₇₄BF₂₄InN₂O₂Si: C 54.02; H 4.60; N 1.74. Found: C 54.15; H 4.48; N 1.73.

Chapter 3: Spiro-orthoester synthesis and polymerizations

As discussed in Chapter 1, the cationic alkyl indium complex $[(\text{NNO})\text{In}(\text{CH}_2\text{SiMe}_3)(\text{THF})][\text{BAR}^{\text{F}}]$ (**30**) was found to be able to catalyze the reaction of ϵ -caprolactone and epoxides to form a product that was tentatively assigned as alternating oligomers. We wanted to understand this transformation as well as identify the resulting product. In this chapter, modification and optimization of previous reported reaction conditions by Dr. Yu were investigated. Detailed characterization of the isolated product from aforementioned reaction confirmed its identity as discrete spiro-orthoester, 2-(hex-5-en-1-yl)-1,4,6-trioxaspiro[4.6]undecane (SOE1). In a similar manner, spiro-orthoesters bearing five and six member ether ring were prepared using δ -valerolactone and γ -butyrolactone as the lactone substrate. Preliminary polymerization studies of synthesized SOE1, spiro-orthoester bearing a seven membered ether ring, is also described with the cationic indium complex **30** as the catalyst.

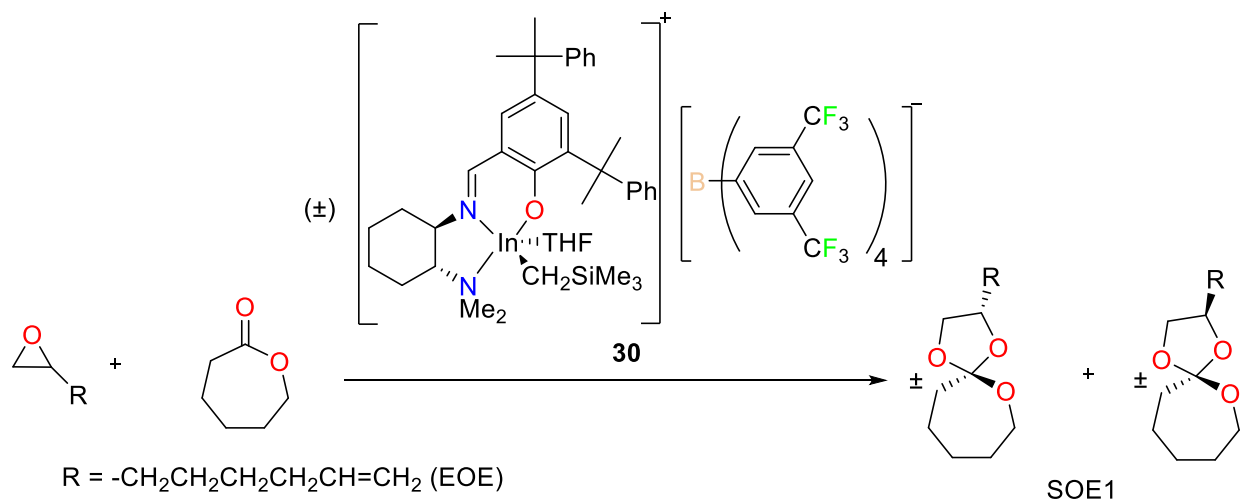


Figure 3.1 SOE1 synthesis catalyzed by **30**.

3.1 Spiro-orthoester (SOE1) synthesis and characterization

Complex **30** catalyzes the reaction of an epoxide and a lactone to form the corresponding spiro-orthoester (Fig. 3.0.1). Reaction of a 1:1 mixture of 1,2-epoxy-7-octene (EOE) and ϵ -caprolactone (CL) with 0.25% catalyst loading, at 60 °C in benzene, forms product with up to 70% conversions of both CL and EOE after 16 h (Fig. 3.2).

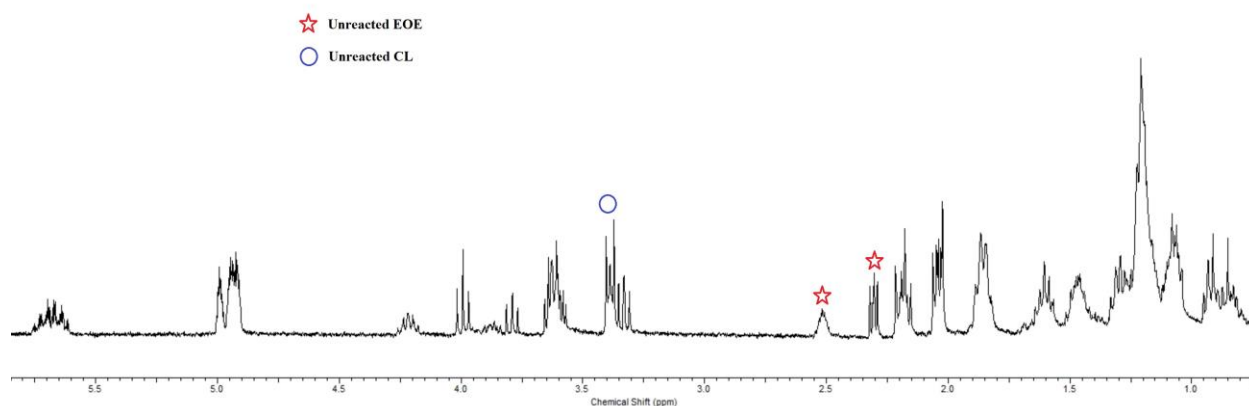


Figure 3.2. ¹H NMR spectrum (300 MHz, C₆D₆, 25 °C) of crude from reaction of EOE and CL in the presence of **30** over 16 h.

The solvent was removed under vacuum after 16 h. The residue was dissolved in a minimum amount of hexane (3 mL) to separate a solid by-product from the mixture solution. The decanted solution was filtered through a silica flash column and the collected solution was dried under vacuum to obtain the desired product as colorless oil. Further purification of the product was done by a vacuum distillation. Analysis of the distilled product by NMR spectroscopy showed the removal of trace impurities, with identical diagnostic signals before and after distillation.

Detailed analysis of the isolated product by NMR spectroscopy, GC-MS, and IR spectroscopy, confirms the structure of the major product as discrete spiro-orthoester. The specific assignment of these peaks can be determined using various NMR techniques. ^1H NMR spectrum (Fig. 3.4) and $^{13}\text{C}\{^1\text{H}\}$ NMR spectrum (Fig. 3.5) of SOE1 both show two sets of resonance signals corresponding to two diastereomers. It is understood that two pairs of enantiomers are formed from the reaction which results in four spiro-orthoesters (Fig. 3.3). For the rest of this thesis, these four different spiro-orthoesters are abbreviated as SOE1 for the ease of understanding.

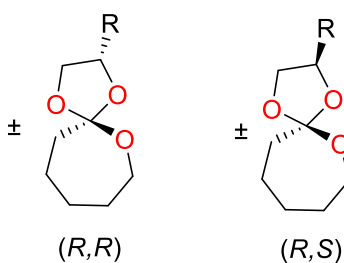


Figure 3.3. Possible structures of SOE1.

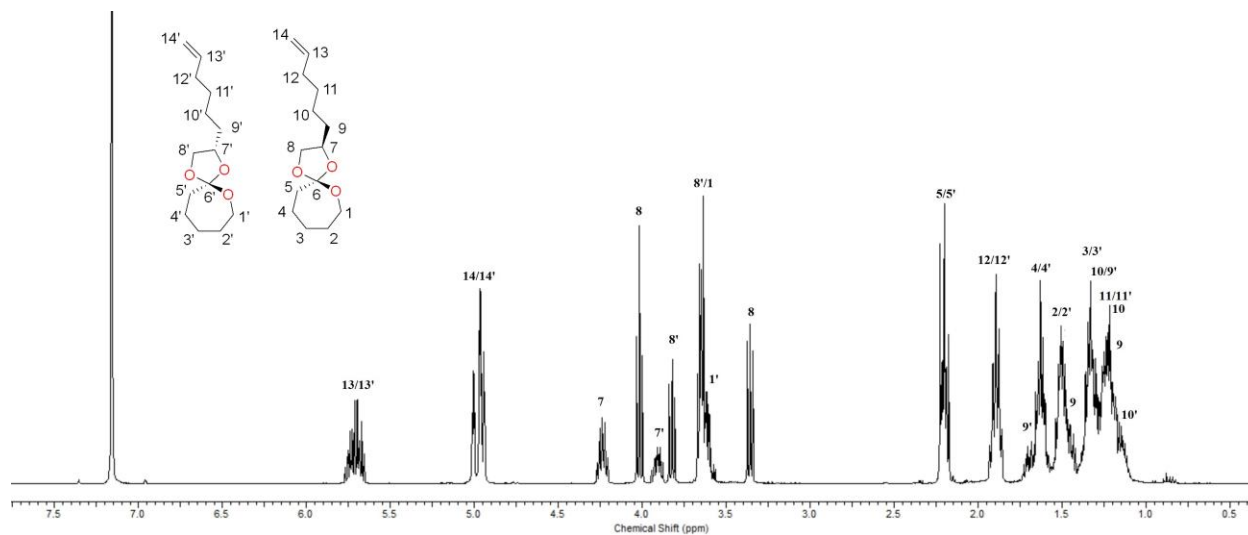


Figure 3.4. ^1H NMR spectrum (400 MHz, C_6D_6 , 25 $^\circ\text{C}$) of SOE1. Two sets of isomeric signals were observed. For example, H7 and H7' are assigned to methane protons of different diastereomers.

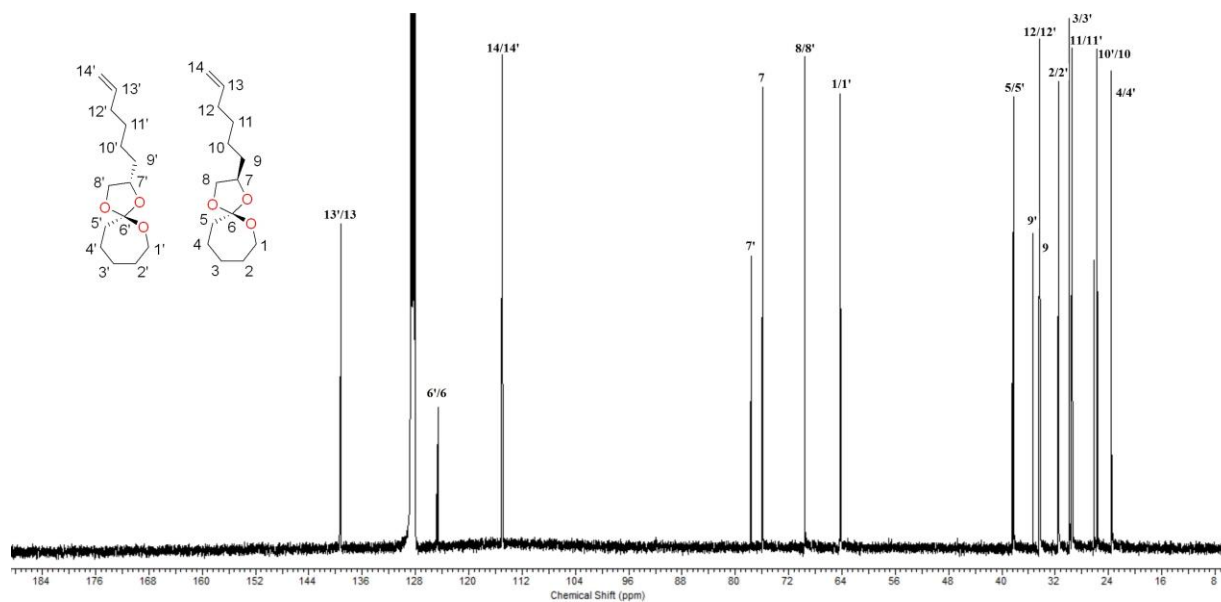


Figure 3.5. $^{13}\text{C}\{^1\text{H}\}$ NMR spectrum (151 MHz, C_6D_6 , 25 $^\circ\text{C}$) of SOE1.

Further 2-dimensional correlation NMR experiments are also consistent with the formation of two discrete diastereomers with absence of correlation between each set of signals. The resonances at 5.72 (H13/H13') and 5.00 (H14/H14') ppm are assigned to terminal alkene protons based on the starting epoxide and the assignment of carbon signals for terminal alkene are determined by ^{13}C - ^1H HSQC NMR spectroscopy to identify correlation from direct one bond CH coupling, The resonances at 124.6 (C6/C6') ppm are assigned to the spiro-orthoester carbon due to the absence of direct one bond CH coupling (Fig. 3.6).

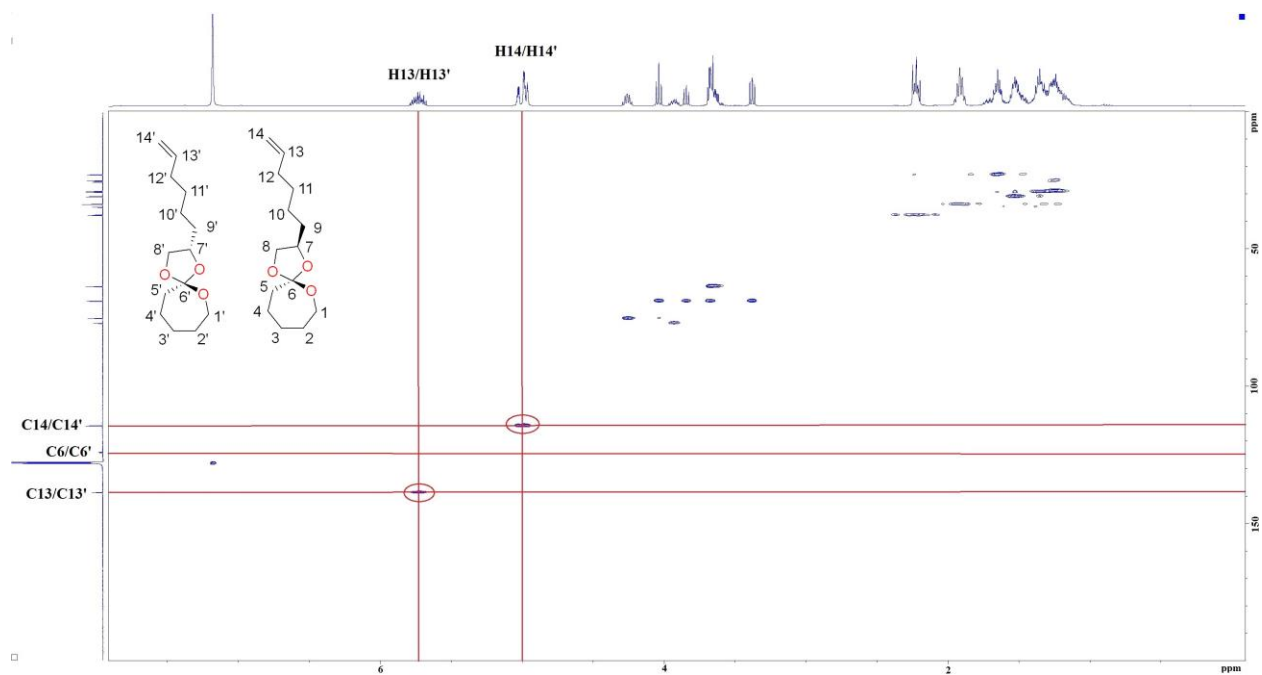


Figure 3.6. ^{13}C - ^1H Heteronuclear Single Quantum Coherence (HSQC) NMR spectrum (CDCl_3 , 25 $^\circ\text{C}$) of SOE1.

Assignments of atomic connectives are determined through series of ^1H - ^1H COSY NMR spectroscopy experiment to identify through bond interactions between different protons, and ^{13}C - ^1H HMBC NMR spectroscopy to identify correlation from long range CH couplings around terminal alkene and spiro-orthoester carbon. For example, the ^{13}C - ^1H HMBC NMR spectrum shows cross peaks between proton signals around 1.88 ppm and both C13/C13' and C14/C14', which are indicative of long range CH coupling between them (Fig. 3.7). As a consequence, these protons around 1.88 ppm are assigned to H12/H12', respectively.

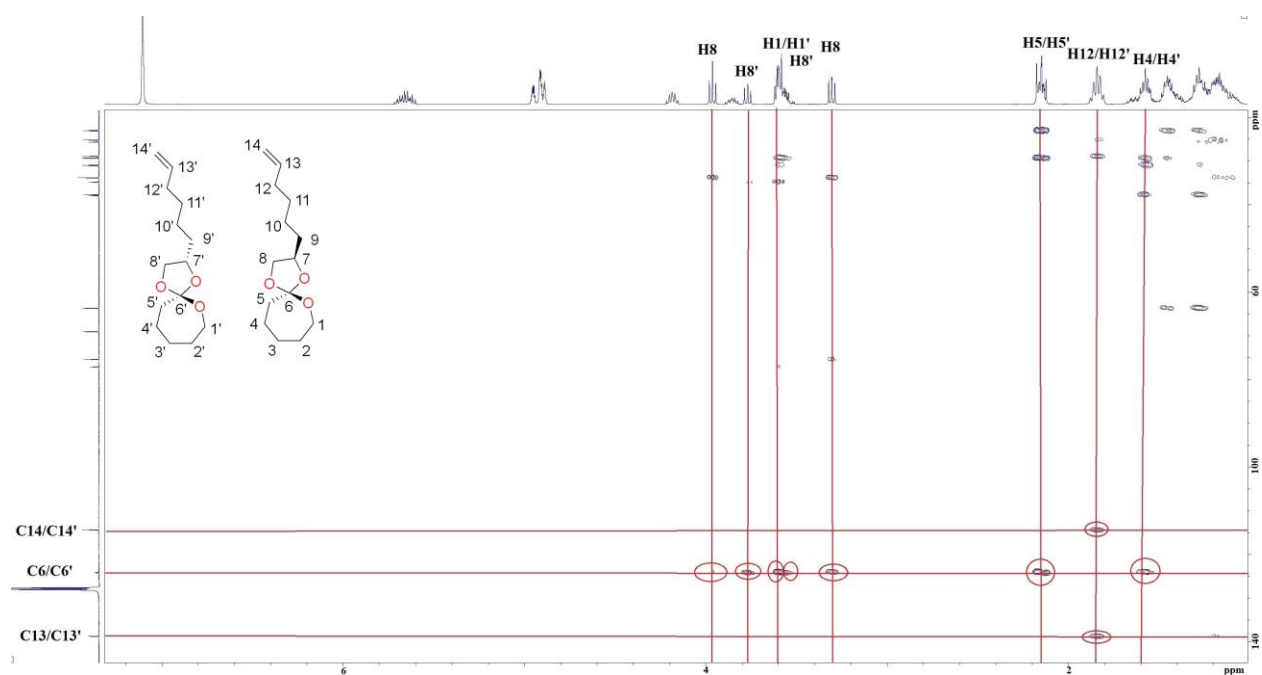


Figure 3.7. ^{13}C - ^1H Heteronuclear Multiple Bond Correlation (HMBC) NMR spectrum (CDCl_3 , 25 $^\circ\text{C}$) of SOE1.

Moreover, HMBC NMR spectra also show coupling between orthoester carbon (C6/C6') and protons around 4.02 ppm, 3.82 ppm, 3.67 ppm, 3.60 ppm, 3.36 ppm, 2.20 ppm, and 1.63 ppm, which suggests long range through bond interaction between them (Fig. 3.7). Based on ^{13}C - ^1H HSQC NMR spectroscopy, protons around 4.02 ppm, 3.82 ppm, 3.67 ppm, and 3.36 ppm are shown to interact with a pair of carbon signals at 69.6 ppm (Fig. 3.8). These protons are likely to be protons at either C1/C1' or C8/C8' positions as the electronegative oxygen would de-shield the neighboring atoms, leading to a downshift in ^1H -NMR spectrum. With very different shifts between these protons ranging from 4.02 ppm to 3.36 ppm, they were assigned to H8/H8'. The stereocenter at C7/C7' is likely to result in a more significant asymmetric interaction between the two protons compared to that influenced by C2/C2'.

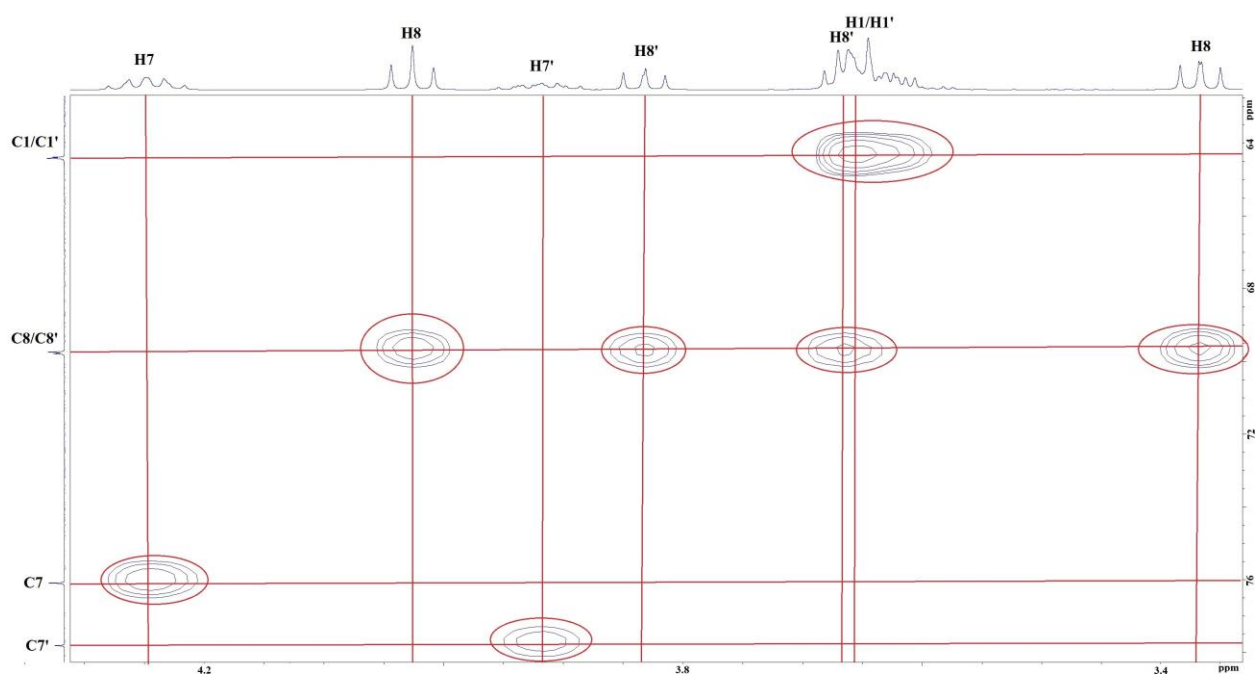


Figure 3.8. Zoomed in ^{13}C - ^1H Heteronuclear Single Quantum Coherence (HSQC) NMR spectrum (CDCl_3 , 25 $^\circ\text{C}$) of SOE1.

An overlapped signal was observed around proton H8' at 3.66 ppm, which also shows long range C-H through bond interaction with orthoester carbon (C6/C6') on HMBC. However, this signal correlates to a different carbon at 64.3 ppm than that of H8/H8' on (Fig. 3.8). Based on the downfield nature of these protons as well as previous assignment of H8/H8', it is logical to assign these protons at 3.66 ppm as H1/H1' and the carbon at 64.3 as C1/C1'. Protons around 2.2 ppm and 1.6 ppm were assigned to H5/H5' and H4/H4' based on the long range C-H correlation between these protons and orthoester carbon (C6/C6'), respectively (Fig. 3.7). The remaining assignments were determined based on previous assignments through a combination of NMR techniques including ^1H - ^1H COSY, ^{13}C - ^1H HSQC, and ^{13}C - ^1H HMBC.

GC-MS analysis of SOE1 shows two signals closely distributed on the chromatogram, which is indicative of two diastereomers of SOE1. Electron ionization mass spectra of these two signals show identical signals with a parent mass of 240.1 m/z, which is consistent with the calculated mass of the expected spiro-orthoester (Fig. 3.9).

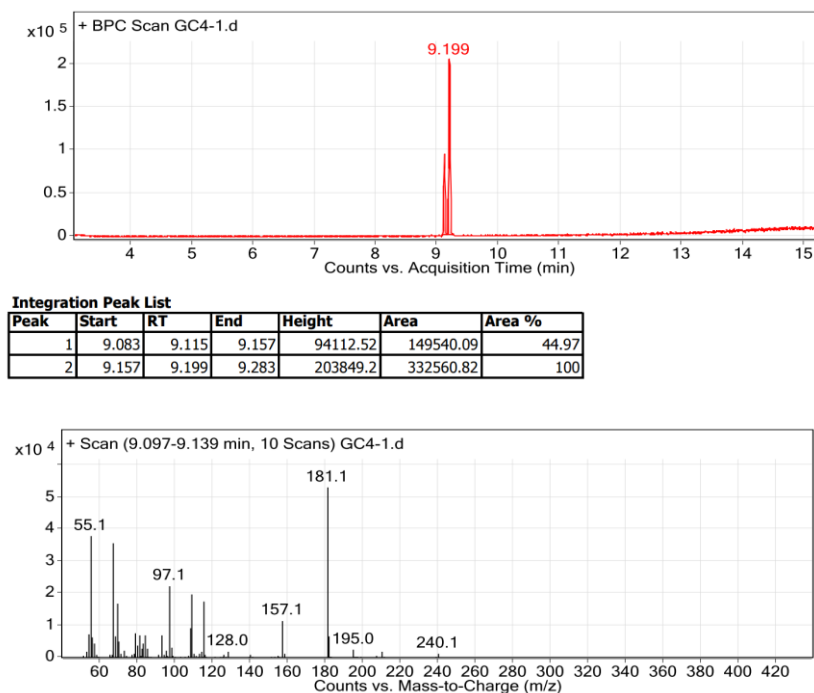


Figure 3.9. GC-MS analysis of SOE1, chromatogram shows two inequivalent peaks, which have identical mass by MS.

A plausible mechanism for the reaction of lactones and epoxides catalyzed by complex **30** is shown in Figure 3.10. Two possible products might be derived from the incorporation of an epoxide unit and a lactone unit. In path A, a lactone unit could be first activated by **30**, followed by a ring opening event through the nucleophilic attack of the oxygen on the epoxide on the activated ester carbon on the lactone. Further intramolecular backbiting could ring open the activated epoxide on either side, leading to the formation of ten-member cyclic esters with two diastereomers. In contrast, an activated epoxide could be ring opened by a lactone unit on either side to form reactive intermediates. Backbiting event of these intermediates would lead to the formation of corresponding spiro-orthoester with two diastereomers in path B.

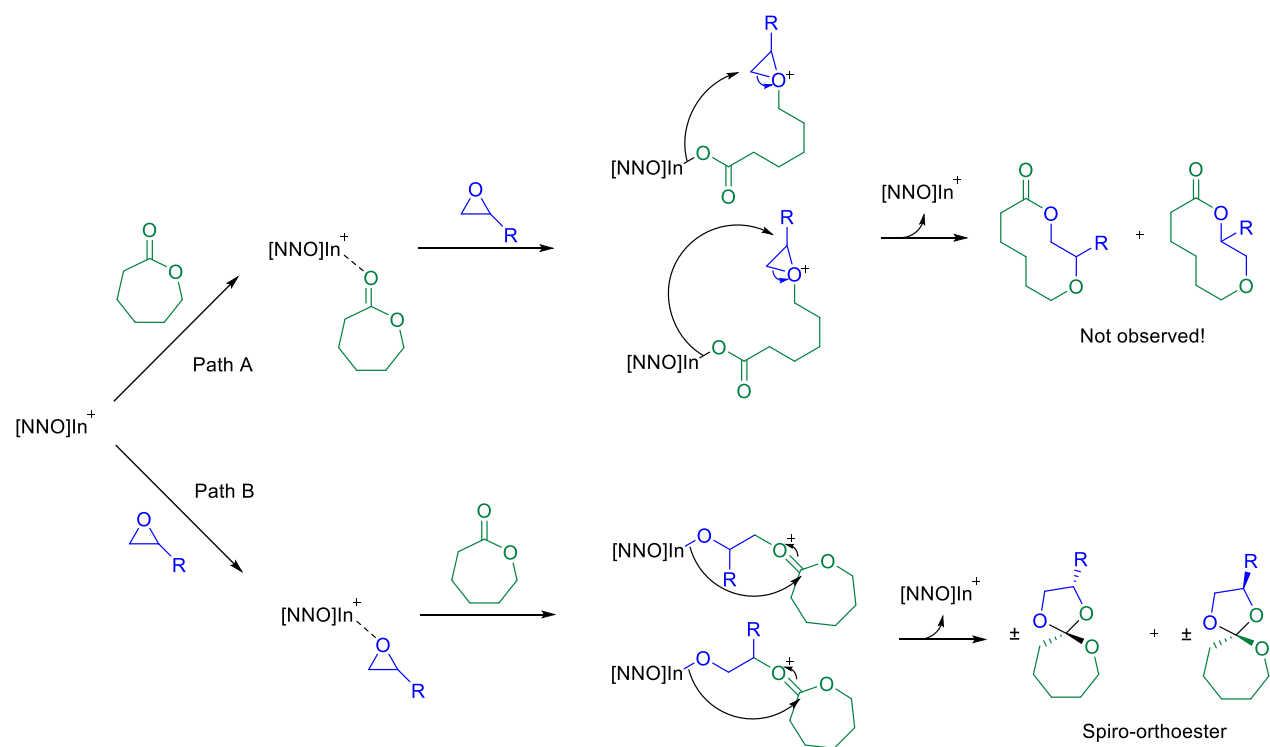


Figure 3.10. Proposed mechanism for the reaction of epoxides and lactones catalyzed by **30**, initial monomer coordination could lead to different products.

Various techniques such as ^{13}C NMR and FTIR spectroscopy were used to distinguish the two possible products. For example, the absence of a $\text{C}=\text{O}$ stretch signal around 1700 cm^{-1} in the IR spectrum of the product (Fig. 3.11) is evidence against the presence of a possible ten-member cyclic esters with an identical parent mass. In addition, the absence of carbon signals on ^{13}C -NMR spectrum between 150 ppm to 220 ppm also suggests the absence of ester type of moiety. These experimental data support the assignment of the product as discrete spiro-orthoester.

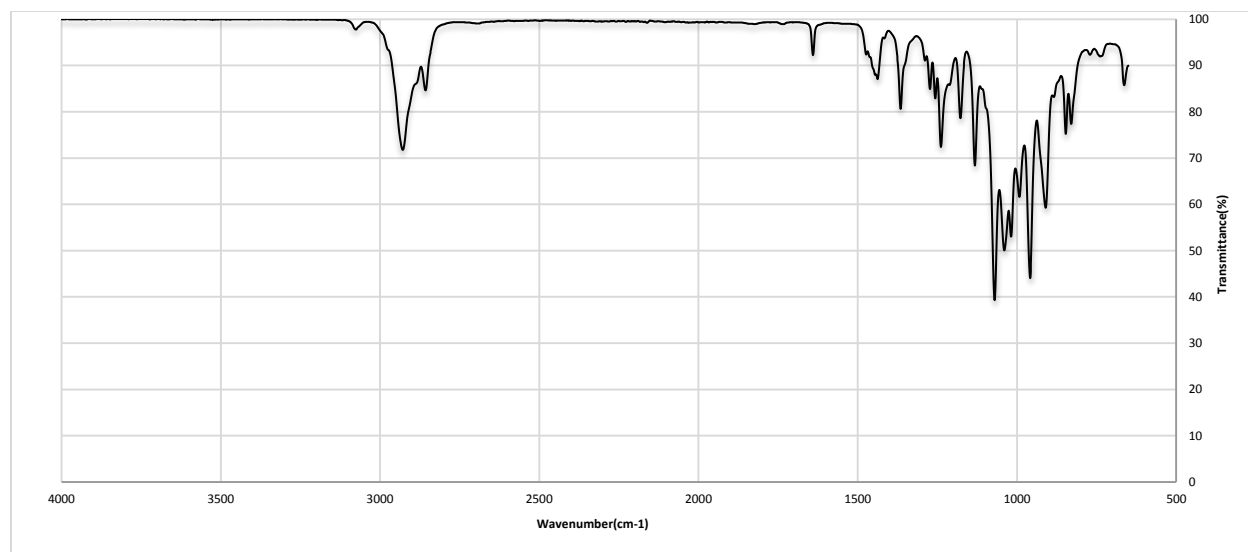


Figure 3.11. FTIR Spectrum of SOE1.

3.2 Spiro-orthoester (SOE1) synthesis optimization

In order to improve the efficiency of spiro-orthoester (SOE1) formation catalyzed by **30**, the aforementioned reaction was carried out at various conditions as illustrated in Table 3.1. In the best condition, reaction of a 1:1 mixture of EOE and CL with 2.5% catalyst loading, at 60 °C in benzene, forms corresponding SOE1 with quantitative conversions of both CL and EOE after 24 h (Table 3.1 Entry 12). After purification, SOE1 can be obtained in greater than 70% isolated yield.

Table 3.1. Synthesis of SOE1 by **30**.

| Entry | [30] | Reaction time | Temperature | Solvent | Conv.% (EOE) | Conv.% (CL) |
|-----------|---------------|---------------|-------------|-------------------------------|--------------|----------------|
| 1 | - | 16 h | 60 °C | C ₆ H ₆ | 0 | 0 |
| 2 | 0.25% | 16 h | 60 °C | C ₆ H ₆ | 68 | 69 |
| 3 | 0.5% | 16 h | 60 °C | C ₆ H ₆ | 74 | 74 |
| 4 | 1% | 16 h | 60 °C | C ₆ H ₆ | 79 | 82 |
| 5 | 1% | 16 h | 60 °C | THF | 37 | 58 |
| 6 | 1% | 16 h | 60 °C | CH ₃ CN | trace | trace |
| 7 | 1% | 24 h | 60 °C | C ₆ H ₆ | 88 | 91 |
| 8 | 1% | 24 h | 25 °C | C ₆ H ₆ | trace | trace |
| 9 | 1% | 24 h | 40 °C | C ₆ H ₆ | 73 | 73 |
| 10 | 1% | 24 h | 80 °C | C ₆ H ₆ | 100 | - ^a |
| 11 | 2.5% | 16 h | 60 °C | C ₆ H ₆ | 87 | 93 |
| 12 | 2.5% | 24 h | 60 °C | C ₆ H ₆ | 100 | 100 |

Reactions performed in 1 mL of solvent, at least two times. [CL] = [EOE] = 0.25 M. Conversions were determined by ¹H NMR spectroscopy. ^a Lactone conversion determination was unsuccessful due to signal overlaps.

Reactions carried out in coordinating solvents such as THF or acetonitrile led to a decrease in reactivity. In the case of acetonitrile, only trace conversions for both substrates were observed over 24 h (Table 3.2 Entry 6). This phenomenon may be due to the coordination of these solvents to the cationic indium center, which could compete with incoming substrates and decrease the reactivity. An increase in reactivity was observed with an increase in reaction temperature from room temperature to 60 °C (Table 3.2, Entry 7-9). At 80 °C, however, a new product was observed in the NMR spectrum with broad signals (Fig. 3.2.1 and Table 3.1 Entry 10). With both quantitative

conversions for CL and EOE, it was suspected that the new product was either a polymeric or a degradation product of SOE1. Reactions of isolated SOE1 in the presence of **30** at 80 °C in benzene also showed the formation of a similar product over 24 h.

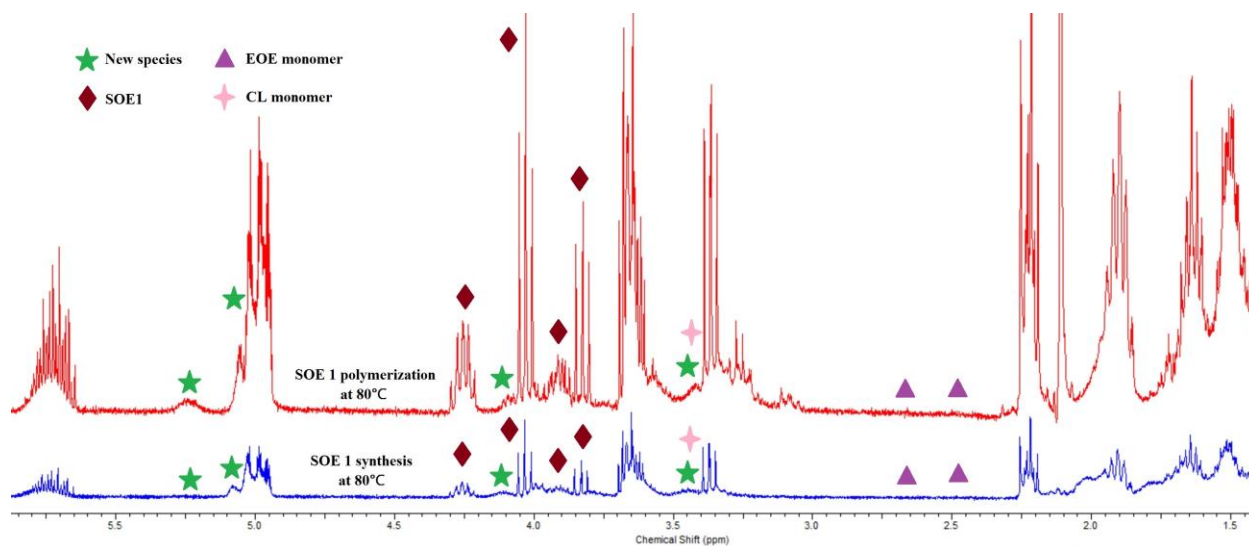


Figure 3.2.1 Overlaid ¹H NMR spectra (300 MHz, C₆D₆, 25 °C) of reaction of CL and EOE in the presence of **30** at 80°C (Bottom) and SOE1 polymerization by **30** at 80°C (Top). CL monomer conversion determination was unsuccessful due to signal overlaps

3.3 Homopolymerization studies of **30** with various monomers

In order to probe the interaction between the cationic indium complex **30** and different monomers as well as understanding the role of catalyst in spiro-orthoesters formation, homopolymerization studies were conducted with various lactones and epoxides as illustrated in Table 3.2. Complex **30** is active for the polymerization of δ -valerolactone (VL), ϵ -caprolactone

(CL), and cyclohexene oxide (CHO); attempts to homopolymerize γ -butyrolactone (BL) and 1,2-epoxy-7-octene (EOE) in identical conditions led to unreacted monomer, yield <1% polymer (Table 3.2).

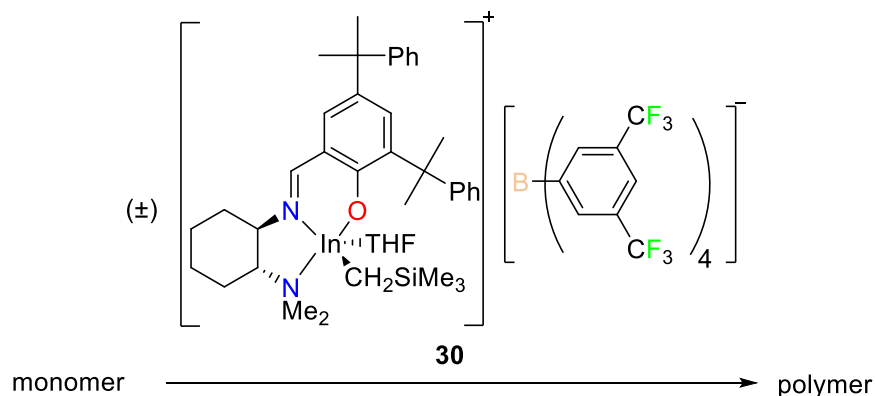
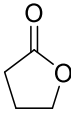
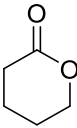
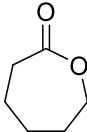
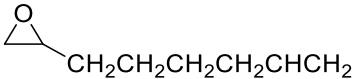
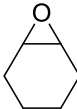


Figure 3.13. Homopolymerization of various monomer by **30**.

The unreactive nature of BL at high temperature is consistent with literature, where polymerization of BL was only reported recently to be achieved at low temperature.¹⁰³ In contrast, polymerization of VL and CL in benzene yields 44% and 74% conversion of the monomer in 24 h, respectively. While complex **30** is inactive towards homopolymerization of EOE, it is shown to be reactive towards homopolymerization of CHO, where quantitative conversion can be achieved in 24 h. The difference in reactivity between EOE and CHO may be attributed to the more strained nature of CHO which translates to higher reactivity.¹⁰⁴⁻¹⁰⁵ Emboldened by these homopolymerization studies, I investigated the spiro-orthoesters formation catalyzed by **30** with incorporation of various lactones with CHO and EOE. Attempts to synthesize spiro-orthoesters from different lactones with cyclohexene oxide (CHO) yielded a mixture of products with

polyester as the major product. This can be rationalized by a more favorable homopolymerization of CHO over spiro-orthoesters formation under the given condition.

Table 3.2. Homopolymerization of various monomers by **30**.

| Entry | | Monomer | Conv.% |
|-------|-----|--|--------|
| 1 | BL |  | Trace |
| 2 | VL |  | 44 |
| 3 | CL |  | 74 |
| 4 | EOE |  | trace |
| 5 | CHO |  | 100 |

Reactions performed in 1 mL of benzene at 60 °C for 24 h, at least two times. [Monomer] = 0.25 M. [**30**] = 2.5%. Conversions were determined by ¹H NMR spectroscopy.

3.4 Spiro-orthoester synthesis with various lactones and EOE

Synthesis of spiro-orthoester with 1,2-epoxy-7-octene (EOE) and δ -valerolactone (VL) was successful under the aforementioned reaction condition (Fig. 3.14). Near quantitative conversion of EOE was achieved over 24 h and the expected spiro-orthoester (SOE2) can be isolated in yields greater than 70% (Table 3.3, Entry 2).

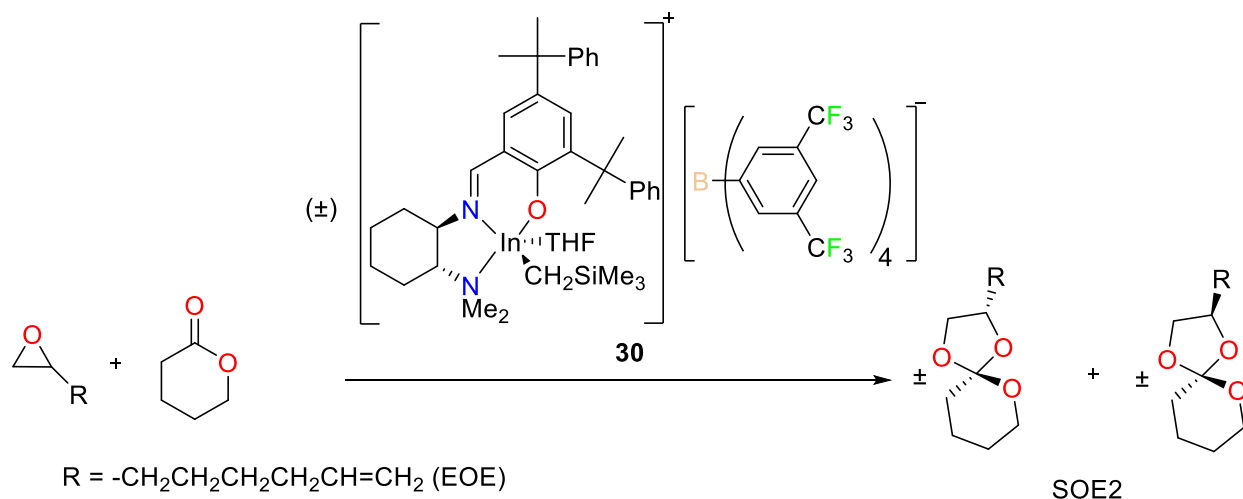


Figure 3.3. Synthesis of SOE2.

Table 3.3. Synthesis of SOEs with different substrates by **30**.

| Entry | Lactone | Epoxide | Conv.% (EOE) | Conv.% (Lactone) | Time (h) | Isolated yield % |
|-------|---------|---------|--------------|------------------|----------|------------------|
| 1 | ε-CL | EOE | 100 | - ^a | 25 | 76 |
| 2 | δ-VL | EOE | 100 | - ^a | 25 | 75 |
| 3 | γ-BL | EOE | 85 | 80 | 72 | 53 |

Reactions performed in 5 mL of benzene at 60 °C. [lactone] = [epoxide] = 0.25 M. [**30**] = 2.5%. Conversions were determined by ¹H NMR spectroscopy. ^aLactone conversion determination was unsuccessful due to signal overlaps.

Detailed analysis of SOE2 by NMR spectroscopy, GC-MS, and IR spectroscopy was carried out in a similar manner to that of SOE1. ¹H NMR and ¹³C{¹H} NMR spectra of SOE2 also showed two sets of resonance signals corresponding to two diastereomers (Fig. 3.15 and Fig. 3.16).

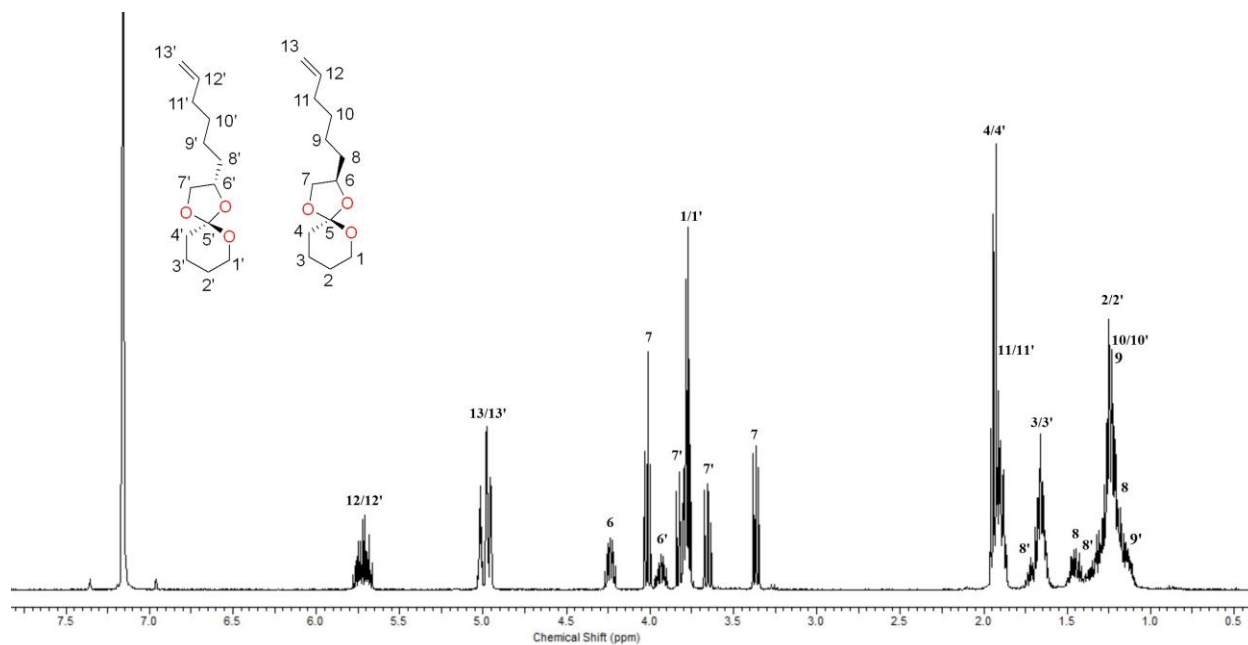


Figure 3.15. ^1H NMR spectrum (400 MHz, C_6D_6 , 25 °C) of SOE2.

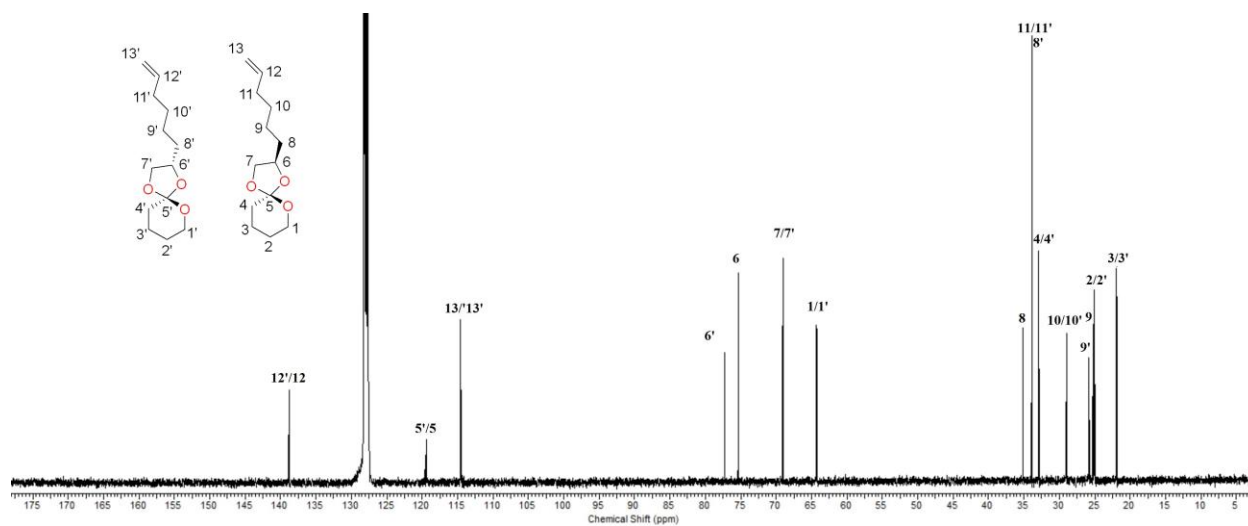


Figure 3.16. $^{13}\text{C}\{^1\text{H}\}$ NMR spectrum (151 MHz, C_6D_6 , 25 °C) of SOE2.

Surprisingly, GC-MS analysis of SOE2 only showed a broad signal corresponding to a parent mass of 226.1 m/z, which was in agreement with the proposed structure. Attempts to resolve the broad signal on GC chromatogram by varying conditions, such as temperature ramping speed

and concentration, were unsuccessful. However, based on NMR evidence of the presence of two diastereomers, this phenomenon may be due to the incapability of the GC column to separate these isomer; which led to the observed of the broad of the signal by GC (Fig. 3.17).

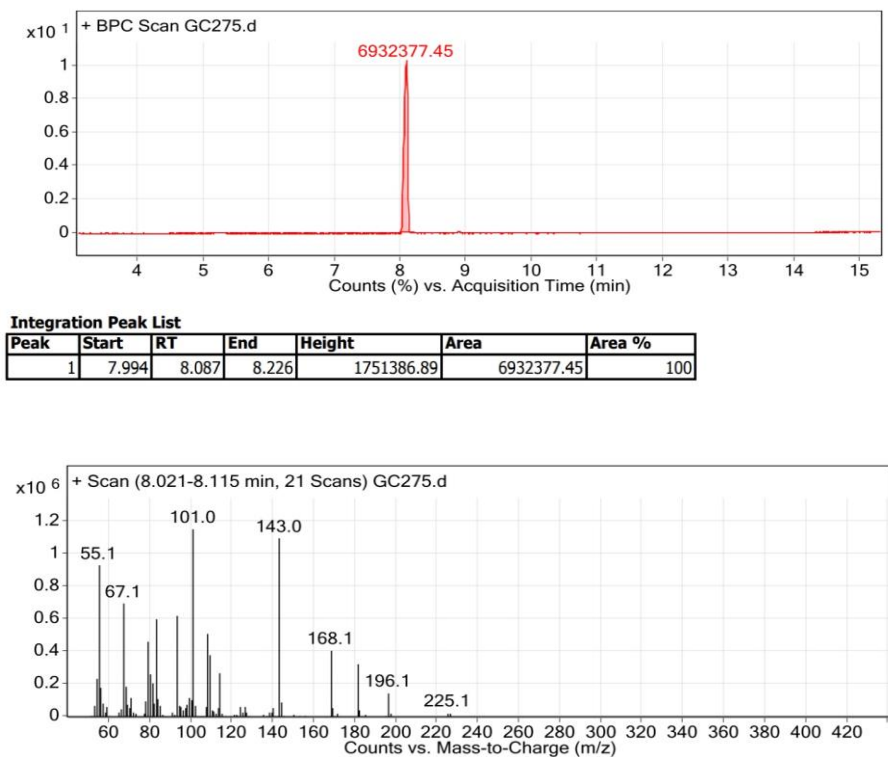


Figure 3.17. GC-MS analysis of SOE2.

In a similar manner, formation of spiro-orthoester with EOE and γ -butyrolactone (BL) was observed (Fig. 3.18). Over 85% conversion of EOE was achieved over 72 h and the corresponding spiro-orthoester (SOE3) was isolated in more than 50 % (Table 3.3, Entry 3).

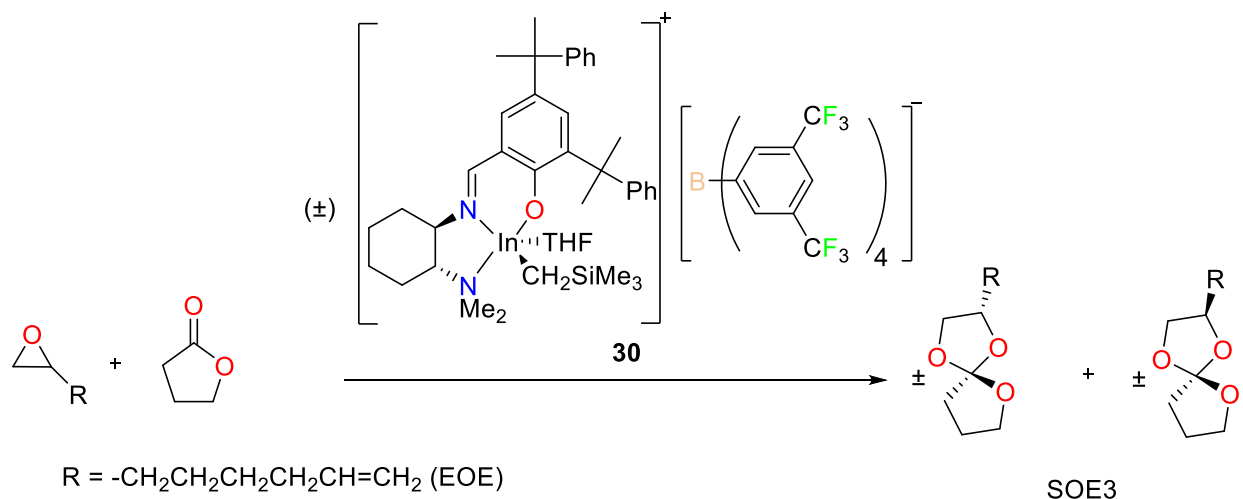


Figure 3.18. Synthesis of SOE3.

Structural characterizations of SOE3 were carried out with NMR spectroscopy, GC-MS and IR spectroscopy. The presence of two sets of signals on both ^1H -NMR and ^{13}C -NMR analysis were also consistent with the formation of diastereomers (Fig. 3.19 and 3.20).

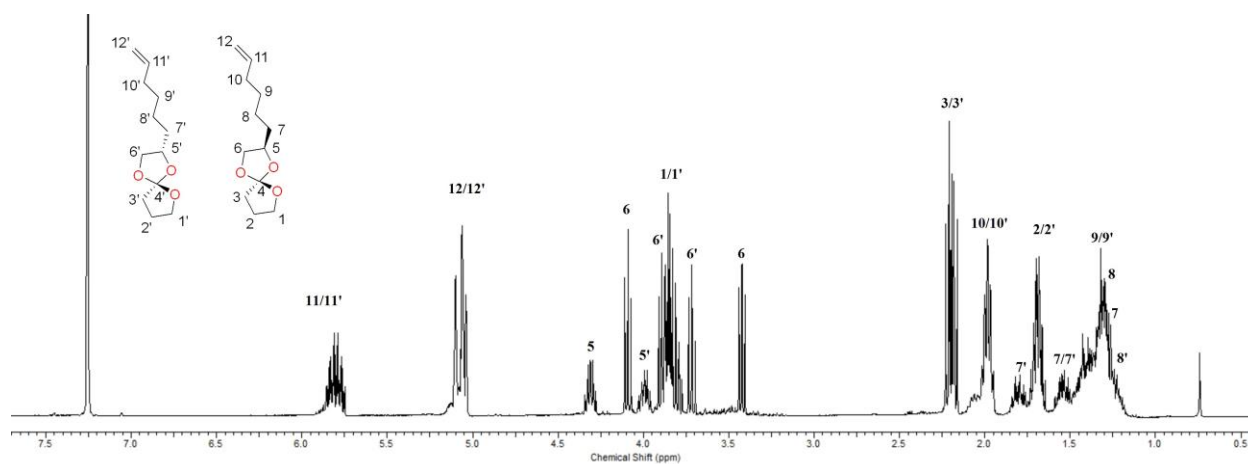


Figure 3.19. ^1H NMR spectrum (400 MHz, C_6D_6 , 25 °C) of SOE3.

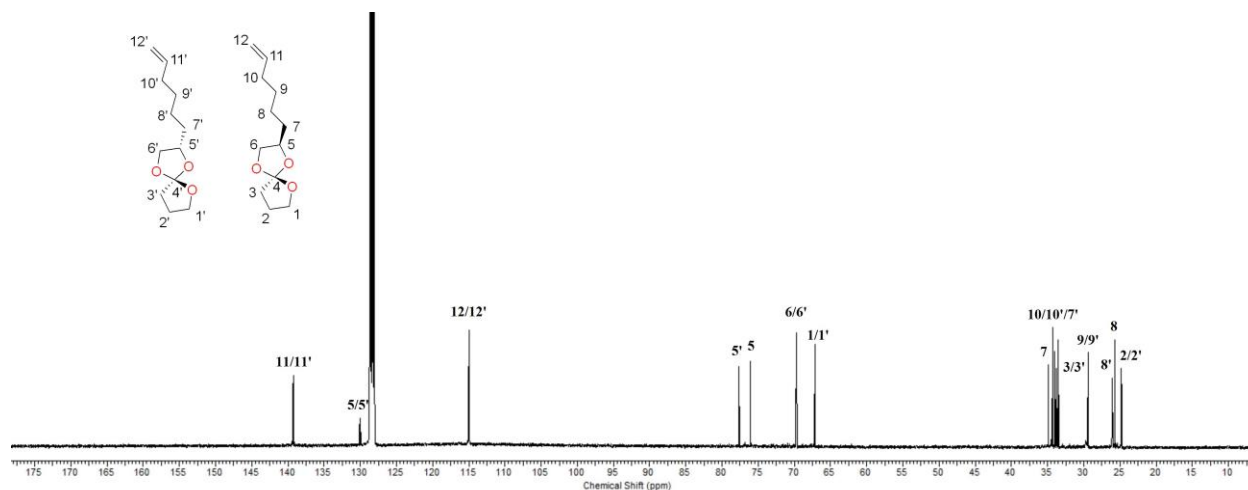


Figure 3.20. $^{13}\text{C}\{^1\text{H}\}$ NMR spectrum (151 MHz, C_6D_6 , 25 °C) of SOE3.

While GC-MS analysis showed several signals on the chromatogram, all species appear to have an identical parent mass of 212 m/z (Fig. 3.21), which is consistent with the mass of proposed spiro-orthoester structure. These GC signals may be rationalized with the formation of enantiomers that were indistinguishable by NMR spectroscopy but were distinguishable by GC column chromatography.

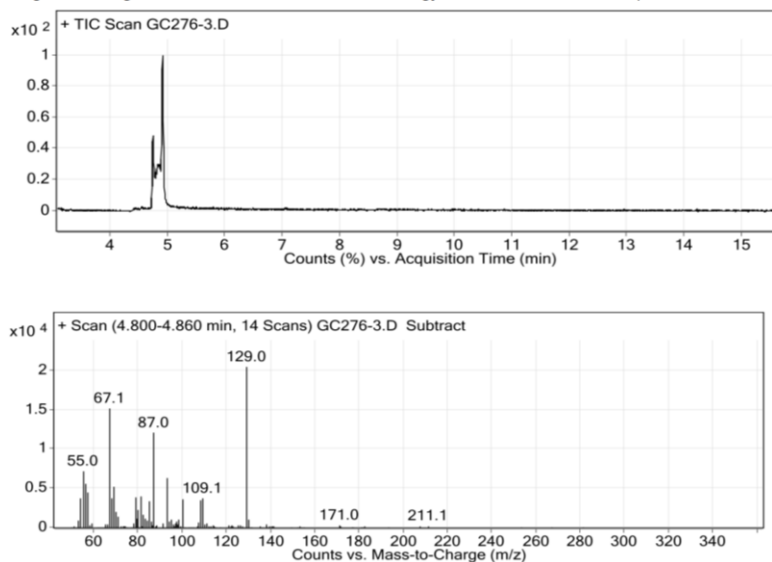


Figure 3.21. GC-MS analysis of SOE3.

3.5 Preliminary polymerization of SOE1

While cationic polymerization of spiro-orthoesters using Lewis acids has been reported,³¹⁻
³³ we are interested to investigate whether the highly Lewis acidic cationic indium species **30** is a
 suitable candidate as a catalyst for spiro-orthoester polymerization to form poly(cyclic orthoester)
 or poly(ether ester). Due to the reported unreactive nature of spiro-orthoesters bearing five and six
 membered ether rings,⁴⁰ SOE1 was chosen as the monomer for this study.

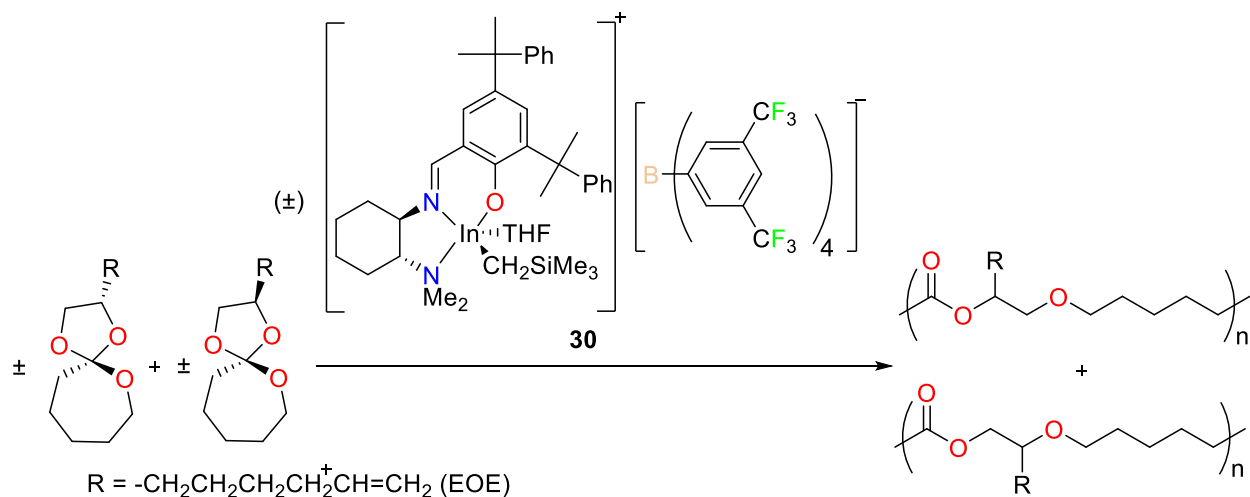


Figure 3.22. Cationic polymerization of SOE1 by **30**.

First attempts at polymerization of SOE1 in the presence of cationic alkyl indium **30** in toluene at room temperature and 60 °C were unsuccessful (Table 3.4). At 200:1 monomer to catalyst ratio, only trace conversion of SOE1 was observed over 240 h in both conditions.

Table 3.4. Attempted SOE1 polymerization by **30** under varying temperatures.

| Entry | Temperature (°C) | Time (h) | Conversion (%) |
|-------|------------------|----------|----------------|
| 1 | 25 | 240 | trace |
| 2 | 60 | 240 | trace |
| 3 | 110 | 96 | 90 |

Reactions performed in 1 mL of toluene at. [SOE1] = 1 M. [**30**] = 0.5%. Conversions were determined by ¹H NMR spectroscopy.

However, the formation of polymeric species was observed at 110 °C over time (Fig. 3.23). Over 90% conversion of SOE1 was achieved over 96 hours. Upon basic work up, the resultant product was isolated as viscous brown oil.

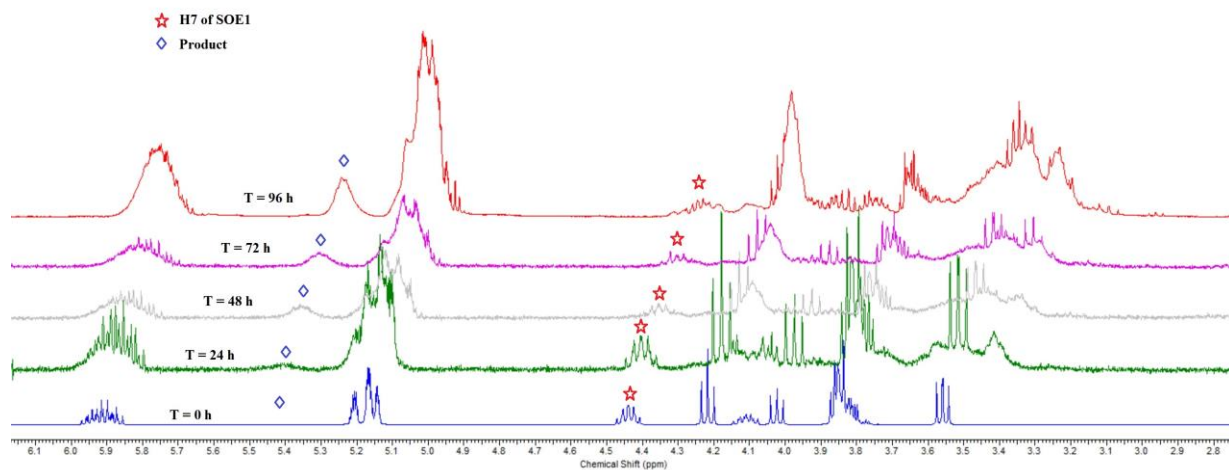


Figure 3.23. Overlaid ¹H NMR spectra (300 MHz, C₆D₆, 25 °C) of SOE1 polymerization at 110 °C overtime.

Initial characterization of the resultant product was conducted by ¹H NMR and ¹³C{¹H} NMR spectroscopy, as well as IR spectroscopy. The broad ¹H NMR signals were indicative of a polymeric species which suggested the successful polymerization of SOE1 by complex **30** at the given conditions. According to the literature, cationic polymerization of spiro-orthoesters at elevated temperature would yield poly(ether ester) type of polymers,⁴² and we were expecting to obtain such a product. Further analysis of the product by ¹³C NMR spectroscopy and IR spectroscopy supported such formation (Fig. 3.24 and 3.25)

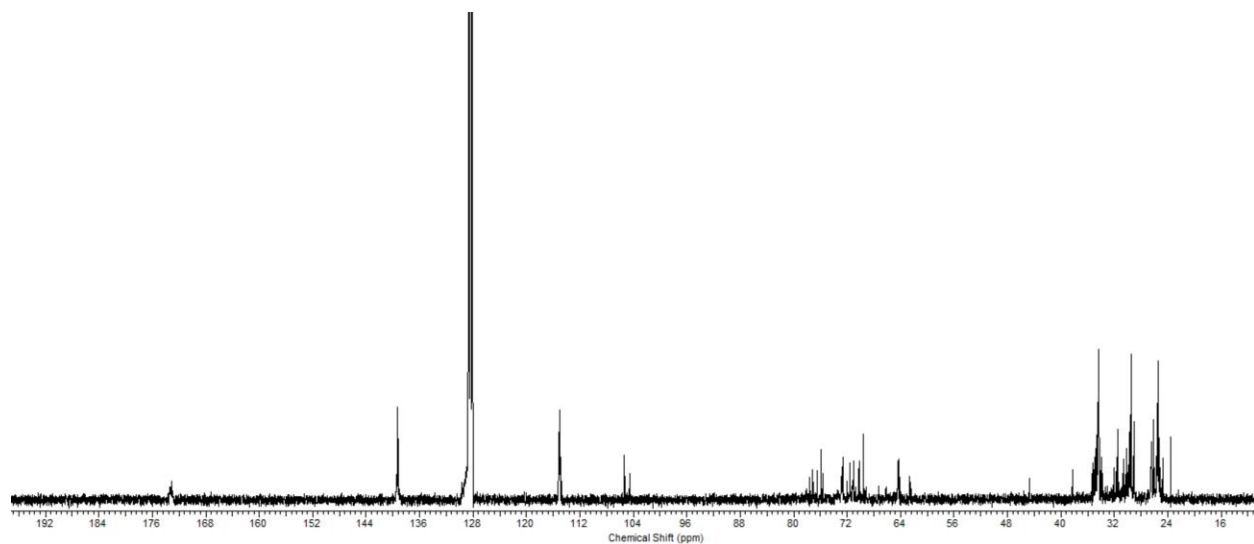


Figure 3.24. $^{13}\text{C}\{^1\text{H}\}$ NMR spectrum (400 MHz, C_6D_6 , 25 °C) of SOE1 polymerization product.

The disappearance of ^{13}C signal corresponding to orthoester carbon (124.6 ppm) suggested the conversion of SOE1 and was also evidence against the formation of poly(cyclic orthoester) type of polymers.³⁹⁻⁴³ Moreover, the presence of ^{13}C signal at 173.1 ppm supported the formation of carbonyl type species which was absent from the starting material, SOE1. IR spectrum of the product showed a strong absorption signal around 1733 cm^{-1} , which also supported the formation of poly(ether ester) type of polymer (Fig. 3.3.3).

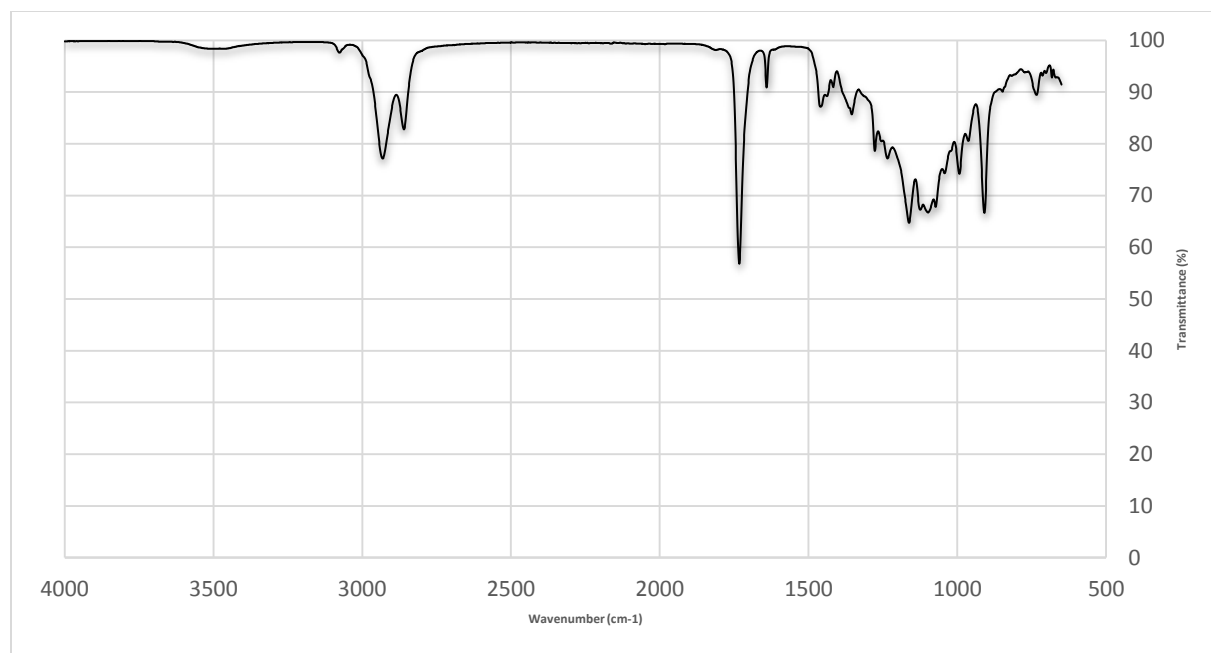


Figure 3.25. FTIR Spectrum of SOE1 polymerization product.

Further MALDI-TOF analysis of the resultant product showed polymeric signals up to 3500 m/z, which was indicative of the presence of low molecular weight polymer. A repeating unit of 240 m/z was observed between every second signals, which suggested the polymerization of SOE1 (Fig. 3.26).

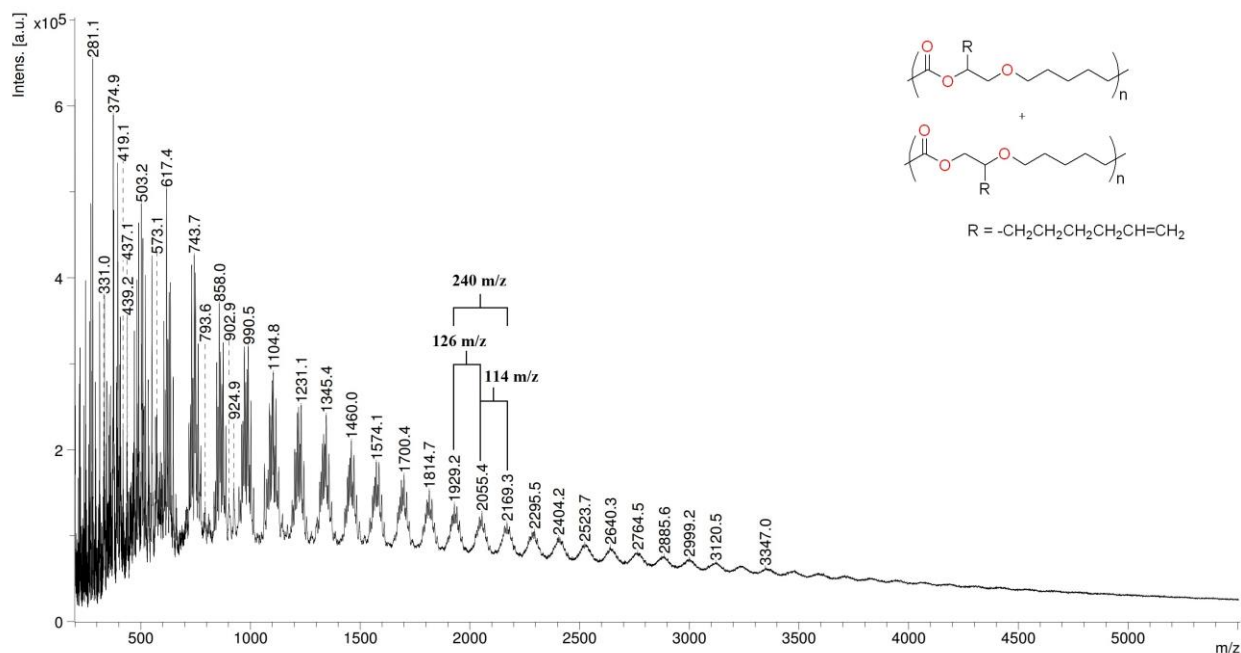


Figure 3.26. MALDI-TOF mass spectrum of SOE1 polymerization product.

However, within each repeating unit of 240 m/z, a signal was observed to be separated by 114 m/z or 126 m/z, which corresponds to a CL unit or an EOE unit. This result suggests the uncontrolled nature of thermal rearrangement at high temperature to form poly(ether ester) that leads to the breakdown of polymer chains at both ester and ether linkages. The observed low molecular weight of the polymer was also consistent with previous literature.³⁸⁻⁴⁷ Potential influences of the cationic agent during matrix preparation in the presence of moisture might breakdown the polymer cationically. Thus, a more accurate molecular weight determination should be conducted by gel permeation chromatography.

3.6 Conclusion

In this chapter, the reaction of EOE and CL catalyzed by cationic alkyl indium $[(\text{NNO})\text{In}(\text{CH}_2\text{SiMe}_3)(\text{THF})][\text{BAr}^{\text{F}}]$ (**30**) was investigated. The resultant product was purified and identified as spiro-orthoester (SOE1) through various spectroscopy techniques. Quantitative conversions of both substrates could be achieved less than 24 hours at 2.5% catalyst loading at 60 °C in benzene, which yielded to more than 70% isolated yield. Spiro-orthoesters bearing various ether rings (SOE2 and SOE3) are prepared with different lactone substrates (VL and BL, respectively) at moderate efficiency. While preliminary polymerization studies of SOE1 suggested the poor activity of complex **30** towards polymerization of SOE at lower temperature, polymerization of SOE1 complex **30** at 110 °C yielded to over 90% conversion of the monomer, and the resultant polymer was tentatively assigned as low molecular weight poly(ether ester). Further characterization of the resultant polymer is necessary to confirm its structure and molecular weight.

3.7 Experimental section

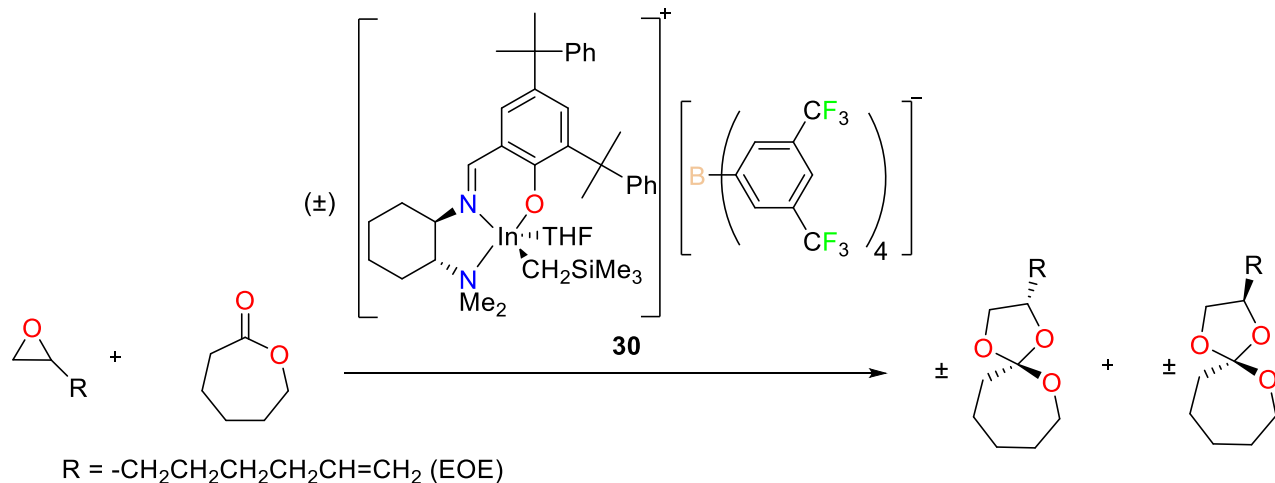
General Considerations. Unless otherwise indicated, all air- and/or water-sensitive reactions were carried out under dry nitrogen using either an MBraun glove box or standard Schlenk line techniques. All reaction vials were placed in an aluminum heat block, which has two different size holes to accommodate multiple 1 mL and 20 mL vials at the same time, preheated to desired temperature on a magnetic hotplate/stirrer and allowed to stabilize prior to usage. Infrared spectra

were recorded using a PerkinElmer Frontier IR Single-Range Spectrometer. GC-MS analyses are conducted through an Agilent GC-MS equipped with an EI ion source. Sample solution was prepared using hexane and 1 uL sample solution was injected using split mode with split ratio of 50:1. The GC column used was HP-5ms. The oven temperature started at 80°C and held for 1 minute, then ramped from 80 to 150 at 30°C/min and from 150 °C to 250 °C at 10°C/min with total run time of 15 minutes. Mass scan range was 50-450.

MALDI mass spectra were obtained on Bruker autoflex MALDI-TOF equipped with Bruker smartbeam-II laser system (wavelength 355nm). The samples were normally dissolved in tetrahydrofuran. DHB (2,5-Dihydroxybenzoic acid) was used as matrix. The solutions of the sample (~1mg/mL) and matrix (20mg/mL) were mixed in the ratio of 1:1 to 1:10 and 1 uL of final mixture was deposited onto the sample target. MALDI mass spectra were acquired in the positive reflectron mode with delay extraction. Spectra were obtained by averaging 3000 laser shots. Calibration was performed externally using various peptides.

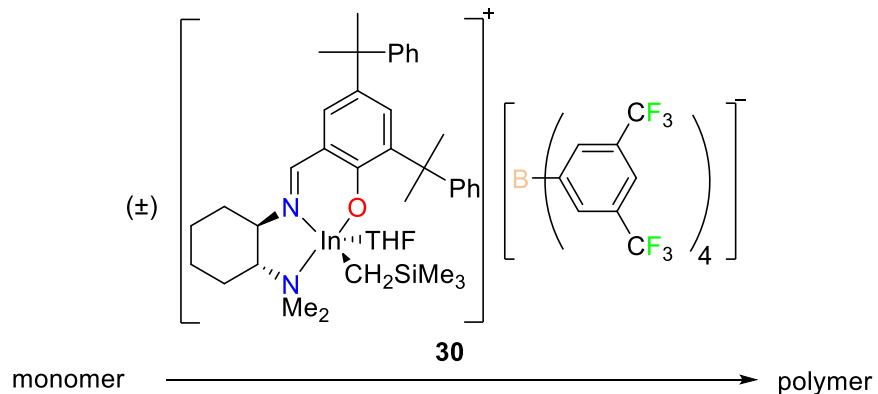
Materials. Solvents hexane was collected from a Solvent Purification System from Innovative Technology, Inc. whose columns are packed with activated alumina. Benzene, diethyl ether, tetrahydrofuran were distilled from Na/benzophenone ketyl and degassed through a series of freeze-pump-thaw cycles. CDCl₃ and C₆D₆ were dried over CaH₂ and Na/benzophenone ketyl, respectively, collected by vacuum distillation and degassed through a series of freeze-pump-thaw cycles.

Representative spiro-orthoester synthesis with complex 30.



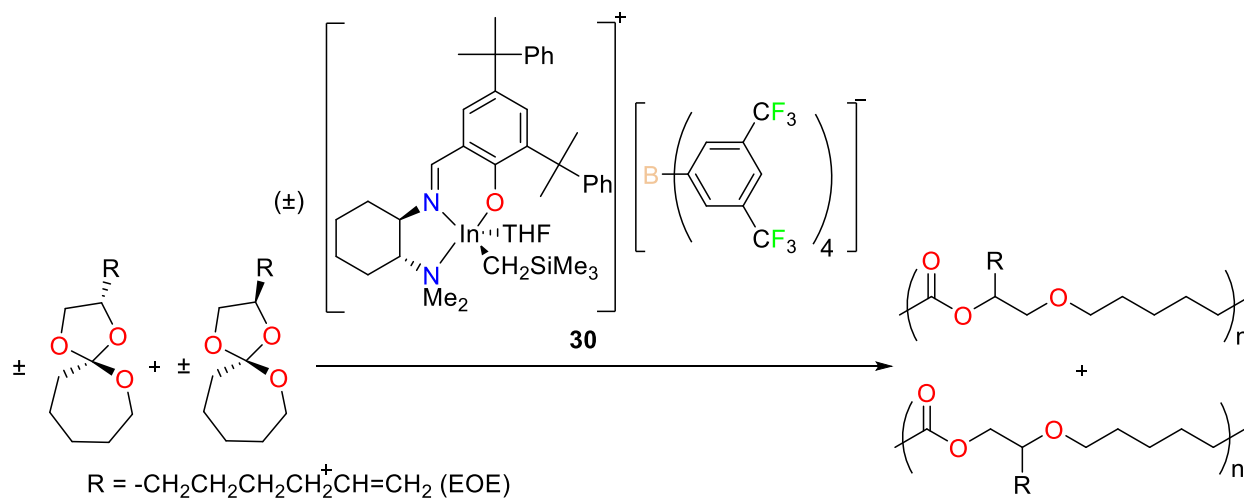
A 20 mL scintillation vial was charged with 0.15 mL and 0.45 mL solution of a 7-hexene-1,2-epoxide and ϵ -caprolactone stock solution, respectively (epoxide: 0.25 mmol; [epoxide] = 1.67 M; CL: 0.25 mmol; [CL] = 0.556 M). 0.15 mL solution of a catalyst stock solution (0.00625 mmol; [30] = 0.0417 M) were added to the vial. 0.25 mL solution of benzene was used to make up to the total volume of 1 mL. The resulting mixture was placed in an aluminum heat block preheated to 60 °C and stirred. A sample of the crude polymerization mixture (ca. 0.05 mL) was dissolved in C_6D_6 to be analyzed by ^1H NMR spectroscopy to determine conversion. The solvent was removed under vacuum after 24 h. The residue was dissolved in a minimum amount of hexane (3 mL) to separate a solid by-product from the mixture solution. The decanted solution was filtered through silica flash column. The collected solution was dried over vacuum to obtain the desired product as colourless oil. The product was dried under high vacuum for 4 h prior to analysis. Further vacuum distillation may be carried out to remove trace impurity. A larger scale can be also carried out in a similar fashion in 5 mL of benzene.

Homopolymerization of various monomers by complex 30.



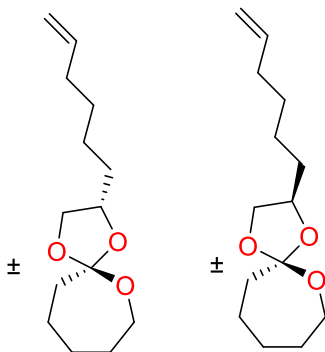
A 20 mL scintillation vial was charged with 0.15 mL (monomer: 0.25 mmol; [monomer] = 1.67 M). 0.15 mL solution of a catalyst stock solution (0.00625 mmol; [30] = 0.0417 M) were added to the vial. 0.70 mL solution of benzene was used to make up to the total volume of 1 mL. The resulting mixture was placed in an aluminum heat block preheated to 60 °C and stirred for 24 h. A sample of the crude polymerization mixture (ca. 0.05 mL) was dissolved in C₆D₆ to be analyzed by ¹H NMR spectroscopy to determine conversion.

Polymerization of spiro-orthoester by complex 30.



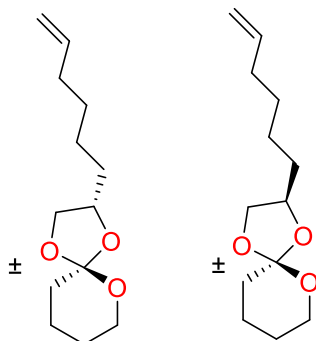
A 20 mL scintillation vial was charged with 240 mg of SOE1 (1 mmol) vial. 0.5 mL of a catalyst stock solution (0.005 mmol, [**30**] = 0.01 mM) and solution of toluene was used to make up to the total volume of 1 mL. The resulting mixture was stirred at appropriate temperature. A sample of the crude polymerization mixture (ca. 0.05 mL) was dissolved in C₆D₆ to be analyzed by ¹H NMR spectroscopy to determine conversion. Few drops of Et₃N were added to stop the reaction upon completion. The reaction mixture was dissolved in dichloromethane and washed with 100 mL saturated NaHCO₃ solution. The organic layer was dried over Na₂SO₄ and the solvent was removed in vacuum to yield to viscous oil. The sample was dried under vacuum for 2 h prior to analysis.

Spiro-orthoester (SOE1; EOE + CL).



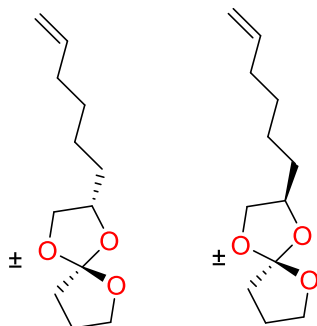
$^{13}\text{C}\{^1\text{H}\}$ NMR (151 MHz, C_6D_6) δ 139.3 (-CH=CH₂ of EOE), δ 139.3 (-CH=CH₂ of EOE), δ 124.7 (-C- of SOE), δ 124.6 (-C-of SOE), δ 115.0 (-CH=CH₂ of EOE), δ 115.0 (-CH=CH₂ of EOE), δ 77.6 (-CH- of EOE), δ 75.9 (-CH- of EOE), δ 69.6 (-CH₂- of EOE), δ 69.6 (-CH₂- of EOE), δ 64.3 (-O-CH₂- of CL), δ 64.3 (-O-CH₂- of CL), δ 38.4 (-C(OR)₂CH₂-), δ 38.2 (-C(OR)₂-CH₂- of CL), δ 35.4 (-CH₂- of EOE), δ 34.4 (-CH₂- of EOE), δ 34.3 (-CH₂- of EOE), δ 31.6 (-CH₂- of CL), δ 31.5 (-CH₂- of CL), δ 29.9 (-CH₂- of EOE), δ 29.9 (-CH₂- of EOE), δ 29.5 (-CH₂- of EOE), δ 29.5 (-CH₂- of EOE), δ 26.2 (-CH₂- of EOE), δ 25.7 (-CH₂- of EOE), δ 23.6 (-CH₂- of CL), δ 23.5 (-CH₂- of CL).

Spiro-orthoester (SOE2; EOE + VL).



$^{13}\text{C}\{^1\text{H}\}$ NMR (151 MHz, C_6D_6) δ 139.3 (-CH=CH₂ of EOE), δ 139.3 (-CH=CH₂ of EOE), δ 120.0 (-C(O)- of VL), δ 119.9 (-C(O)- of VL), δ 115.0 (-CH=CH₂ of EOE), δ 115.0 (-CH=CH₂ of EOE), δ 77.7 (-CH- of EOE), δ 75.8 (-CH- of EOE), δ 69.6 (-CH₂- of EOE), δ 69.5 (-CH₂- of EOE), δ 64.8 (-O-CH₂- of VL), δ 64.7 (-O-CH₂- of VL), δ 35.6 (-CH₂- of EOE), δ 34.4 (-CH₂- of EOE), δ 34.3 (-CH₂- of EOE), δ 33.4 (-C(OR)₂CH₂- of VL), δ 33.4 (-C(OR)₂CH₂- of VL), δ 29.5 (-CH₂- of EOE), δ 29.4 (-CH₂- of EOE), δ 26.3 (-CH₂- of EOE), δ 25.7 (-CH₂- of EOE), δ 25.5 (-CH₂- of VL), δ 25.5 (-CH₂- of VL), δ 22.4 (-CH₂- of VL), δ 22.4 (-CH₂- of VL).

Spiro-orthoester (SOE3; EOE + BL).



$^{13}\text{C}\{^1\text{H}\}$ NMR (151 MHz, C_6D_6) δ 139.3 (-CH=CH₂ of EOE), 139.2 (-CH=CH₂ of EOE), 130.0(-C(O)- of BL), 130.0 (-C(O)- of BL), 115.0 (-CH=CH₂ of EOE), 115.0 (-CH=CH₂ of EOE), 77.6 (-CH- of EOE), 76.1 (-CH- of EOE), 69.7 (-CH₂- of EOE), 69.7 (-CH₂- of EOE), 67.2 (-O-CH₂- of BL), 67.2 (-O-CH₂- of BL), 34.9 (-CH₂- of EOE), 34.3 (-CH₂- of EOE), 34.3 (-CH₂- of EOE), 34.0 (-CH₂- of EOE), 33.8 (-C(O)-CH₂- of BL), 33.5 (-C(O)-CH₂- of BL), 29.5 (-CH₂- of EOE), 29.4 (-CH₂- of EOE), 26.1 (-CH₂- of EOE), 25.7 (-CH₂- of EOE), 24.8 (-CH₂- of BL), 24.7 (-CH₂- of BL).

Conclusion and future works

In this thesis, I described the project that I worked on during my graduate studies in the Mehrkhodavandi group. The project was started by Dr. Yu to investigate the reactivity of cationic indium complex **29** bearing a coordinating ether. Preliminary studies suggested that complex **29** is active towards homopolymerization of CL but not epoxides. In addition, attempts to copolymerize CL and epoxide yielded a viscous oil that was tentatively assigned as copolymers. Through modification of procedure developed by Dr. Yu, I synthesized a cleaner cationic indium complex **30** bearing a coordinating THF. As well I carried on the investigation of isolated product from the attempted copolymerization of EOE and CL with complex **30** and identified the product as spiro-orthoester (SOE1).

In chapter 2, the synthesis and characterization of complex **30** was discussed. Through a protonolysis reaction of the neutral indium alkyl complex **28** with $[\text{HNMe}_2\text{Ph}][\text{BAr}^{\text{F}}]$ in THF, the corresponding cationic indium complex **30** can be isolated in more than 75% yield. Various NMR spectroscopy techniques were used to confirm the structure. As well, solid state structure of **30** was obtained through X-ray diffraction techniques. The variant in bond distances of In-C and In-O (THF) between **30** and literature compounds suggested the potential tunability of the cationic indium complex through ligand design. With limited reactive cationic indium complexes reported in the literature, exploring the reactivity of other cationic indium complexes bearing different ligand platforms and counterions will be continued in the Mehrkhodavandi group.

In chapter 3, the reaction of EOE and CL by the cationic indium complex **30** was investigated. Through careful purification and characterization, the isolated product was identified as spiro-orthoester (SOE1) through various spectroscopy techniques. Attempts to increase reaction efficiency by varying catalyst loading, reaction temperature, solvent, and reaction time were conducted. In the best condition, quantitative conversions of both substrates are achieved under 24 hours at 2.5% catalyst loading at 60 °C in benzene. Moreover, other spiro-orthoesters bearing 5 and 6 membered ether ring (SOE2 and SOE3) were synthesized with different lactones as substrates. Preliminary polymerization of SOE1 studies suggested that complex **30** is active towards SOE polymerization only at high temperature. The resultant low molecular weight polymer was tentatively assigned as poly(ether ester) based on various NMR techniques and FTIR. Further structural analysis of the isolated polymer will be conducted to confirm its structure and molecular weight.

With promising nature of spiro-orthoesters as expandable building blocks towards tunable functionalized biodegradable materials, further investigation of such monomers and their polymerizations could lead to potential industrial applications. For example, synthesis of various spiro-orthoesters with functionalized epoxides and functionalized lactones would allow us to create a library of available spiro-orthoesters for further polymerization studies. While we are able to successfully incorporate various epoxides and lactones to form various spiro-orthoesters, incorporation of lactams and cyclic carbonates instead of lactones would also be an interesting direction that provides us access to different monomers and polymers, respectively. As previous reports have suggested the low molecular weight nature of spiro-orthoester polymers, improving the molecular weight of such polymers is one major challenge that needs to be addressed. Attempts

to optimize the polymerization condition for higher molecular polymers will be investigated by Hyuk Joon Jung in the group. Subsequently, in collaboration with chemical engineering department at UBC, the material properties of these polymers can be evaluated to determine their potential industrial application.

References

1. Bai, Y.; Feng, X.; Xing, H.; Xu, Y.; Kim, B. K.; Baig, N.; Zhou, T.; Gewirth, A. A.; Lu, Y.; Oldfield, E.; Zimmerman, S. C. *J. Am. Chem. Soc.* **2016**, *38*, 11077.
2. Zhang, D.; Boopathi, S. K.; Hadjichristidis, N.; Gnanou, Y.; Feng, X. *J. Am. Chem. Soc.* **2016**, *138*, 11117.
3. Cheng, C.; Watts, A.; Hillmyer, M. A.; Hartwig, J. F. *Angew. Chem. Int. Ed.* **2016**, *55*, 11872.
4. Ding, Y.; Yu, G. *Angew. Chem. Int. Ed.* **2016**, *55*, 4772.
5. Li, P.; Ma, S.; Dai, Y.; Liu, X.; Jiang, Y.; Wang, S.; Wei, J.; Chen, J.; Zhu, J. *ACS Sustainable Chem. Eng.* **2017**, *5*, 1228.
6. Raj, T.; Sharma, H.; Mayank; Singh, A.; Aree, T.; Kaur, N.; Singh, N.; Jang, D. O. *ACS Sustainable Chem. Eng.* **2017**, *5*, 1468.
7. Anastas, P. T.; Warner, J. C. *Green Chemistry: Theory and Practice*, Oxford University Press: New York, 1998, p.30. By permission of Oxford University Press.
8. Statista. <http://www.statista.com/statistics/282732/global-production-of-plastics-since-1950/> (accessed Dec, 2015).
9. Gómez, E. F.; Michel Jr., F.C. *Polym. Degrad. Stab.* **2013**, *98*, 2583.
10. Wang, X.L.; Yangand, K.K.; Wang, Y.Z. *J. Macromol. Sci. Polym. Rev.* **2003**, *43*, 385.
11. Oh, J. K. *Soft Matter.* **2011**, *7*, 5096.
12. Hussain, M.A.; Mollic, J.A. *J. Pharm. Sci.* **1993**, *82*, 553.
13. Jamshidian, M.; Tehrany, E.A.; Imran, M.; Jacquot, M.; Desobry, S. *Compr. Rev. Food Sci. Food Saf.* **2010**, *9*, 552.
14. Briassoulis, D. *J. Polym. Environ.* **2004**, *12*, 65.
15. Jakubiak, J.; Linden, L. A. *Polimery*, **2001**, 7-8, 522.
16. Boaro, L. C.; Gonçalves, F.; Guimarães, T. C.; Ferracane, J. L.; Versluis, A.; Braga, R. R. *Dent. Mater.* **2010**, *26*, 1144.
17. Schneider, L. F. J.; Cavalcante, L. M.; Silikas, N. *J. Dent. Biomech.* **2010**, *1*, 131630.
18. Wang, C.; Zhou, B. *J. Mater. Sci. Lett.*, **1999**, *18*, 1259–1262.
19. Li, Z.; Cho, Y. H.; Kawakami, Y. *Polym Int*, **2007**, *56*, 666–673.
20. Fu, J.; Liu, W.; Liu, X.; Sapna, L. T.; Wan, Q.; Wang, H. *J. Wuhan. Univ. Technol. Mater. Sci. Ed.* **2014**, *29*, 384.
21. Bailey, W. J.; *Elastoplast*, **1973**, *5*, 142.
22. Chikaoka, S.; Takata, T.; Endo, T. *Macromolecules.* **1994**, *27*, 2380.
23. Hall Jr., H. K.; DeBlauwe, F.; Pyriadi, T. *J. Am. Chem. Soc.*, **1975**, *97*, 3854.
24. Endo, T.; Sato, H.; Takata, T. *Macromolecules*, **1987**, *20*, 1416.
25. Bodenbenner, K. *Justus Liebigs Ann.* **1959**, *625*, 183.
26. Igarashi, M.; Takata, T.; Endo, T. *Macromolecules.* **1994**, *27*, 2628.
27. Matejka, L.; Dusek, K.; Chabanne, P.; Pascault, J. P. *J. Polym. Sci. Part A: Polym Chem.* **1997**, *35*, 665.

28. Nishida, H.; Sanda, F.; Endo, T.; Nakahara, T.; Ogata, T.; Kusumoto, K. *J. Polym. Sci. Part A: Polym Chem.*, **2000**, *38*, 68.
29. Nishida, H.; Morikawa, H.; Nakahara, T.; Ogata, T.; Kusumoto, K.; Endo, T. *Polymer* **2005**, *46*, 2531.
30. Tortoreto, C.; Achard, T.; Egger, L.; Guenee, L.; Lacour J. *Org. Lett.* **2016**, *18*, 240.
31. Chabanne, P.; Tighzert, L.; Pascault, J. P. *J. Polym. Sci. Part A: Polym Chem.* **1994**, *53*, 787.
32. Bailey, W. J.; Iwama, H.; Tsushima, R. *J. Polym. Sci. Symp.*, **1976**, *56*, 117.
33. Takata, T.; Endo, T. *Prog. Polym. Sci.*, **1993**, *18*, 839.
34. Hsu, Y.; Wan, Y. *J. Polym. Sci. Part A: Polym Chem.*, **2009**, *47*, 3680.
35. Hsu, Y.; Wan, Y.; Lin, W.; Hsieh, W. *Macromolecules*. **2010**, *43*, 8430.
36. Chikaoka, S.; Takata, T.; Endo, T. *J. Polym. Sci., Polym. Chem. Ed.* **1990**, *28*, 3101.
37. Bailey, W. J.; Sun, R. L. *Am. Chem. Soc., Div. Polym. Chem.* **1972**, *13*, 281.
38. Matyjaszewski, K. *J. Polym. Sci. Part A: Polym Chem.* **1984**, *22*, 29.
39. Chikaoka, S.; Takata, T.; Endo, T. *Macromolecules*, **1991**, *24*, 6557.
40. Yokozawa, T.; Sato, M.; Endo, T. *J. Polym. Sci. Part A: Polym Chem.* **1990**, *28*, 1841.
41. Chikaoka, S.; Takata, T.; Endo, T. *Macromolecules*. **1991**, *24*, 331.
42. Chikaoka, S.; Takata, T.; Endo, T. *Macromolecules*, **1992**, *25*, 625.
43. Chikaoka, S.; Takata, T.; Endo, T. *Polym. Repr. Jpn.* **1989**, 1437.
44. Nishida, H.; Morikawa, H.; Nakahara, T.; Ogata, T.; Kusumoto, K.; Endo, T. *Polymer*. **2005**, *46*, 2531.
45. Kume, M.; Hirano, A.; Ochiai, B.; Endo, T. *J. Polym. Sci. Part A: Polym Chem.* **2006**, *44*, 3666.
46. Canadell, J.; Mantecon, A.; Cadiz, V. *J. Polym. Sci. Part A: Polym Chem.* **2007**, *45*, 1920.
47. Canadell, J.; Hunt, B.J.; Cook, A.G.; Mantecon, A.; Cadiz, V. *Polym. Degrad. Stab.* **2007**, *92*, 1482.
48. Frost, C. G.; Hartley, J. P. *Mini-Rev. Org. Chem.* **2004**, *1*, 1.
49. Loh, T. P.; Chua, G. L. *Chem. Commun.* **2006**, 2739.
50. Shen, Z. L.; Wang, S. Y.; Chok, Y. K.; Xu, Y. H.; Loh, T. P., *Chem. Rev.* **2013**, *113*, 271.
51. Maudoux, N.; Roisnel, N.; Carpentier, J.-F.; Sarazin, Y. *Organometallics* **2014**, *33*, 5740.
52. Ghosh, S.; Gowda, R. R.; Jagan, R.; Chakraborty, D. *Dalton Trans.* **2015**, *44*, 10410.
53. Schnee, G.; Bolley, A.; Hild, F.; Specklin, D.; Dagonne, S. *Catalysis Today*, In Press, Corrected Proof, Available online 24 August 2016.
54. Kremer, A. B.; Osten, K. M.; Yu, I.; Ebrahimi, T.; Aluthge, D. C.; Mehrkhodavandi, P. *Inorg. Chem.* **2016**, *55*, 5365.
55. Horeglad, P.; Cybularczyk, M.; Litwińska, A.; Dąbrowska, A. M.; Dranka, M.; Z.Żukowska, G.; Urbańczyk, M.; Michalak, M. *Polym. Chem.* **2016**, *7*, 2022.
56. Maudoux, N.; Tan, E.; Hu, Y.; Roisnel, T.; Dorcet, V.; Carpentier, J.-F.; Sarazin, Y. *Main Group Met. Chem.* **2016**, *39*, 131
57. Douglas, A. F.; Patrick, B. O.; Mehrkhodavandi, P. *Angew. Chem. Int. Ed.* **2008**, *47*, 2290.

58. Yu, I.; Acosta-Ramirez, A.; Mehrkhodavandi, P., *J. Am. Chem. Soc.* **2012**, *134*, 12758.
59. Acosta-Ramirez, A.; Douglas, A. F.; Yu, I.; Patrick, B. O.; Diaconescu, P. L.; Mehrkhodavandi, P. *Inorg. Chem.* **2010**, *49*, 5444.
60. Osten, K. M.; Yu, I.; Duffy, I. R.; Lagaditis, P. O.; Yu, J C.-C.; Wallis, C. J.; Mehrkhodavandi, P. *Dalton Trans.* **2012**, *41*, 8123.
61. Osten, K. M.; Aluthge, D. C.; Patrick, B. O.; Mehrkhodavandi, P. *Inorg. Chem.* **2014**, *53*, 9897.
62. Osten, K. M.; Aluthge, D. C.; Mehrkhodavandi, P. *Dalton Trans.* **2015**, *44*, 6126.
63. Aluthge, D. C.; Patrick, B. O.; Mehrkhodavandi, P. *Chem. Commun.* **2013**, *49*, 4295.
64. Atwood, D. A.; Jegier, J. A.; Rutherford, D. *J. Am. Chem. Soc.* **1995**, *117*, 6779.
65. Munoz-Hernandez, M.-A.; McKee, M. L.; Keizer, T. S.; Yearwood, B. C.; Atwood, D. A. *J. Chem. Soc., Dalton Trans.* **2002**, 410.
66. Jegier, J. A.; Munoz-Hernandez, M.-A.; Atwood, D. A. *J. Chem. Soc., Dalton Trans.* **1999**, 2583.
67. Liu, S.; Muñoz-Hernandez, M.-A.; Atwood, D. A. *J. Organomet. Chem.* **2000**, *596*, 109.
68. Dagonne, S.; Bouyahyi, M.; Vergnaud, J.; Carpentier, J.-F. *Organometallics* **2010**, *29*, 1865.
69. Nakata, N.; Saito, Y.; Ishii, A. *Organometallics.* **2014**, *33*, 1840.
70. Emig, N.; Nguyen, H.; Krautscheid, H.; Reau, R.; Cazaux, J.-B.; Bertrand, G. *Organometallics.* **1998**, *17*, 3599.
71. Dagonne, S.; Lavanant, L.; Welter, R.; Chassenieux, C.; Haquette, P.; Jaouen, G. *Organometallics.* **2003**, *22*, 3732.
72. Dagonne, S. *C. R. Chim.* **2006**, *9*, 1143.
73. Dagonne, S.; Janowska, I.; Welter, R.; Zakrzewski, J.; Jaouen, G. *Organometallics.* **2004**, *23*, 4706.
74. Dagonne, S. *J. Organomet. Chem.* **2006**, *691*, 4797.
75. Dagonne, S.; Le Bideau, F.; Welter, R.; Bellemin-Laponnaz, S.; Maise-Francois, A. *Chem. Eur. J.* **2007**, *13*, 3202.
76. Milione, S.; Grisi, F.; Centore, R.; Tuzi, A. *Organometallics.* **2006**, *25*, 266.
77. Saunders Baugh, L.; Sissano, J. A. *J. Polym. Sci. A: Polym. Chem.* **2002**, *40*, 1633.
78. Lewiński, J.; Horeglad, P.; Dranka, M.; Justyniak, I. *Inorg. Chem.* **2004**, *43*, 5789.
79. Delpech, F.; Guzei, I. A.; Jordan, R. F. *Organometallics.* **2002**, *21*, 1167.
80. Peckermann, I.; Robert, D.; Englert, U.; Spaniol, T. P.; Okuda, J. *Organometallics* **2008**, *27*, 4817.
81. Robson, D. A.; Bylikin, S. Y.; Cantuel, M.; Male, N. A. H.; Rees, L. H.; Mountford, P.; Schroder, M. *J. Chem. Soc., Dalton Trans.* **2001**, 157.
82. Chamazi, N. N.; Heravi, M. M.; Breyhan, T.; Neumuller, B. Z. *Anorg. Allg. Chem.* **2007**, *633*, 1243.
83. Cheng, F.; Friend, S. I.; Hector, A. L.; Levason, W.; Reid, G.; Webster, M.; Zhang, W. *Inorg. Chem.* **2008**, *47*, 9691.

84. Peckermann, I.; Dols, T. S.; Spaniol, T. P.; Okuda, J. *J. Organomet. Chem.* **2010**, *695*, 2325.
85. Surendra, K.; Corey, E. J. *J. Am. Chem. Soc.* **2014**, *136*, 10918.
86. Michelet, B.; Colard-Itte, J. R.; Thiery, G.; Guillot, R.; Bour, C.; Gandon, V. *Chem. Commun.* **2015**, *51*, 7401.
87. Kessler, M.; Knapp, C.; Zogaj, A. *Organometallics.* **2011**, *30*, 3786.
88. Yu, I. Ph.D. Thesis, University of British Columbia, BC, Canada, 2012
89. Li, Y. F.; Ward, D. G.; Reddy, S. S.; Collins, S. *Macromolecules.* **1997**, *30*, 1875.
90. Yasuda, H.; Yamamoto, H.; Yokota, K.; Miyake, S.; Nakamura, A. *J. Am. Chem. Soc.* **1992**, *114*, 4908.
91. Osman, K. M.; Powell, D. R.; Wehmschulte, R. J. *Inorg. Chem.* **2015**, *54*, 9195.
92. Sarazin, Y.; Carpentier, J. F., *Chem. Rev.* **2015**, *115*, 3564.
93. Chang, C.; Yu, I.; Mehrkhodavandi, P. *Manuscript in preparation.*
94. Zhang, X.; Emge, T. J.; Hultsch, K. C. *Angew. Chem. Int. Ed.* **2012**, *51*, 394.
95. Beachley, O. T.; Rusinko, R. N. *Inorg. Chem.* **1979**, *18*, 1966.
96. Bulc, N.; Golic, L. *Acta Cryst.* **1983**, C39, 174.
97. Pei, J.; Lin, M.; Loh, T.-P. *Chem. Commun.* **1996**, 2315.
98. Patric Lindqvist-Reis, P.; Muñoz-Pa'ez, A.; Dí'az-Moreno, S.; Pattanaik, S.; Persson, I.; Sandstrom, M. *Inorg. Chem.* **1998**, *37*, 6675.
99. Seward, T. M.; Henderson, C. M. B.; Charnock, J. M. *Chemical Geology.* **2000**, *167*, 117.
100. Rudolph, W. W.; Fischer, D.; Tomney, M. R.; Pye, C. C. *Phys. Chem. Chem. Phys.* **2004**, *6*, 5145.
101. Hua, M.; Wang, M.; Zhang, P.; Wang, L.; Zhu, F.; Sun, L. *Inorg. Chem. Commun.* **2010**, *13*, 968.
102. Lakin, N. M.; Varberg, T. D.; Brown, J. M. *J. Mol. Spectrosc.* **1997**, *183*, 34.
103. Hong, M.; Chen, E. Y.-X. *Nat. Chem.* **2016**, *8*, 42.
104. Morgan, K. M.; Gronert, S. *J. Org. Chem.* **2000**, *65*, 1461.
105. Morgan, K. M.; Ellis, J.A.; Lee, J.; Fulton, A.; Wilson, S. L.; Dupart, P. S.; Dastoori, R. *J. Org. Chem.* **2013**, *78*, 4303.
106. Thanks to Prof Sammis for his suggestion of other possible products from the reaction of lactone and epoxide.

Appendices

A. Characterization of compounds in solution

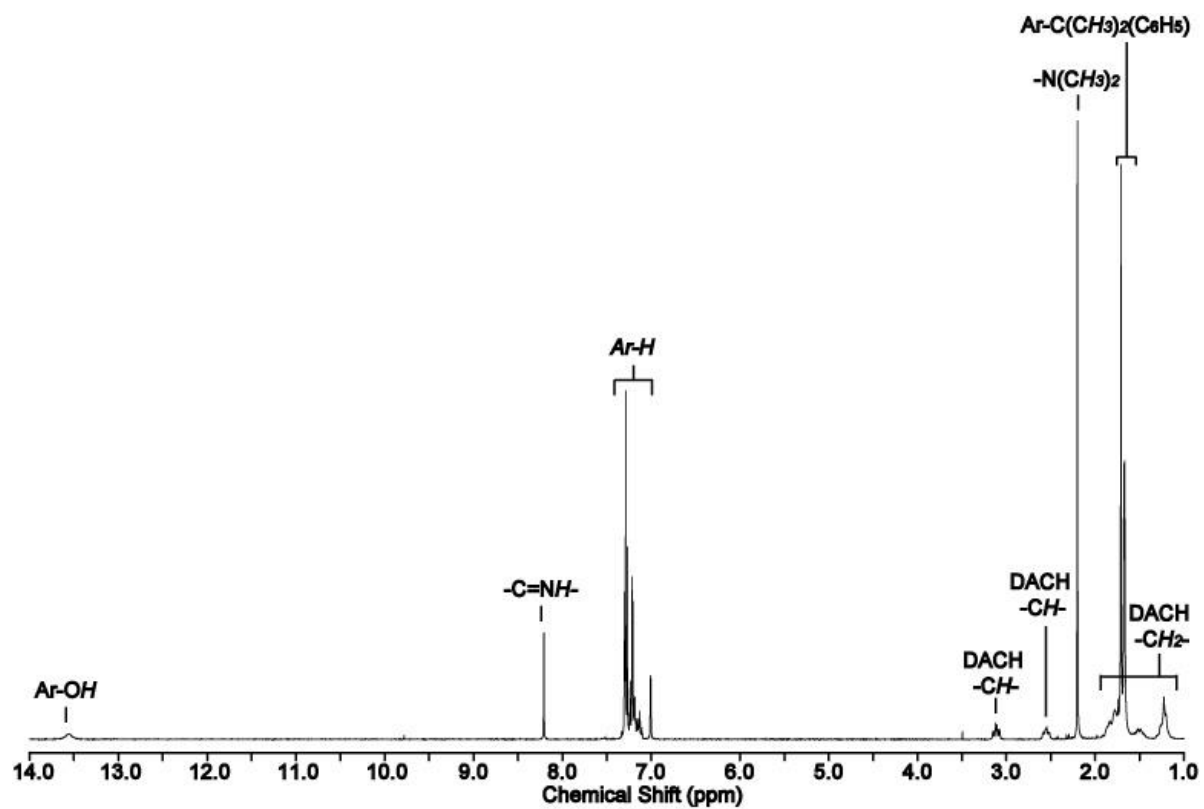


Figure A-1. ^1H NMR spectrum (300 MHz, CDCl_3 , 25 °C) of (\pm)-H(NNO) (**27**).

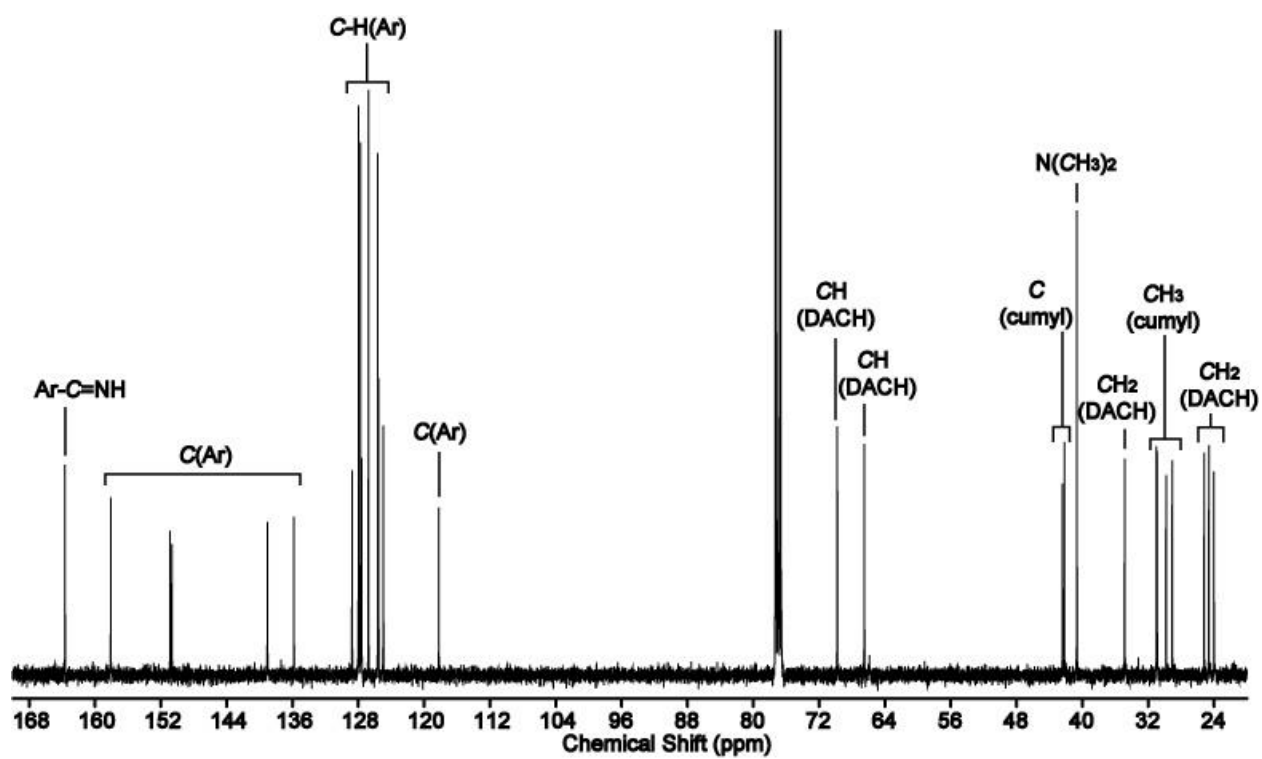
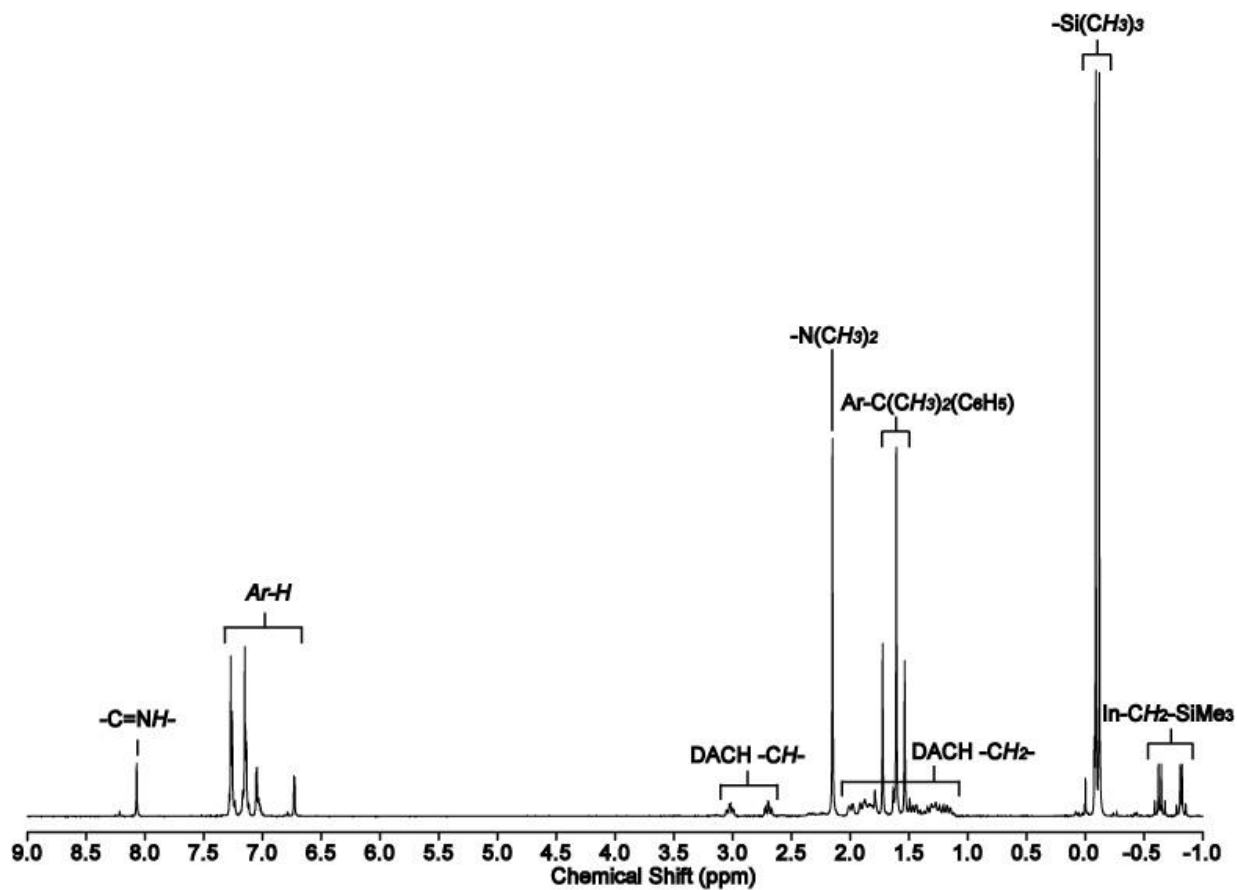


Figure A-2. $^{13}\text{C}\{^1\text{H}\}$ NMR spectrum (101 MHz, CDCl_3 , 25 °C) of (\pm)-H(NNO) (**27**).



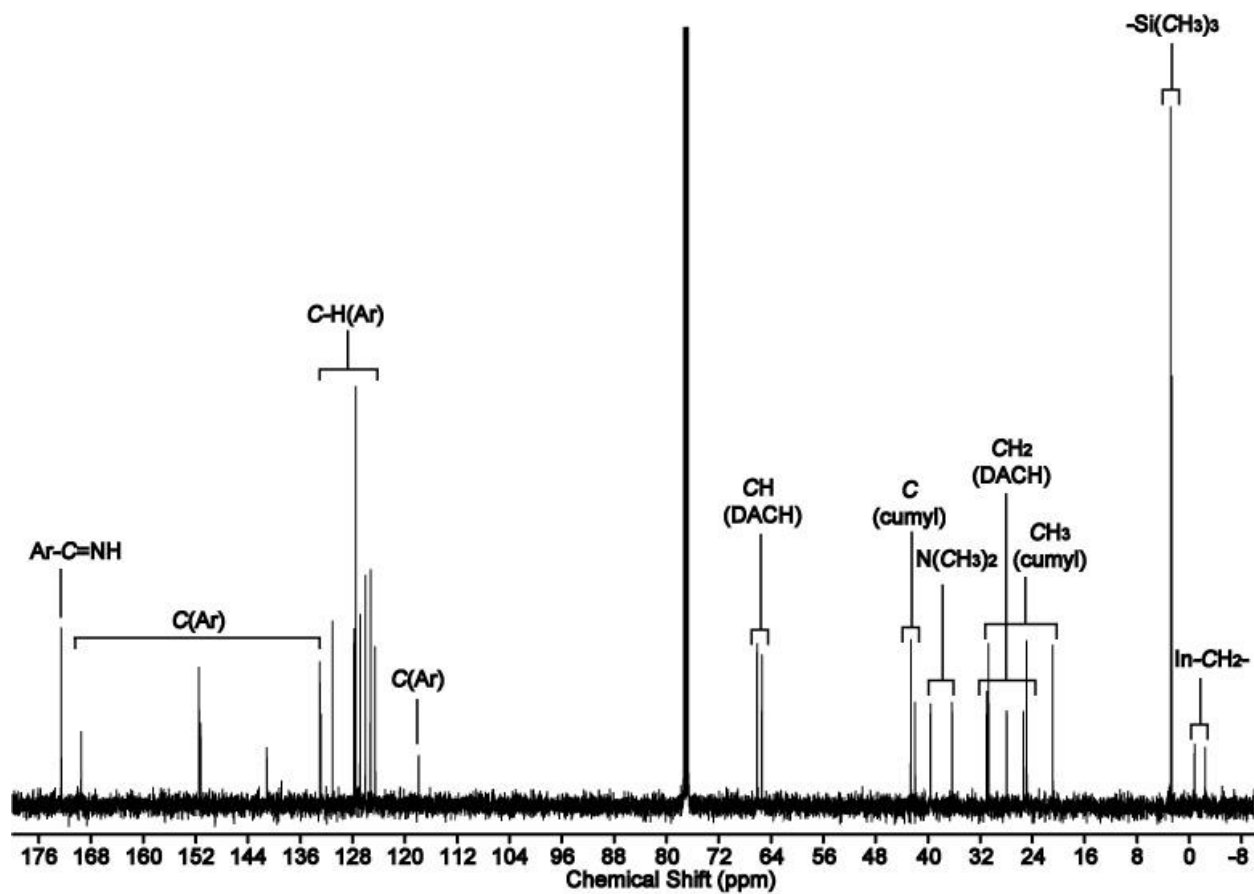


Figure A-4. $^{13}\text{C}\{^1\text{H}\}$ NMR spectrum (101 MHz, CDCl_3 , 25 °C) of $(\pm)\text{-(NNO)In(CH}_2\text{SiMe}_3)_2$ (28).

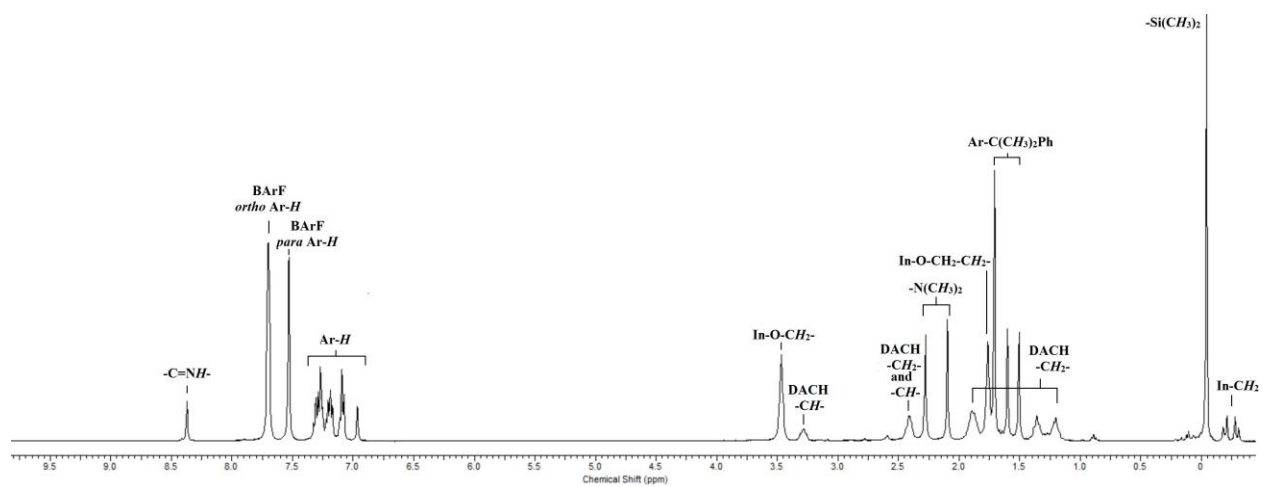


Figure A-5. ^1H NMR spectrum (400 MHz, CDCl_3 , 25 $^\circ\text{C}$) of (\pm) - $[(\text{NNO})\text{In}(\text{CH}_2\text{SiMe}_3)(\text{THF})][\text{BAr}^{\text{F}}]$ (**30**).

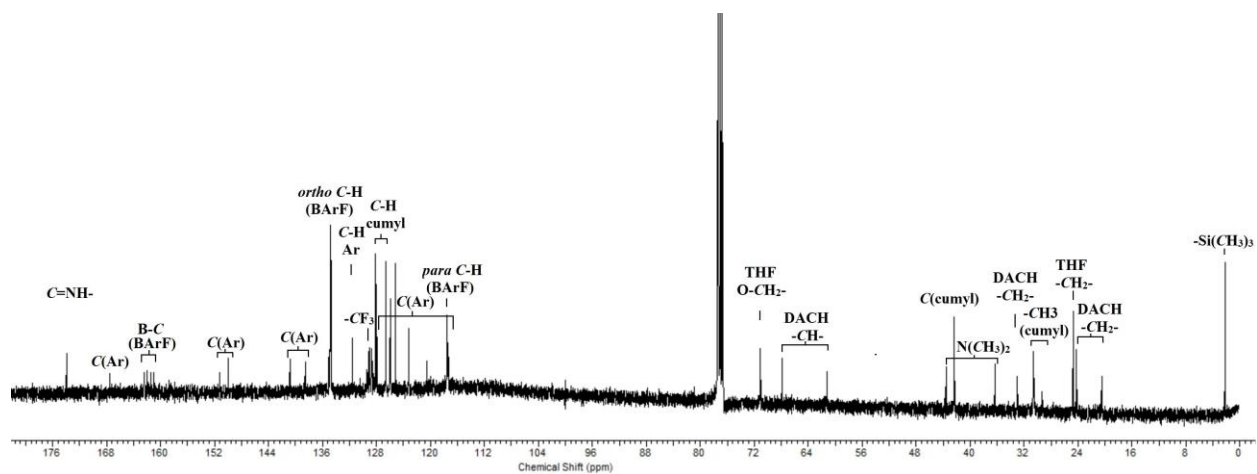


Figure A-6. $^{13}\text{C}\{^1\text{H}\}$ NMR spectrum (400 MHz, CDCl_3 , 25 $^\circ\text{C}$) of (\pm)- $[(\text{NNO})\text{In}(\text{CH}_2\text{SiMe}_3)(\text{THF})][\text{BAr}^{\text{F}}]$ (**30**).

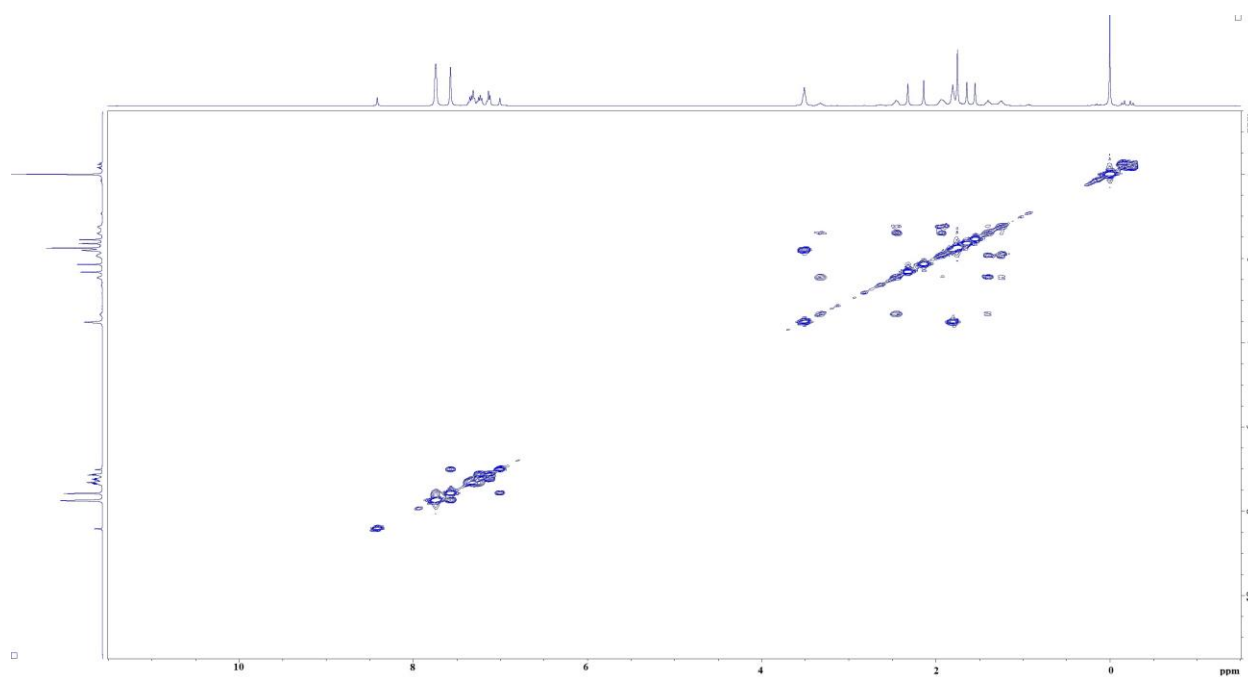


Figure A-7. 2D ^1H - ^1H COSY NMR spectrum (CDCl_3 , 25 $^\circ\text{C}$) of (\pm)- $[(\text{NNO})\text{In}(\text{CH}_2\text{SiMe}_3)(\text{THF})][\text{BAR}^{\text{F}}]$ (**30**).

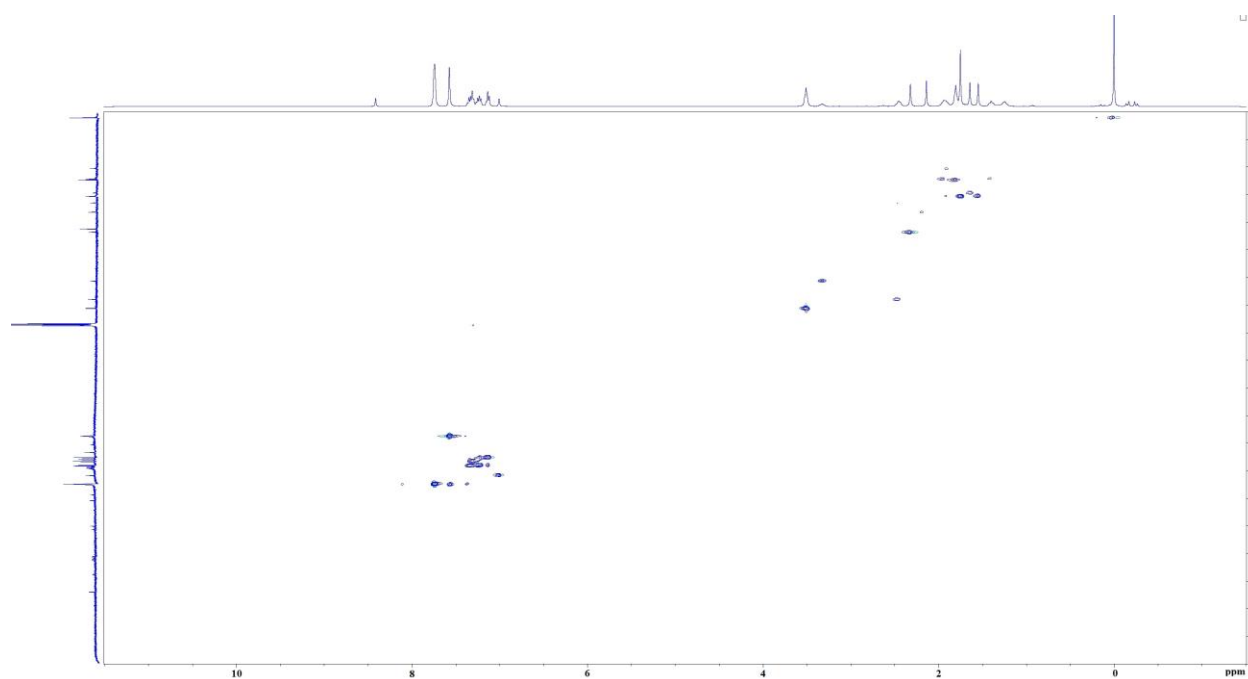


Figure A-8. 2D ^{13}C - ^1H Heteronuclear Single Quantum Coherence (HSQC) NMR spectrum (CDCl_3 , 25 $^\circ\text{C}$) of (\pm)- $[(\text{NNO})\text{In}(\text{CH}_2\text{SiMe}_3)(\text{THF})][\text{BAr}^{\text{F}}]$ (**30**).

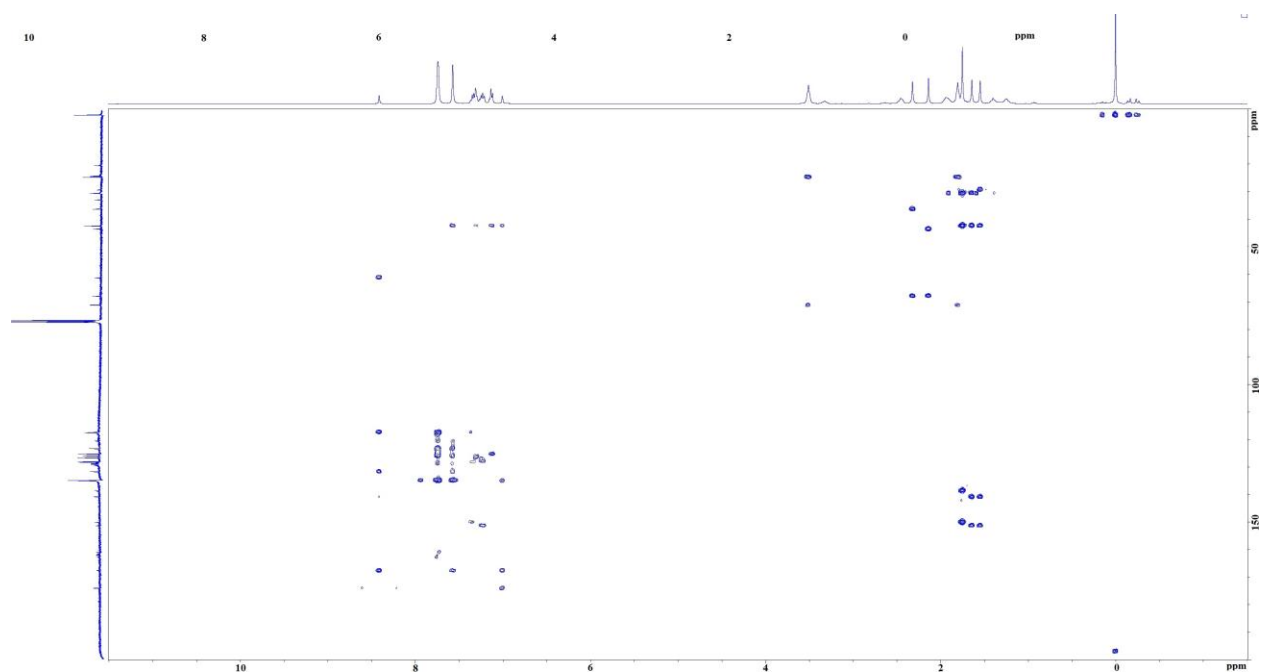


Figure A-9. 2D ^{13}C - ^1H Heteronuclear Multiple Bond Correlation (HMBC) NMR spectrum (CDCl_3 , 25 $^\circ\text{C}$) of (\pm) - $[(\text{NNO})\text{In}(\text{CH}_2\text{SiMe}_3)(\text{THF})][\text{BAr}^{\text{F}}]$ (**30**).

B. Characterization of compounds in the solid state

Table B-1. Crystallography table

| | 28 | 30 | 30•H₂O |
|--|---|---|---|
| empirical formula | C ₄₁ H ₆₃ InN ₂ OSi ₂ | C ₇₃ H ₇₂ B ₁ F ₂₄ InN ₂ O ₂ Si | C ₇₃ H ₇₂ BF ₂₄ InN ₂ O ₂ Si |
| fw | 770.93 | 1619.04 | 1619.04 |
| <i>T</i> (K) | 100 | 296.15 | 90 |
| <i>a</i> (Å) | 11.6281(15) | 21.188(5) | 13.8359(13) |
| <i>b</i> (Å) | 13.7428(16) | 13.401(4) | 14.8225(14) |
| <i>c</i> (Å) | 25.852(3) | 30.278(7) | 20.389(2) |
| <i>α</i> (deg) | 90 | 90 | 94.893(2) |
| <i>β</i> (deg) | 96.798(3) | 109.686(4) | 107.042(2) |
| <i>γ</i> (deg) | 90 | 90 | 106.266(2) |
| volume (Å ³) | 4102.2(9) | 8095(4) | 3773.5(6) |
| <i>Z</i> | 4 | 4 | 2 |
| cryst syst | monoclinic | monoclinic | triclinic |
| space group | <i>P</i> 2 ₁ /c | <i>P</i> 2 ₁ /c | <i>P</i> -1 |
| <i>d</i> _{calc} (g/cm ³) | 1.248 | 1.329 | 1.425 |
| <i>μ</i> (Mo Kα) (cm ⁻¹) | 6.66 | 4.04 | 4.33 |
| 2 <i>θ</i> _{max} (deg) | 59.5 | 55.1 | 55.1 |
| absor corr (<i>T</i> _{min} , <i>T</i> _{max}) | 0.695, 0.925 | 0.673, 0.746 | 0.708, 0.746 |
| total no. of reflns | 54 400 | 78 600 | 66 700 |
| no. of indep reflns (<i>R</i> _{int}) | 11 490 (0.0499) | 18 685 (0.0382) | 16 850 (0.0435) |
| residuals (refined on <i>F</i> ²): <i>R</i> ₁ ; <i>wR</i> ₂ | 0.0840, 0.1645 | 0.0953, 0.2136 | 0.0818, 0.1501 |
| GOF | 1.336 | 0.908 | 1.034 |
| no. obsrvns [<i>I</i> > 2σ(<i>I</i>)] | 9781 | 14723 | 12950 |
| residuals (refined on <i>F</i> ² : <i>R</i> ₁ ^{<i>a</i>} ; <i>wR</i> ₂ ^{<i>b</i>}) | 0.0677, 0.1539 | 0.0748, 0.1918 | 0.0563, 0.1328 |

$${}^a R_1 = \sum ||F_o| - |F_c|| / \sum |F_o|. {}^b wR_2 = [\sum (w (F_o^2 - F_c^2)^2) / \sum w(F_o^2)_2]^{1/2}$$

C. Spiro-orthoesters characterization

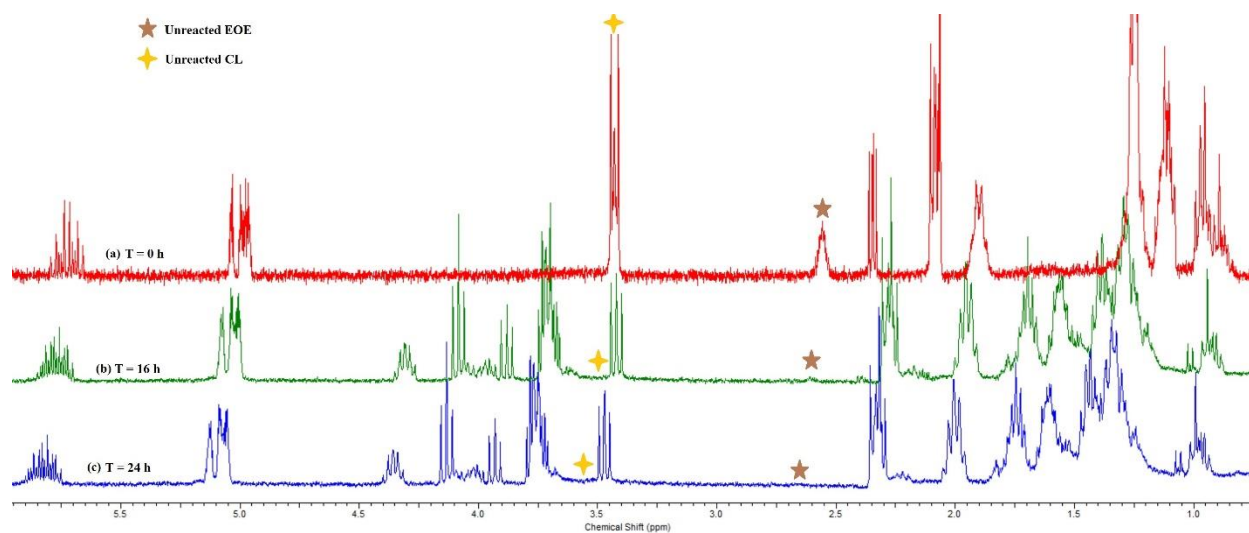


Figure C-1. Overlaid ¹H NMR spectra (300 MHz, C₆D₆, 25 °C) of spiro-orthoester synthesis of 40:40:1 mixture of CL:EOE:**30** overtime.

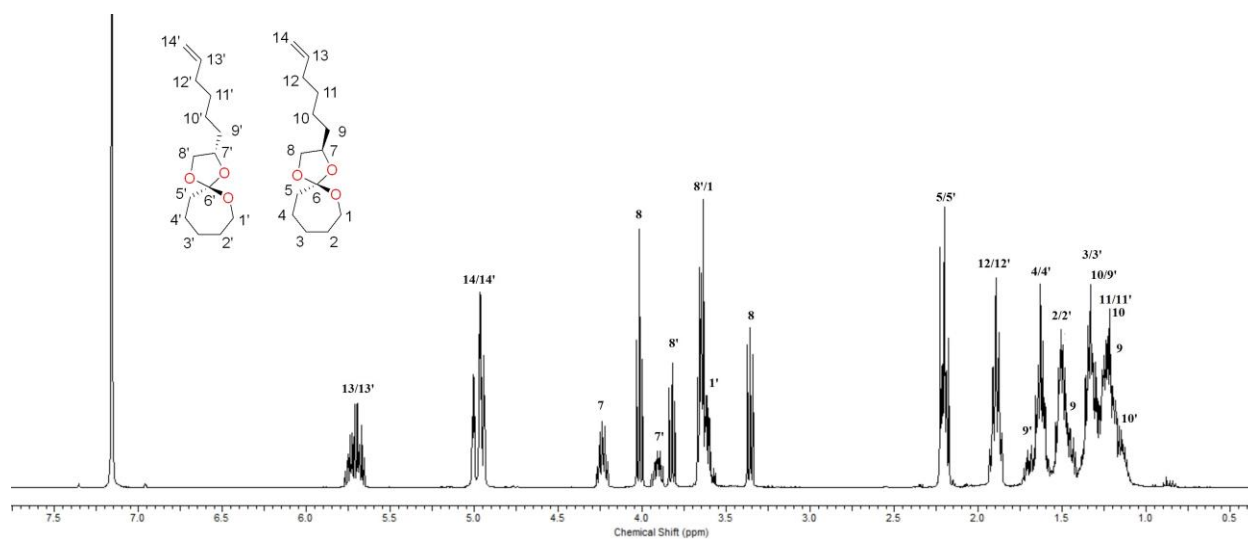


Figure C-2. ¹H NMR spectrum (400 MHz, C₆D₆, 25 °C) of SOE1 (CL+EOE).

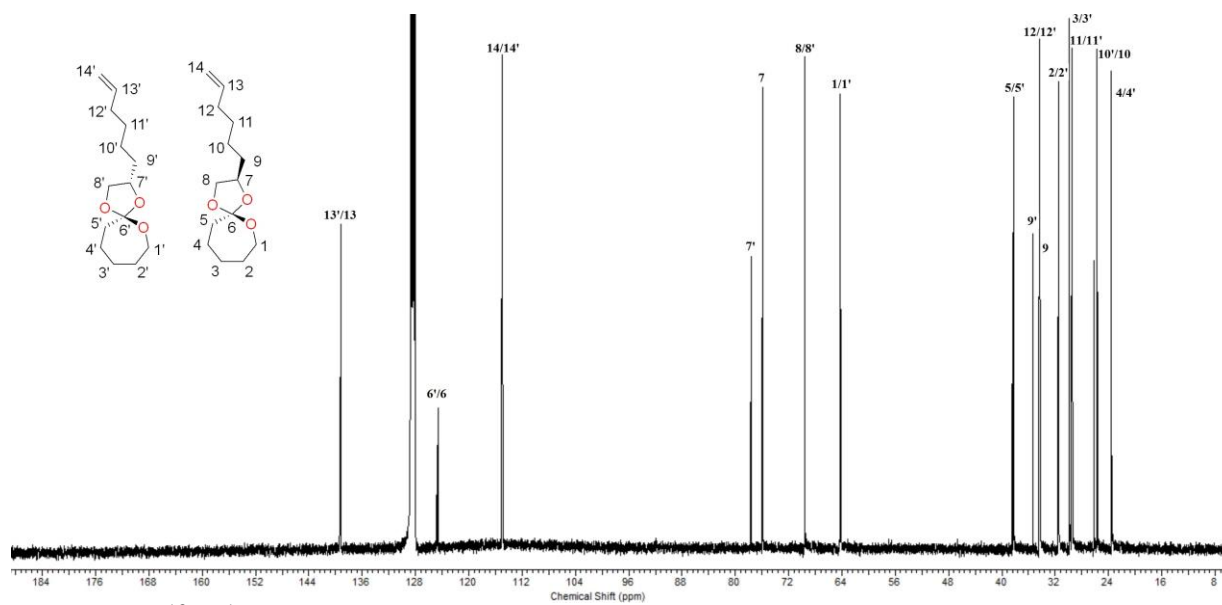


Figure C-3. $^{13}\text{C}\{^1\text{H}\}$ NMR spectrum (151 MHz, C_6D_6 , 25 °C) of SOE1 (CL+EOE).

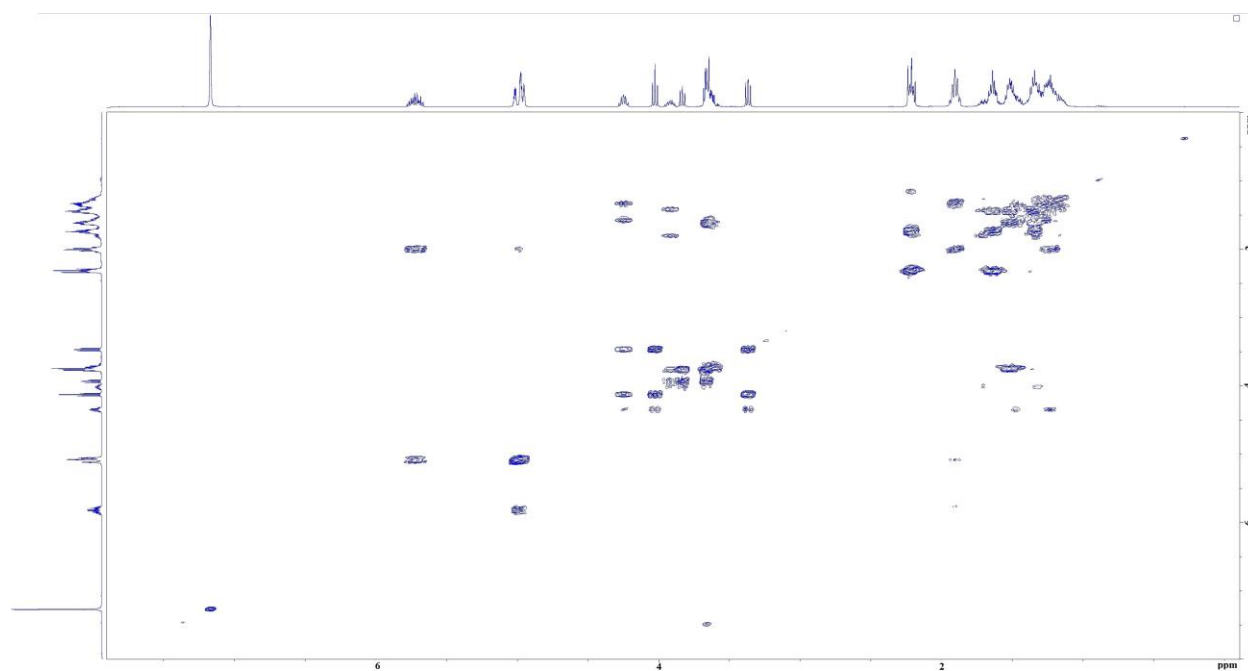


Figure C-4. 2D ^1H - ^1H COSY NMR spectrum (C_6D_6 , 25 $^\circ\text{C}$) of SOE1 (CL+EOE).

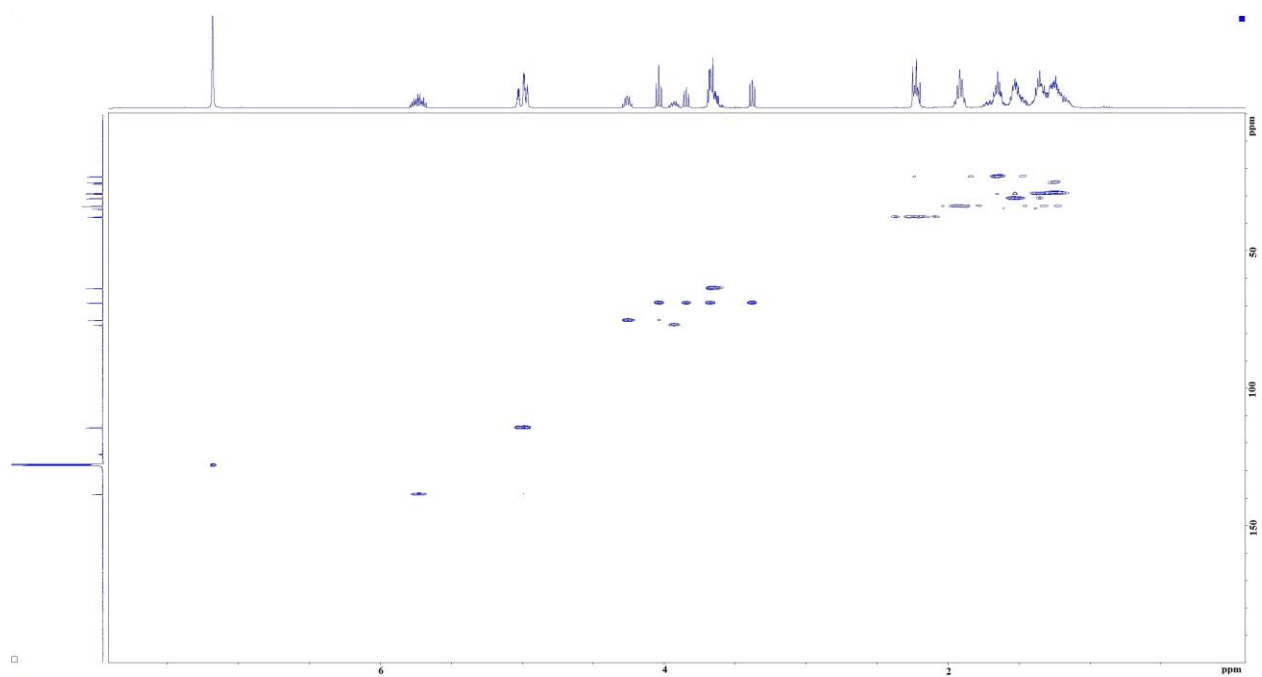


Figure C-5. 2D ^{13}C - ^1H Heteronuclear Single Quantum Coherence (HSQC) NMR spectrum (C_6D_6 , 25 °C) of SOE1 (CL+EOE).

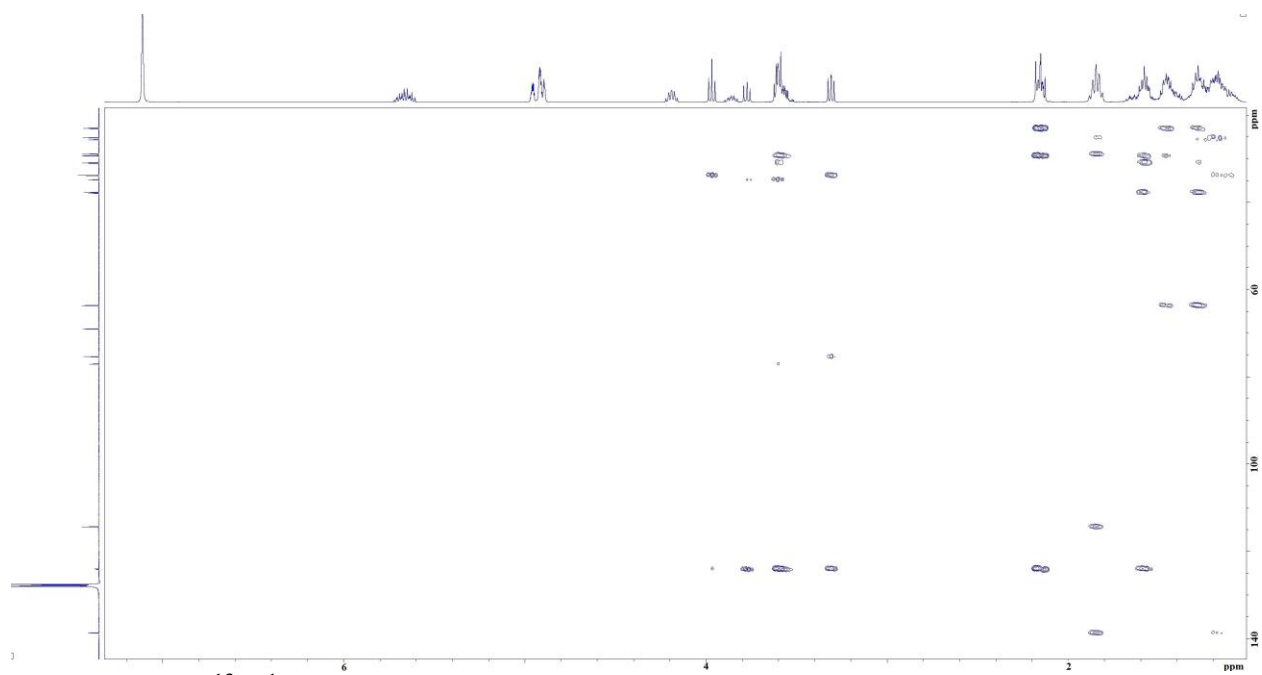


Figure C-6. 2D ^{13}C - ^1H Heteronuclear Multiple Bond Correlation (HMBC) NMR spectrum (C_6D_6 , 25 $^\circ\text{C}$) of SOE1 (CL+EOE).

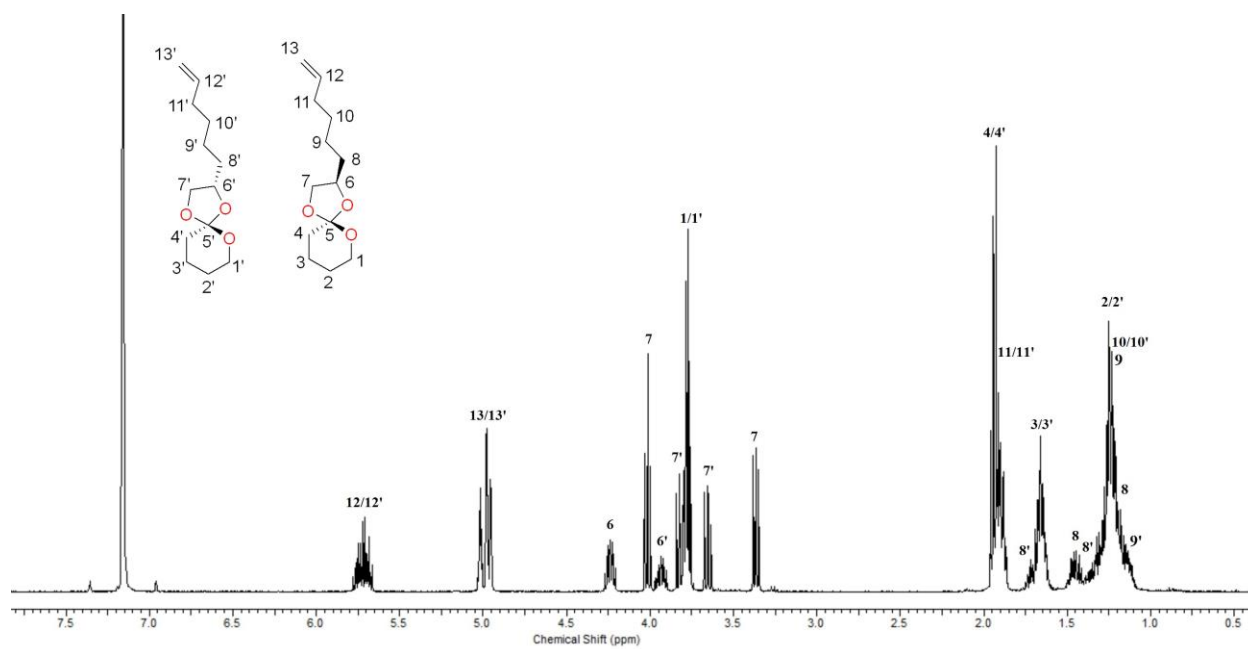


Figure C-7. ^1H NMR spectrum (400 MHz, C_6D_6 , 25 $^\circ\text{C}$) of SOE2 (VL+EOE).

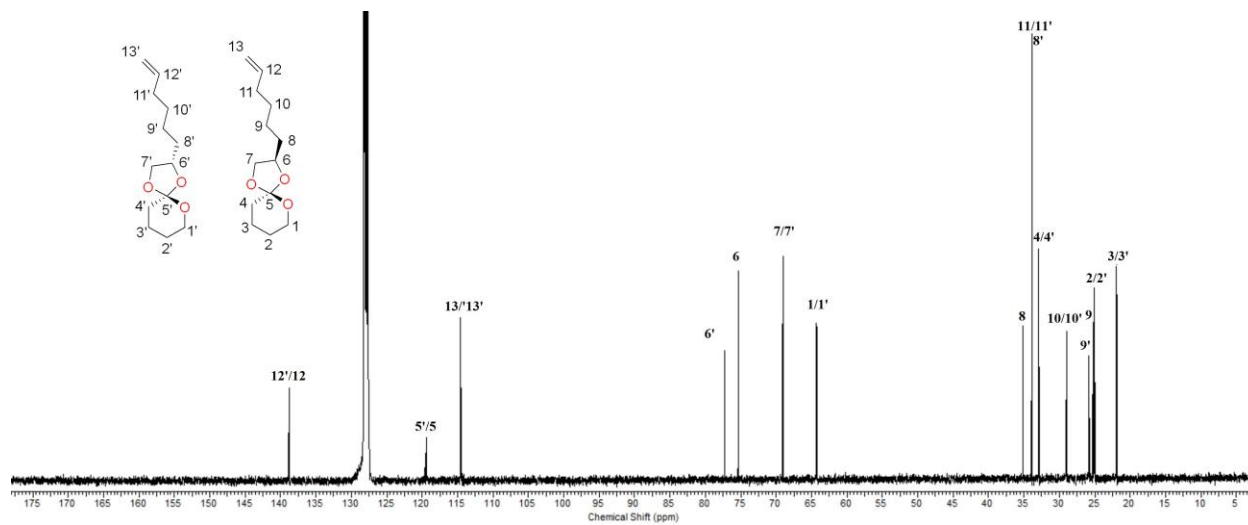


Figure C-8. $^{13}\text{C}\{^1\text{H}\}$ NMR spectrum (151 MHz, C_6D_6 , 25 °C) of SOE2 (VL+EOE).

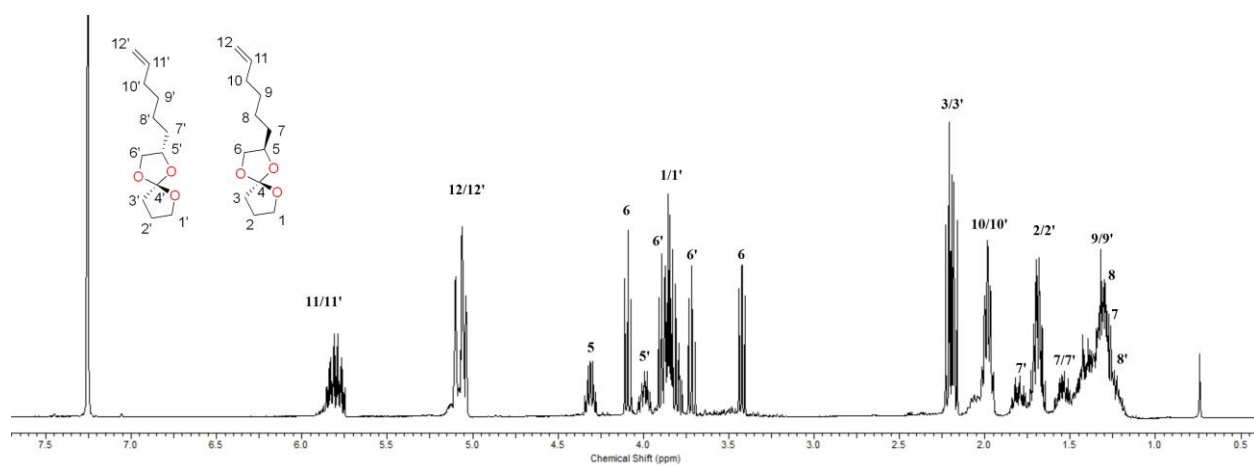


Figure C-9. ¹H NMR spectrum (400 MHz, C₆D₆, 25 °C) of SOE3 (BL+EOE).

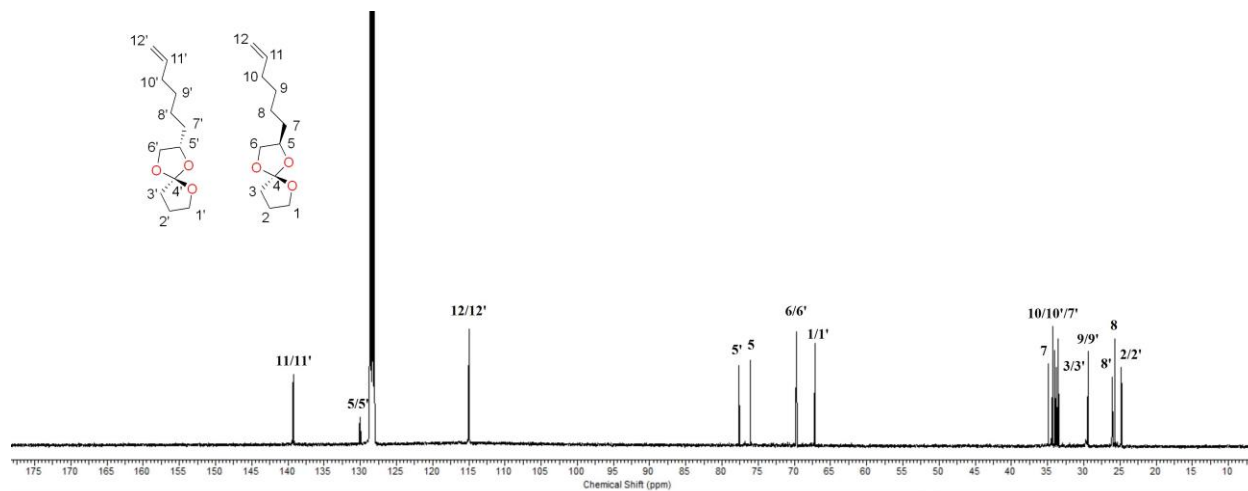


Figure C-10. $^{13}\text{C}\{^1\text{H}\}$ NMR spectrum (151 MHz, C_6D_6 , 25 °C) of SOE3 (BL+EOE).

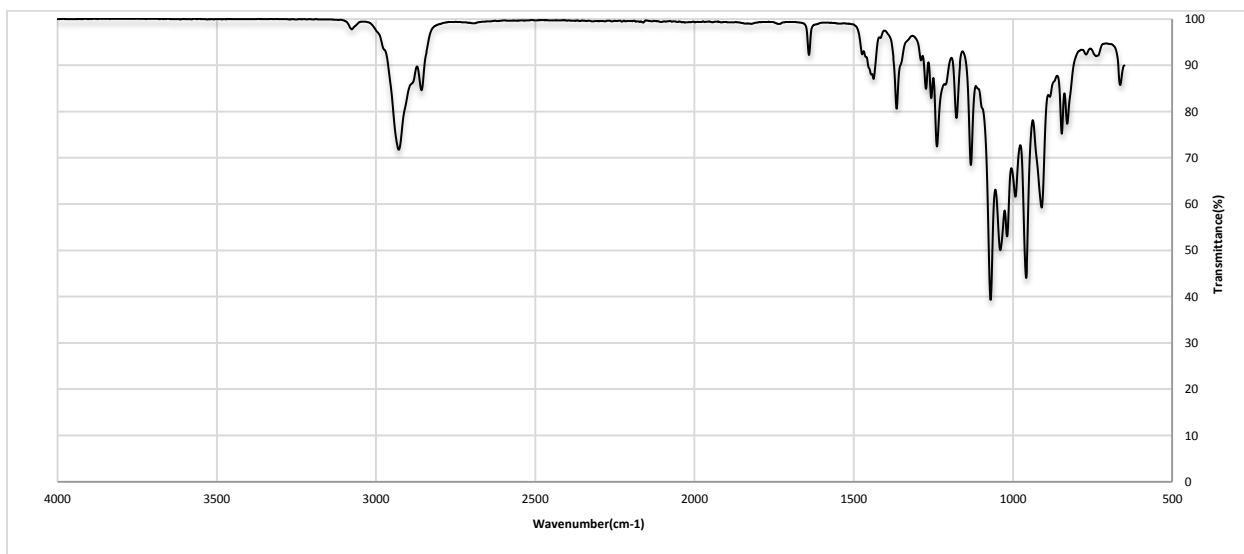


Figure C-11. FTIR Spectrum of SOE1 (CL+EOE).

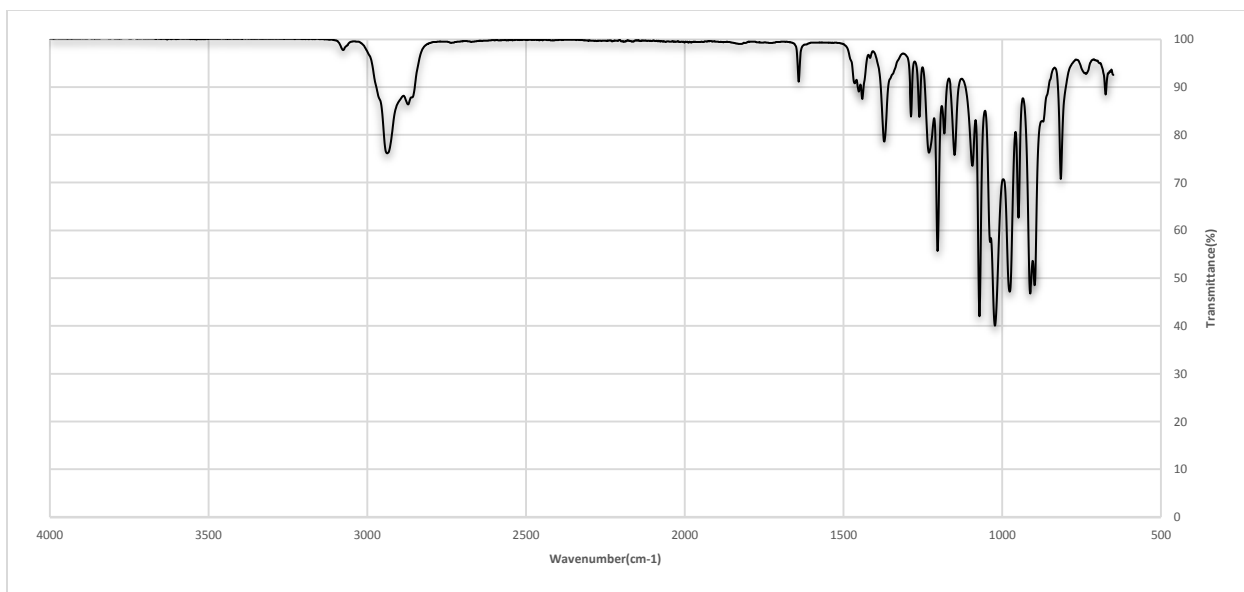


Figure C-12. FTIR Spectrum of SOE2 (VL+EOE).

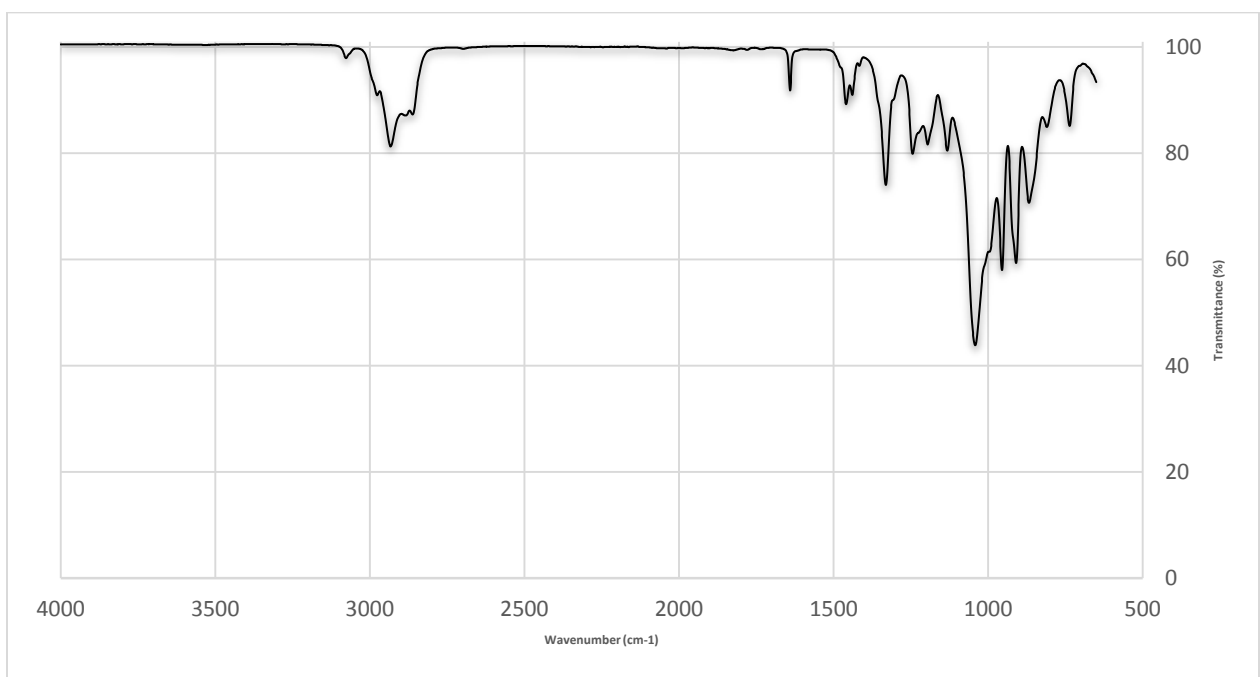
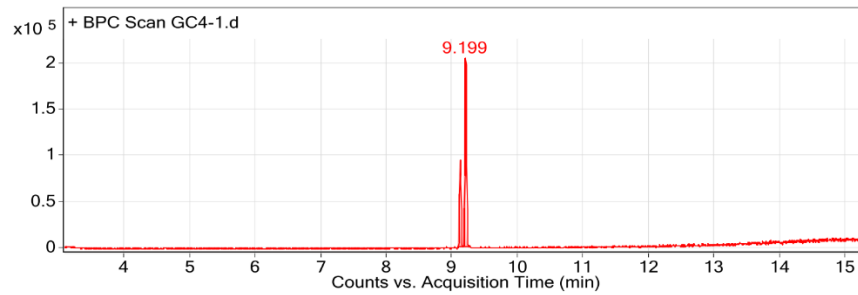


Figure C-13. FTIR Spectrum of SOE3 (BL+EOE).



Integration Peak List

| Peak | Start | RT | End | Height | Area | Area % |
|------|-------|-------|-------|----------|-----------|--------|
| 1 | 9.083 | 9.115 | 9.157 | 94112.52 | 149540.09 | 44.97 |
| 2 | 9.157 | 9.199 | 9.283 | 203849.2 | 332560.82 | 100 |

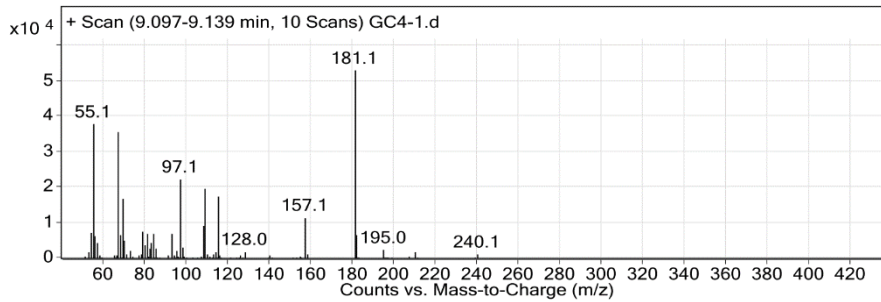
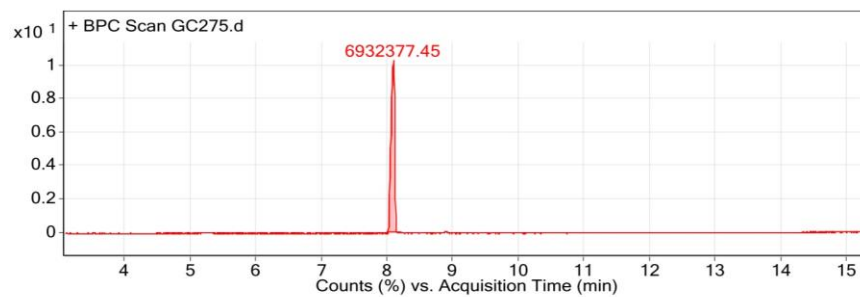


Figure C-14. GC-EIMS report for SOE1 (CL+EOE).



Integration Peak List

| Peak | Start | RT | End | Height | Area | Area % |
|------|-------|-------|-------|------------|------------|--------|
| 1 | 7.994 | 8.087 | 8.226 | 1751386.89 | 6932377.45 | 100 |

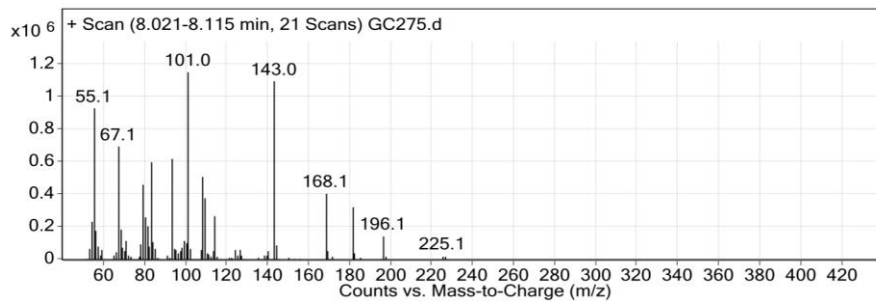


Figure C-15. GC-EIMS report for SOE2 (VL+EOE).

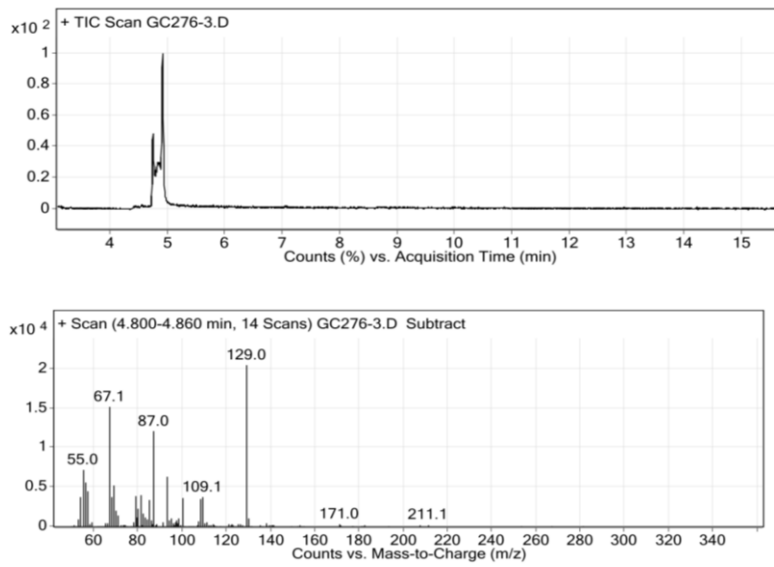


Figure C-16. GC-EIMS report for SOE3 (BL+EOE).

D. Spiro-orthoester (SOE1) polymerization

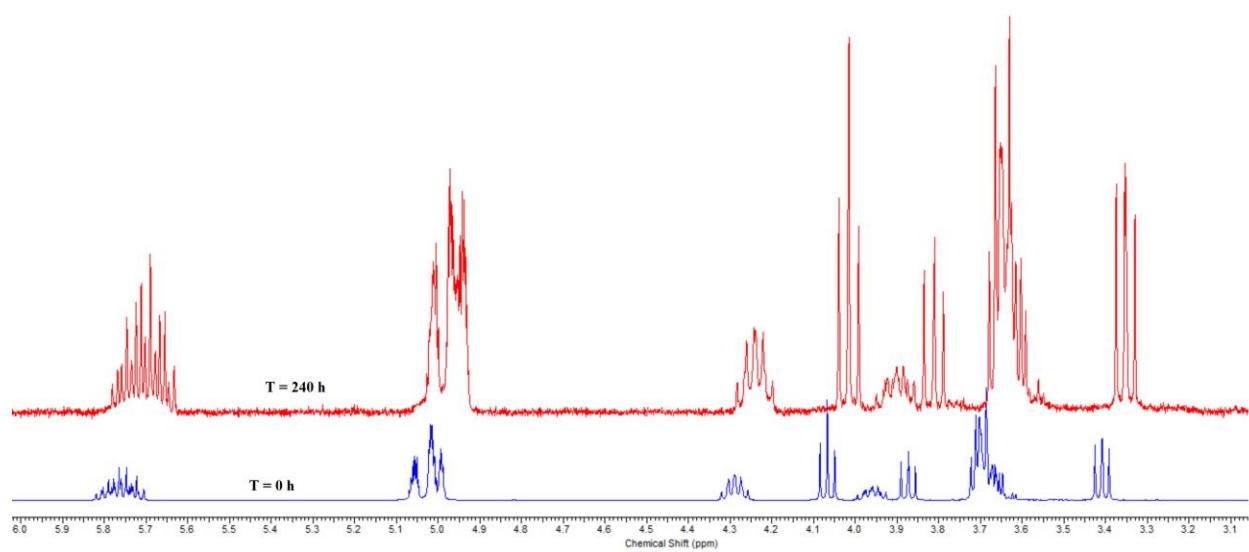


Figure D-1. Overlaid ^1H NMR spectra (300 MHz, C_6D_6 , 25 °C) of SOE1 polymerization at 25 °C overtime.

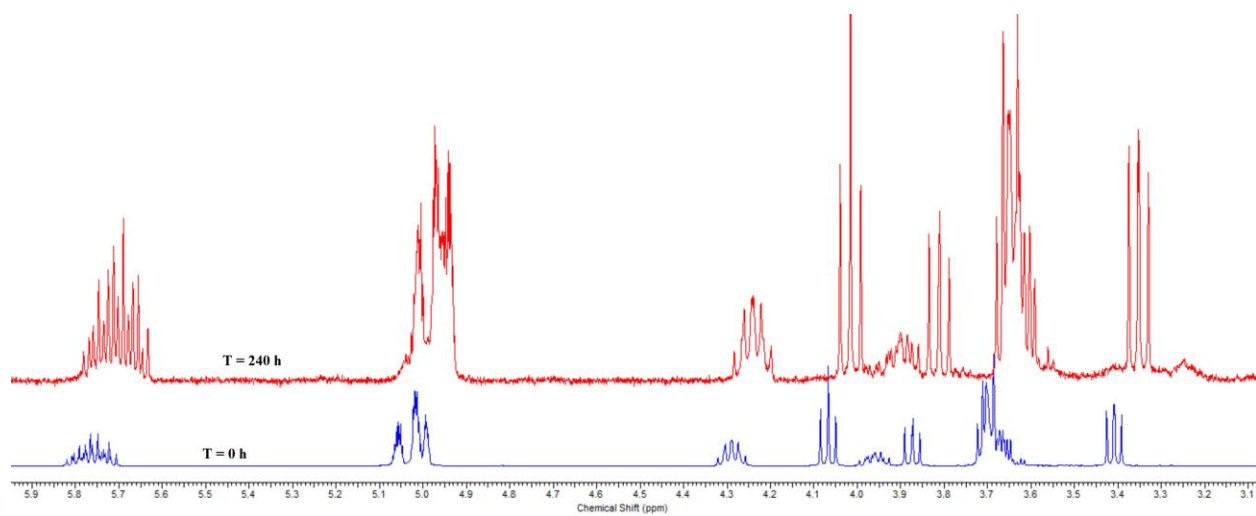


Figure D-2. Overlaid ¹H NMR spectra (300 MHz, C₆D₆, 25 °C) of SOE1 polymerization at 60 °C overtime.

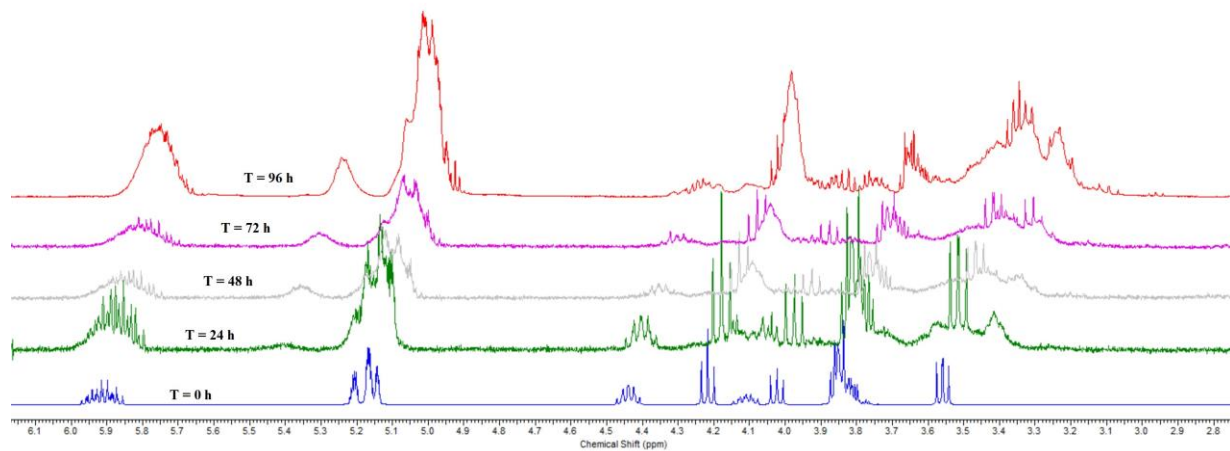


Figure D-3. Overlaid ¹H NMR spectra (300 MHz, C₆D₆, 25 °C) of SOE1 polymerization at 110°C overtime.

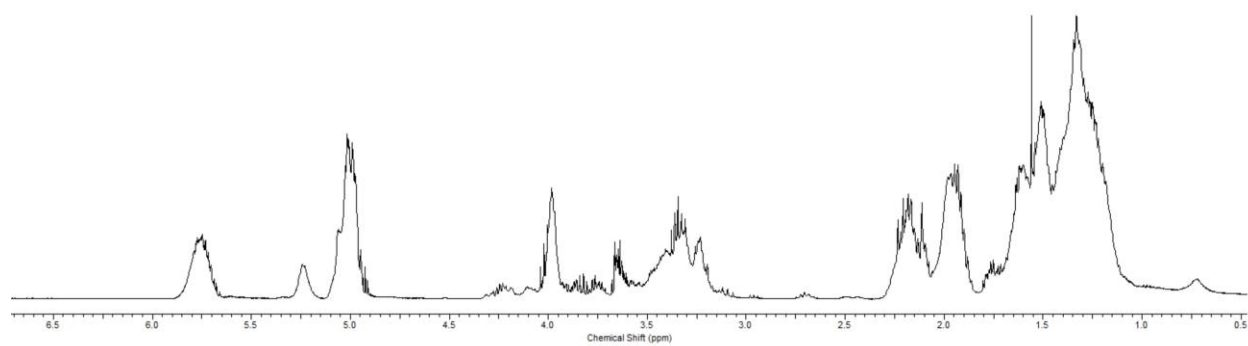


Figure D-4. ^1H NMR spectrum (400 MHz, C_6D_6 , 25 $^\circ\text{C}$) of polymerization product of SOE1.

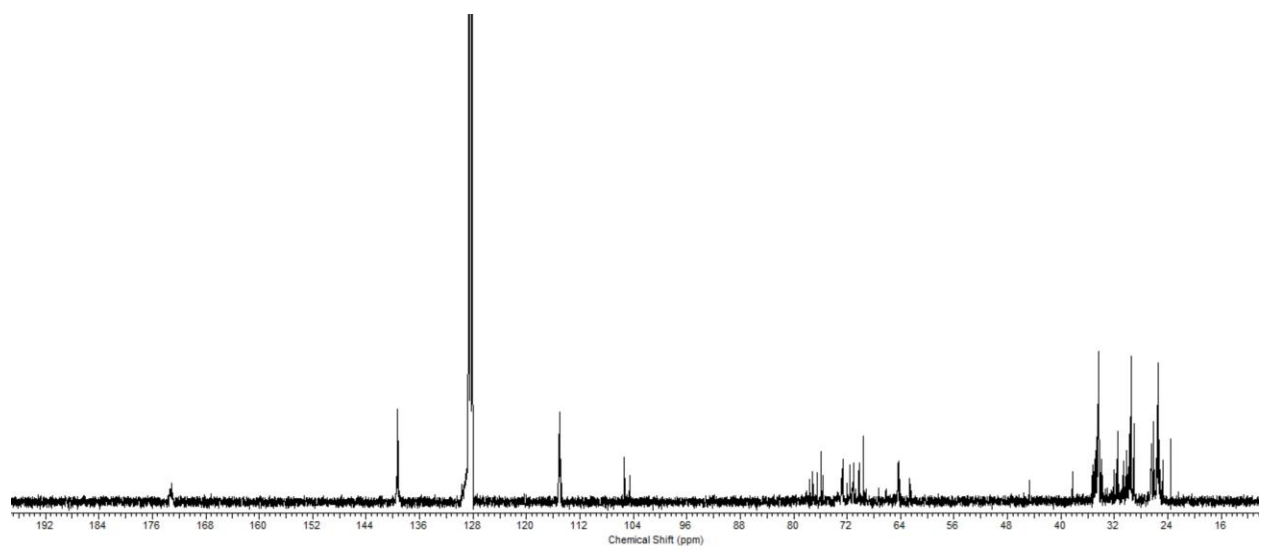


Figure D-5. $^{13}\text{C}\{^1\text{H}\}$ NMR spectrum (400 MHz, C_6D_6 , 25 °C) of polymerization product of SOE1.

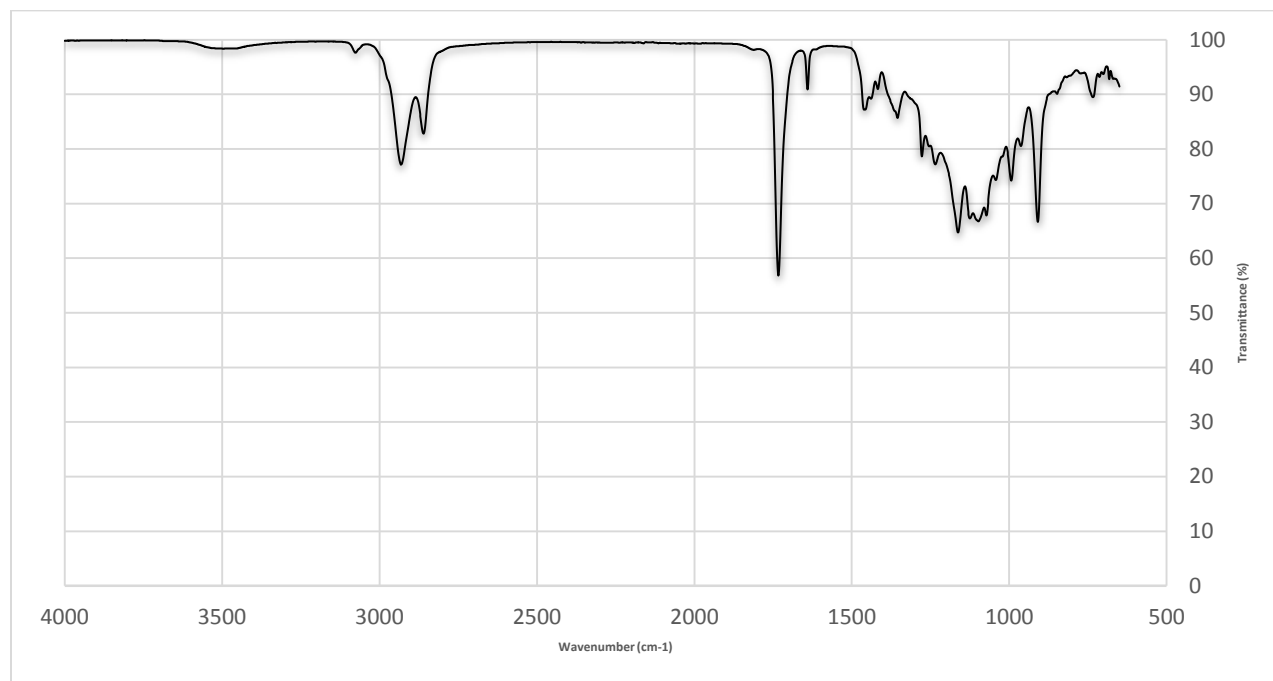


Figure D-6. FTIR Spectrum of polymerization product of SOE1.

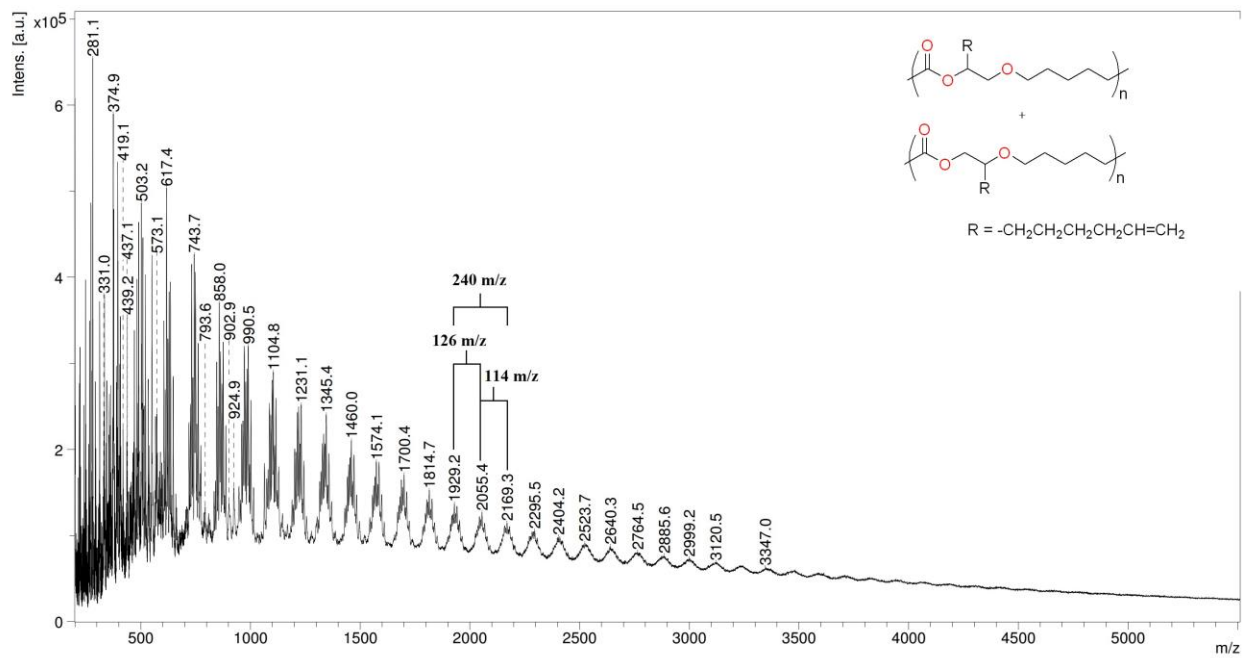


Figure D-7. MALDI-TOF mass spectrum of polymerization product of SOE1.